Non-Fermi liquid behavior in multi-orbital Anderson impurity models and possible relevance for strongly correlated lattice models

Thesis submitted for the degree of

Philosophiæ Doctor

Candidate:
Lorenzo De Leo

Supervisor:
Prof. Michele Fabrizio

October, 29th 2004

Contents

Introduction

Soon after the discovery of high T_c in cuprates, it was observed that some of their peculiar non-Fermi liquid properties could be explained phenomenologically by assuming a singular frequency (but not momentum) dependence of the electron self-energy, which was named as *marginal-Fermi liquid* behavior[1]. This observation stimulated a lot of activity in single-impurity models showing non-Fermi liquid behavior [2–5], which are the simplest cases where a singular frequency dependence may show up. Meanwhile non-Fermi liquid behavior started to be observed in uranium and cerium heavy-fermion compounds [6], which also admitted simple explanations through exotic single-impurity models [6] or phenomenological descriptions in terms of magnetic susceptibilities with anomalous frequency- but conventional momentum-dependence[7, 8].

All these theoretical attempts assumed, more or less implicitly, that a single-impurity behavior had chance to survive even in a translationally invariant system. This assumption is however not easy to justify theoretically. For instance, in the case of heavy-fermion compounds, one rather expects that, once the density of impurities is increased, the effects of the single-impurity singular behavior should be smoothened[9] and the non-Fermi liquid character lost. Even more difficult it is to relate the single-impurity behavior to the physics of cuprates, where the strength of the hybridization between the strongly correlated copper d-orbitals and the oxygen p-orbitals is comparable to the charge transfer gap. For these reasons and especially in the case of high T_c superconductors, the original interest towards anomalous single-impurity models lessened rapidly. Actually a connection between lattice models and impurity models was just near to come and what was lacking in the earlier approaches was indeed fixed by dynamical mean field theory (DMFT)[10–12], which improves ordinary Hartree-Fock theory by treating exactly temporal fluctuations while considering spatial fluctuations within mean-field. This theory provided a rigorous frame-

work in which a lattice model is mapped onto an Anderson impurity model (AIM) subject to a self-consistency condition which relates the impurity Green's function to the hybridization function with the conduction bath. The quasiparticle bandwidth of the lattice model transforms into the Kondo temperature T_K of the AIM. As in the case of classical mean-field theory, DMFT is exact only for infinite lattice connectivity, which is its main limitation. In finite dimensional systems, DMFT amounts to neglect the spatial dependence of the electron self-energy, while keeping its frequency dependence, which is presumably a safe approximation provided all relevant correlations are local.

Now that this tool is at disposal, the natural next step would be to apply it to those impurity models that are known to exhibit non-Fermi liquid behavior. The latter may emerge in impurity models for two distinct reasons. The first one is that, by construction, the conduction electrons may not be able to perfectly Kondo-screen all the impurity degrees of freedom. This is realized for instance in multi-channel Kondo models. The second mechanism is the competition between the Kondo effect and other couplings which may by their own screen the impurity degrees of freedom. In fact, the Kondo exchange takes advantage of letting the impurity tunnel among all available electronic configurations. This quantum tunneling is hampered by any term which splits the degeneracy and tends to trap the impurity into a given state. Therefore either the Kondo exchange overwhelms the intra-impurity splitting mechanism, or vice-versa, which leads respectively to a Kondo-screened phase or an unscreened one. When none of the two effects prevails, a non trivial behavior may appear. The two simplest models possessing either the first or the second ingredient are the over-screened multi-channel Kondo model[13] and the two $S = 1/2$-impurity Kondo model (2IKM)[14–17].

In the former an impurity-spin of magnitude S interacts antiferromagnetically with k conduction bands of electrons. If $k > 2S$ (over-screened model) the conduction electrons are not able to perfectly screen the impurity and the low-energy fixed point has non-Fermi liquid properties.

In the latter model two $S = 1/2$ impurities interact antiferromagnetically with each other (inter-impurity coupling) and with a conduction band of electrons (ordinary Kondo coupling). In this case the Kondo interaction favors the screening of the impurity spins by the conduction electrons, while the inter-impurity coupling tends to force the impurities into a non-degenerate singlet, which gets decoupled from the

conduction band. Under particular circumstances[18], the competition of these two screening-mechanisms originates an unstable non-Fermi liquid fixed point.

Unfortunately there is no lattice model that can be mapped through DMFT into any of these impurity models, because none of them can be interpreted as the low-energy (large U) limit of a single AIM. This is obvious in the two-impurity Kondo model. For what it concerns the multi-channel Kondo, one has to notice that any AIM has by construction a number of screening channels always such as to screen all impurity degrees of freedom, hence it generally gives rise to a perfectly-screened Kondo model rather than to a non-Fermi liquid over-screened one. This fact stresses the importance of finding realistic AIMs with non-Fermi liquid behavior. Examples of lattice models with purely local interactions suitably designed to exhibit non-Fermi liquid phases in infinite dimensions were proposed in Ref. [19]. These models are extensions of heavy-fermion lattice models which include besides strongly-correlated orbitals hybridizing with conduction bands also several non-hybridizing screening channels.

Here we are going to follow an alternative route which leads to simpler lattice models. As we saw, among the possible mechanisms for non-Fermi liquid behavior in AIMs, there is the competition between different screening processes. Since this fixed point requires fine tuning of the model parameters, it is tempting to conclude that it is of little physical relevance. In reality a similar competition is at the heart of any strongly-correlated electron lattice model near a Mott transition. Here the kinetic energy profits by the electrons hopping coherently through the whole lattice, which implies that each single site visits democratically all available local electronic-configurations, with the only constraint imposed by the average electron number. On the contrary, the strong correlation tries to optimize local energetics by favoring a well defined electronic-configuration, thus opposing against the hopping. This local physics involves at least two different energy scales. The higher one is the so-called Hubbard U, which tends to suppress on-site valence fluctuations, namely to fix the local charge to a well defined value. The lower one, let us define it generically by J, governs the splitting among on-site electronic configurations at fixed charge. J may be for instance controlled by the exchange-splitting (Hund's rules), by the crystal field, by local distortion modes or even by short-range inter-site correlations, as *e.g.* the super-exchange.

Within DMFT such a lattice model is mapped into a suitable AIM. The quasi-

particle bandwidth W_{qp} of the lattice translates into the Kondo temperature T_K of the AIM, while J becomes an alternative screening mechanism competing with the Kondo screening. As the model is driven towards a Mott metal-insulator transition (MIT), either by increasing repulsion at integer filling or by doping at large repulsion, it necessarily encounters a regime in which the coherent W_{qp} is of the same order as J, which we expect is essentially unaffected by U as it just determines the multiplet splitting at fixed charge. Translated into the AIM language, this implies that, before the MIT, the effective AIM has to reach a regime in which $T_K \sim J$, just where non-trivial behavior is expected to emerge. This is in short the route we are going to follow to design lattice models which, within DMFT, might show anomalous non-Fermi liquid behavior.

In order to realize the above mentioned competition between Kondo screening and another built-in screening mechanism, the simple AIM is clearly inadequate and generalizations are required. The most obvious one consists in considering multi-orbital impurities. Actually the Anderson impurity model was initially introduced to study $3d$-impurities in non-magnetic metals, hence the orbital degeneracy was a natural ingredient of the model. In multi-orbital impurities additional interactions are indeed permitted, like Hund's coupling, crystal-field splitting and Jahn-Teller effect. In particular the latter represents an appealing possibility to favor a non-degenerate singlet ground state and hence to compete against the Kondo effect. Preliminary attempts along this direction were reported in Refs. [20, 21], where lattice models of molecules with degenerate orbitals in the presence of a dynamical Jahn-Teller effect were analyzed. If the Jahn-Teller effect is strong enough to reverse the sign of the effective Hund's coupling, the isolated molecule has a non-degenerate singlet ground state for even number of electrons. In this case, a lattice of molecules coupled by an inter-molecular hopping undergoes a transition from a metal into a non-magnetic Mott insulator, a local version of a valence bond insulator, as the strength of the hopping decreases with respect to the Coulomb repulsion. However the transition as described by DMFT turns out to be not direct. Indeed it was found that a superconducting region intrudes between the metal and the singlet Mott insulator[22]. It was later realized that this superconducting phase, which was named strongly correlated superconductivity (SCS), has anomalous properties, as for instance a huge superconducting gap[23]. Although it was speculated that this unexpected behavior might reflect anomalous properties of the effective AIM onto which the lattice model maps by DMFT[22], a

more detailed analysis was lacking.

In this thesis we try to fill this gap by uncovering the physical behavior of the AIMs which correspond within DMFT to the lattice models analyzed in Refs. [22, 23], which are basically two- and three-orbital Hubbard models in the presence of an exchange splitting which can give rise either to ordinary or inverted Hund's rules, in the latter case mimicking *e.g.* a dynamical Jahn-Teller effect. In order to study these impurity models, we employ the Wilson numerical renormalization group (NRG) technique supplemented by conformal field theory (CFT) as well as Fermi-liquid theory arguments, all together providing us with a rather exhaustive characterization of the models.

We discover that the phase diagrams of both the two-orbital and the three-orbital models contain a non-Fermi liquid unstable fixed point (UFP) at intermediate coupling, which, as expected, is generated by the competition between the Kondo effect (whose associated energy scale is the Kondo temperature T_K) and the *inverted* Hund's rule (acting at an energy scale J) . This fixed point is in general robust with respect to particle-hole symmetry breaking, and this feature is important for the properties of the corresponding lattices since it implies that the properties driven by the UFP are robust to doping.

The two-orbital model can be seen as an on-site version of the 2IKM, having a quite similar phase diagram and in particular sharing the same unstable non-Fermi liquid fixed point, as we demonstrate by comparing the finite-size spectrum at the UFP with that predicted by CFT for the 2IKM.

We also calculate by NRG the spectral function of the impurity in the full range of parameters. In particular we study in detail the behavior of the spectral function across the UFP. We notice that the model contains three relevant parameters, the impurity Hubbard U, the Kondo temperature T_K and the inverted Hund's rule coupling J. The former is the highest energy scale, below which the valence of the impurity is practically frozen leaving aside only the degrees of freedom corresponding to the electronic configurations at that fixed charge. The next energy corresponds to a scale, which we denote by T_+, below which these residual degrees of freedom start to be quenched. This scale coincides with T_K, if $T_K \gg J$, and with J, if $J \gg T_K$. Naïvely we expect $T_+ \sim Max(T_K, J)$ or either $T_+ \sim T_K + J$. However, around the fixed point, not all the impurity degrees of freedom are involved in the screening processes which take place below T_+. Some of them have to wait until a lower energy scale,

T_-, is crossed. Roughly speaking these degrees of freedom correspond to the fact that the model has two screening mechanisms at its disposal, T_K and J. If $T_K > J$, the impurity finally use the Kondo screening to get rid of these left-over degrees of freedom, otherwise, if $J > T_K$, it prefers the inverted Hund's coupling. Right at the UFP, the impurity is unable to choose among T_K and J, and these degrees of freedom stay unscreened down to zero temperature, leaving a residual entropy of value $1/2 \log 2$. Therefore T_- controls the deviation from the fixed point, which occurs when $J = J_* \sim T_K$, and, in particular,

$$T_- \sim \frac{(J - J_*)^2}{J_*}.$$

All the above energy scales, $U > T_+ > T_-$, show up in the impurity density of states (DOS). We find that the DOS, besides the Hubbard peaks, whose position is controlled by U, is characterized by a low energy broad resonance of width T_+. On top of this resonance we find, in the Kondo screened side of the fixed point, a narrower one of width T_-, which vanishes as UFP is approached, leaving right at the UFP only the broad resonance. On the unscreened side of the UFP, this narrow resonance transforms into a narrow pseudo-gap, of width still controlled by T_-. Through Fermi liquid and scattering theory arguments we can also obtain a model low-energy spectral function which fits perfectly all the numerical results and provides us with a numerical estimate of both T_+ and T_-.

Then we set up a local Fermi liquid theory description that allows a better understanding of the relevant perturbations close to the UFP, in other words of the local susceptibilities which are singular at the UFP. This is an important information to understand the behavior of the lattice model which corresponds by DMFT to that AIM. Indeed, as we said, near the Mott transition the AIM onto which the lattice model maps is necessarily driven towards the UFP, in other words towards a regime with strongly enhanced, eventually singular, local susceptibilities. However, through the DMFT self-consistency, these singularity may turn into true bulk instabilities, leading to spontaneous generation of a bulk order parameter in a whole region around the single-impurity UFP. Since we do know all channels which are singular at the single-impurity fixed point, we can predict all the symmetry broken phases which can appear in the lattice model. Specifically, our two-orbital AIM at the UFP is unstable in several particle-hole channels as well as in a particle-particle one. Hence we foresee that, unless band-structure singularities, like nesting, are present, the most likely

instability is towards superconductivity. This supports and justifies the DMFT results of Refs. [22, 23], and it has been also recently confirmed also in the two-orbital Hubbard model[24].

We have also checked the stability of the UFP with respect to various symmetry breaking terms. In particular we find that the particle-hole symmetry breaking, which is the analog of doping in the corresponding lattice model, does not spoil the UFP and further extends the relevance of the results to lattice models away from half filling.

Finally we perform a similar analysis in the case of the three-orbital AIM corresponding to the lattice model of Refs. [22, 23]. As before, the competition between the Kondo effect and the dynamical Jahn-Teller effect, mimicked again by an inverted Hund's coupling, splits the phase diagram into two regions separated by an UFP with non-Fermi liquid properties. In the specific case analyzed in Refs. [22, 23], which corresponds to an average impurity occupancy of two electrons, we recover a very similar picture as in the two-orbital AIM; namely two Fermi-liquid phases, one Kondo screened and the other unscreened, separated by an UFP, still singular in the particle-particle channel. Again this confirms and clarify the DMFT finding of [22, 23]. More interesting is what we find for an average impurity occupancy of three electrons, corresponding to half-filling in the lattice model and to particle-hole symmetry in the AIM. Here the UFP separates the Kondo screened Fermi-liquid phase from a whole non-Fermi liquid *stable* phase. Unless the lattice model would break spontaneously particle-hole symmetry, this result suggests that the half-filling case, not yet studied by DMFT, might present much more interesting and anomalous behavior than what found in Refs. [22, 23].

From a purely theoretical point of view, the three-orbital AIM turns out to represent also a quite novel situation in boundary conformal field theory, which is the appropriate field theory framework to describe impurity models. Indeed the stable and unstable fixed points which we find realize several possible boundary conditions of three-state Potts models in two dimensions.

This thesis is organized as follows:

- In Chapter 1 we introduce the basic language of DMFT, stressing the relation between lattice and impurity models obtained through the self-consistency imposed on the impurity. We analyze the general properties of the simplest impurity model, the Anderson model, and then those of more other impurity models that present interesting features like non-Fermi liquid behavior.

- In Chapter 2 we present the method we used in this thesis to study impurity problems. We introduce the Numerical Renormalization Group method in some detail. We also briefly introduce the some concepts of Conformal Field Theory that will be useful in particular to interpret the data of the three-orbital model.
- In Chapter 3 and 4 we present the results for the two-orbital and three-orbital models respectively. These two Chapters contain the original contribution of this thesis.

Chapter 1

Dynamical mean field theory and impurity models

1.1 Dynamical mean field theory

Dynamical Mean Field Theory is the natural generalization to quantum many-body problems of the classical Weiss mean field theory. The underlying idea is that it is possible to describe a lattice using a single site embedded in a self consistent medium. As in traditional mean field theory, the DMFT approximation becomes exact in the limit of infinite dimensions, but contrary to the classical case not all the fluctuations are frozen. Indeed DMFT neglects the spatial fluctuations but treats exactly the temporal ones (from which the name "dynamical"). The effective field of the classical Weiss mean field theory, in that case simply a number, is replaced in DMFT by a function of (imaginary) time because now it has to describe the temporal fluctuations of the effective medium. This implies that the single site problem is still a non-trivial quantum many-body problem, but allows the use of the machinery developed to solve impurity problems in this different context.

The DMFT approach to a strongly correlated lattice problem with local interactions consists in focusing the attention on one site of the lattice and formally integrating out all the others obtaining an effective dynamics for the selected site. This effective action is greatly simplified by the assumption of infinite coordination of the lattice and can be interpreted as that of an AIM provided that a self-consistency condition is satisfied.

To understand the basic steps that lead to this construction it is useful to consider the simple case of the Hubbard model

$$H = -\sum_{\langle ij\rangle,\sigma} t_{ij}\left(c^{\dagger}_{i\sigma}c_{j\sigma} + h.c.\right) + U\sum_{i} n_{i\uparrow}n_{i\downarrow}, \tag{1.1}$$

with action

$$S = \int_0^{\beta} d\tau \left(\sum_{i} c^{\dagger}_{i\sigma}\left(\partial_{\tau} - \mu\right)c_{i\sigma} - \sum_{\langle ij\rangle,\sigma} t_{ij}c^{\dagger}_{i\sigma}c_{j\sigma} + U\sum_{i} n_{i\uparrow}n_{i\downarrow}\right) \tag{1.2}$$

in the absence of symmetry breaking, i.e. in the paramagnetic phase.

In order to give sensible results (finite kinetic energy per site) when the dimensionality is sent to infinity the hopping integral must be appropriately scaled $t \sim t^*/\sqrt{z}$, where t^* is a constant value and z is the number of nearest neighbors[11].

We concentrate on site 0 and to obtain an effective action for that site we decompose the original action into three pieces: a part containing the local terms involving only site 0, a part involving all the other sites but site 0 and a part connecting site 0 with the rest of the system:

$$S\left(c^{\dagger}_{i}, c_{i}\right) = S_0\left(c^{\dagger}_{0}, c_{0}\right) + S^{(0)}\left(c^{\dagger}_{i\neq 0}, c_{i\neq 0}\right) + \Delta S. \tag{1.3}$$

The $S^{(0)}\left(c^{\dagger}_{i\neq 0}, c_{i\neq 0}\right)$ term describes the original system in which the site 0 is removed, thus creating a "cavity".

Now all the fields $c^{\dagger}_{i\neq 0}, c_{i\neq 0}$ are formally integrated out giving rise to an effective action containing the generating functional of all the connected Green's functions of the system with the cavity:

$$S_{eff} = S_0 + \sum_{n=1}^{\infty}\sum_{i_1\ldots j_n} \tag{1.4}$$
$$\int t_{0j_1}c^{\dagger}_0(\tau_{j_1})\ldots t_{0j_n}c^{\dagger}_0(\tau_{j_n})G^{(0)}_{i_1\ldots j_n}\left(\tau_{i_1}\ldots\tau_{i_n},\tau_{j_1}\ldots\tau_{j_n}\right)t_{0i_1}c_0(\tau_{i_1})\ldots t_{0i_n}c_0(\tau_{i_n}).$$

where spin labels are omitted here and in the following to simplify the notation.

This derivation is valid in any dimension, but in the limit $d\to\infty$ this effective action simplifies because only the two-point Green's function $G^{(0)}_{ij}(\tau_i,\tau_j)$ survives while higher-point Green's functions are suppressed by inverse power of the dimensionality. This allows to write the $d=\infty$ effective action as

$$S_{eff} = -\int_0^{\beta} d\tau \int_0^{\beta} d\tau' c^{\dagger}_{0\sigma}(\tau)\mathcal{G}_0^{-1}(\tau-\tau')c_{0\sigma}(\tau') + U\int_0^{\beta} d\tau n_{0\uparrow}n_{0\downarrow} \tag{1.5}$$

where in Matsubara frequencies $\mathcal{G}_0^{-1}$ is given by

$$\mathcal{G}_0^{-1}(i\omega_n) = i\omega_n + \mu - \sum_{ij} t_{0i} t_{0j} G_{ij}^{(0)}(i\omega_n). \tag{1.6}$$

It can be shown that the term containing the cavity Green's functions $G_{ij}^{(0)}$ is related to the local on-site component of the original lattice Green's function, defined as

$$G_{loc}(i\omega_n) = \sum_{\mathbf{k}} G(\mathbf{k}, i\omega_n), \tag{1.7}$$

by the relation

$$-\sum_{ij} t_{0i} t_{0j} G_{ij}^{(0)}(i\omega_n) = G_{loc}^{-1}(i\omega_n) - R[G_{loc}(i\omega_n)] \tag{1.8}$$

where $R[G_{loc}]$ is the reciprocal function of the Hilbert transform of the density of states corresponding to the lattice considered. Given the non-interacting density of states $\rho(\epsilon)$ the Hilbert transform is defined as

$$\tilde{\rho}(\zeta) = \int_{-\infty}^{\infty} d\epsilon \frac{\rho(\epsilon)}{\zeta - \epsilon} \tag{1.9}$$

and its reciprocal function as

$$R[\tilde{\rho}(\zeta)] = \zeta. \tag{1.10}$$

The solution of the effective action (1.5) gives the interacting site-0 Green's function $G(i\omega_n)$ defined by

$$G(\tau - \tau') = -\langle T c_0(\tau) c_0^{\dagger}(\tau') \rangle_{S_{eff}} \tag{1.11}$$

and the translational invariance of the system implies that

$$G(i\omega_n) = G_{loc}(i\omega_n). \tag{1.12}$$

Equations (1.6), (1.8) and (1.12) provide a closed set of conditions that, once solved, gives the fully interacting local lattice Green's function.

Different lattices have different densities of states and the only place where these differences enter is in the Hilbert transform. In particular, in the case of the Bethe lattice the DMFT relations become very simple. The density of states of the Bethe lattice in $d = \infty$ is semicircular

$$\rho(\epsilon) = \frac{1}{2\pi t^2} \sqrt{4t^2 - \epsilon^2}, \qquad |\epsilon| < 2t \tag{1.13}$$

and the Hilbert transform and its inverse are

$$\tilde{\rho}(\zeta) = \left(\zeta - \mathrm{sgn}(\mathrm{Im}\zeta)\sqrt{\zeta^2 - 4t^2}\right)/2t^2 \quad (1.14)$$

$$R[G] = t^2 G + 1/G. \quad (1.15)$$

Given these expressions, the relations (1.6) and (1.8) become

$$\mathcal{G}_0^{-1}(i\omega_n) = i\omega_n + \mu - t^2 G(i\omega_n). \quad (1.16)$$

Up to here this mapping is of poor practical use. The crucial intuition due to George and Kotliar[12] is that this effective action can be interpreted as the action of an Anderson impurity model. Indeed if we introduce auxiliary fields that hybridize with site 0 providing a mechanism for the temporal fluctuation, it is possible to formulate the problem in an Hamiltonian form:

$$H_{AIM} = \sum_{\mathbf{k}\sigma} \epsilon_{\mathbf{k}} a^\dagger_{\mathbf{k}\sigma} a_{\mathbf{k}\sigma} + \sum_{\mathbf{k}\sigma} V\left(a^\dagger_{\mathbf{k}\sigma} c_{0\sigma} + c^\dagger_{0\sigma} a_{\mathbf{k}\sigma}\right) - \mu \sum_\sigma n_{0\sigma} + U n_{0\uparrow} n_{0\downarrow} \quad (1.17)$$

where the fields a represent a bath of electrons.

If we integrate out the a fields we obtain exactly S_{eff} in which

$$\mathcal{G}_0^{-1}(i\omega_n) = i\omega_n + \mu - \int_{-\infty}^{\infty} d\epsilon \frac{\Delta(\epsilon)}{i\omega_n - \epsilon} \quad (1.18)$$

where $\Delta(\epsilon) = \pi V^2 \rho(\epsilon)$ is the hybridization function and $\rho(\epsilon)$ is the density of states of the electron bath.

Hamiltonian (1.17) is precisely that of the Anderson impurity model that we will present in the next Section. In terms of this model, in the case of the Bethe lattice, the self-consistency condition (1.16) becomes

$$t^2 G(i\omega_n) = \int_{-\infty}^{\infty} d\epsilon \frac{\Delta(\epsilon)}{i\omega_n - \epsilon}. \quad (1.19)$$

In this way the DMFT self-consistency becomes a practical recipe: to solve a lattice model in infinite dimension we have to solve an AIM in which the density of states is that of the non-interacting lattice; from the solution we obtain the impurity Green's function G that must be related to the hybridization function of the electron bath through (1.12) and (1.18). From this procedure we obtain a new hybridization function that is plugged back into the AIM and the procedure restarts. When the convergence is achieved the Green's function obtained coincides with the local Green's

function of the original lattice model. To solve the AIM in principle we can employ any technique able to obtain the impurity Green's function.

One of the first applications of DMFT was the description of the Mott metal-insulator transition in the half-filled Hubbard model. Indeed it is known that upon increasing U the Hubbard model, which for $U = 0$ is a metal, becomes more and more correlated and at a critical value of U becomes an insulator due to the strong correlation between the electrons. Using DMFT it was proven that this happens with the progressive shift of the electron spectral weight from the quasiparticle peak that lies at the Fermi energy and represents the coherent component of conduction electrons, to the so called Hubbard bands, representing the on-site charge excitations induced by U. Close to the Mott metal-insulator transition the two Hubbard bands are well separated from the quasiparticle peak that shrinks progressively disappearing exactly at the transition.

This brief presentation of the DMFT equations justifies the interest in the AIM and provides a rigorous connection between the physics of impurities and that of lattice models in infinite dimension.

1.2 Anderson impurity model

The Anderson impurity model was originally introduced[25] to explain the experimental fact that some impurities with unfilled $3d$ shell have well defined magnetic moments when dissolved in simple metals, such as copper, whereas others are non-magnetic.

In order to describe transition metal impurities in a non-magnetic host, rather than starting from a realistic band structure calculation, Anderson proposed a model able to show realistic dynamical behavior and still simple enough to allow explicit calculations.

In this model the metal is represented as an electronic band with energy $\epsilon_{\mathbf{k}}$ for momentum $\mathbf{k}$ while the impurity is represented as an extra orbital with two spin orientations $\sigma = \uparrow, \downarrow$ and energy ϵ_d. The transition between this orbital and the conduction band is allowed by a hybridization term with amplitude $V_{\mathbf{k}d}$. Furthermore, Anderson introduced an intra-atomic Coulomb repulsion between two electrons at the localized level to reduce the probability of double occupation. This term results essential to the formation of a magnetic moment on the localized orbital, since in order to be

"magnetic" this orbital must be singly occupied. Collecting all terms the Anderson Hamiltonian is:

$$H_{AIM} = \sum_{\mathbf{k}\sigma} \epsilon_{\mathbf{k}} c^\dagger_{\mathbf{k}\sigma} c_{\mathbf{k}\sigma} + \sum_{\mathbf{k}\sigma} V_{\mathbf{k}d} \left(c^\dagger_{\mathbf{k}\sigma} d_\sigma + d^\dagger_\sigma c_{\mathbf{k}\sigma} \right) + \epsilon_d n_d + U n_{d\uparrow} n_{d\downarrow} \tag{1.20}$$

where $c^\dagger_{\mathbf{k}\sigma}$ creates conduction electrons with momentum $\mathbf{k}$ and spin σ, $d^\dagger_\sigma$ creates localized electrons with spin σ and $n_{d\sigma} = d^\dagger_\sigma d_\sigma$ is the occupation number of the localized level. This Hamiltonian is equivalent to (1.17), simply rewritten in the notation that is usual in impurity models. The model in which $\epsilon_d = -U/2$ is particle-hole symmetric and is usually called the symmetric Anderson model.

The Anderson model in this formulation does not take into account the orbital degeneracy of the d-level. As we will see, orbital degeneracy brings into play additional interactions that can in turn generate interesting new phenomena.

If $U = 0$ the problem is exactly solvable. In this simple case, due to the presence of the hybridization term in (1.20), electrons can remain on the localized level for a finite time only, eventually hopping back to the conduction band. The width of this resonance is

$$\Delta = \pi V^2 \rho_0(\epsilon_d) \tag{1.21}$$

where V^2 denotes an appropriate average of $|V_{\mathbf{k}d}|^2$ and $\rho_0(\epsilon_d)$ is the density of states of the conduction electrons at the energy of the resonant level.

The impurity Green's function is given by

$$G_{0,\sigma}(\omega + i\varepsilon) = \frac{1}{\omega - \epsilon_d + i\Delta} \tag{1.22}$$

where the subscript 0 indicates that the Coulomb interaction has not been taken into account. The impurity density of states is a lorentzian of width Δ

$$\rho_\sigma(\omega) \equiv -\frac{1}{\pi} \lim_{\varepsilon \to 0^+} \left(\mathrm{Im} G_{0,\sigma}(\omega + i\varepsilon) \right) = \frac{1}{\pi} \frac{\Delta}{(\omega - \epsilon_d)^2 + \Delta^2}. \tag{1.23}$$

The conduction electron Green's function can be expressed through the free electron Green's function and the scattering T-matrix as

$$\mathcal{G}_{\mathbf{k}\mathbf{k}',\sigma}(\omega) = \delta_{\mathbf{k}\mathbf{k}'} \mathcal{G}^{(0)}_{\mathbf{k},\sigma}(\omega) + \mathcal{G}^{(0)}_{\mathbf{k},\sigma}(\omega) T_{\mathbf{k}\mathbf{k}',\sigma}(\omega) \mathcal{G}^{(0)}_{\mathbf{k}',\sigma}(\omega) \tag{1.24}$$

where

$$\mathcal{G}^{(0)}_{\mathbf{k},\sigma}(\omega + i\varepsilon) = \frac{1}{\omega - \epsilon_{\mathbf{k}} + i\varepsilon} \tag{1.25}$$

and in the non-interacting case

$$T_{\mathbf{k}\mathbf{k}',\sigma}(\omega) = V_{\mathbf{k}d} G_{0,\sigma}(\omega) V_{d\mathbf{k}'}. \tag{1.26}$$

For $U \neq 0$, a simple Hartree-Fock solution of this model pointed out the distinction between a magnetic and a non-magnetic state. In the Hartree-Fock picture this model has a transition between a phase in which $\langle n_{d\uparrow} \rangle = \langle n_{d\downarrow} \rangle$, corresponding to a non-magnetic impurity, to a phase in which $\langle n_{d\uparrow} \rangle \neq \langle n_{d\downarrow} \rangle$ and the impurity is magnetic. The condition for the onset of a magnetic state can be written

$$U\rho_d^{(0)}(0) > 1 \tag{1.27}$$

where $\rho_d^{(0)}(0)$ is the density of states at the Fermi level of the impurity when $U = 0$. The presence of a sharp phase transition is an artifact of the Hartree-Fock approximation, but this simple analysis already unveils the presence of two qualitatively different regimes of the model.

Many other important observations followed the introduction of the AIM. It was demonstrated by Schrieffer and Mattis[26] that there is no transition between a non-magnetic and a magnetic state in the model as predicted by the Hartree-Fock solution but rather a smooth cross-over. In the same work it was recognized that the diagrammatic expansion of the self-energy in terms of U is formally identical to that of the electron self-energy in an interacting Fermi liquid (except for the lack of momentum conservation). Langreth[27] pointed out that the most important consequence of this result was that the impurity self-energy retains the property that characterizes Fermi liquids

$$\mathrm{Im}\Sigma(\omega \sim 0) \sim \omega^2. \tag{1.28}$$

This property implies that the low energy physics can be described by Fermi liquid theory and in particular by a single phase shift. Indeed, for $U \neq 0$, the impurity Green's function can be written as

$$G_\sigma(\omega + i\varepsilon) = \frac{1}{\omega - \epsilon_d - \Sigma(\omega + i\varepsilon) + i\Delta}; \tag{1.29}$$

combining (1.26) with the interacting expression (1.29) and using the property (1.28) we can obtain the T-matrix at zero energy

$$T_{\mathbf{k}\mathbf{k}',\sigma}(\omega = 0 + i\varepsilon) \;=\; V_{\mathbf{k}d} \left\{ \frac{1}{\omega - \epsilon_d - \mathrm{Re}\Sigma(\omega) + i\Delta} \right\}_{\omega = 0 + i\varepsilon} V_{d\mathbf{k}'}$$

$$= \frac{1}{\pi\rho_0}\left\{\frac{1}{\omega-\epsilon_d-\mathrm{Re}\Sigma(\omega)+i\Delta}\right\}_{\omega=0+i\varepsilon} \tag{1.30}$$

and from this the phase shift at zero energy

$$\delta_\sigma(\omega=0)=\cot^{-1}\left(\frac{\epsilon_d+\mathrm{Re}\Sigma(\omega=0)}{\Delta}\right). \tag{1.31}$$

Using the previous results Langreth has also given a general rigorous derivation of the Friedel sum rule. Assuming that the scattering can be described in terms of phase shifts, this sum rule expresses the total number N of extra electrons associated with the impurity in terms of the phase shift as

$$N=\frac{1}{\pi}\sum_\sigma \delta_\sigma(\omega=0) \tag{1.32}$$

1.3 Kondo model

The fact that for large U the impurity tends to behave as a spin rather than as a non-magnetic impurity suggests a connection with another impurity model, the $s-d$ exchange model, also known as Kondo model. In this model a conduction band of electrons interacts with a single spin-$1/2$ impurity S via an exchange interaction. The Hamiltonian is

$$H_K=\sum_{\mathbf{k}\alpha}\epsilon_{\mathbf{k}}c^\dagger_{\mathbf{k}\alpha}c_{\mathbf{k}\alpha}-J_K\vec{s}\cdot\vec{S} \tag{1.33}$$

where $\vec{s}=\sum_{\mathbf{k}\mathbf{k}'}c^\dagger_{\mathbf{k}\alpha}\frac{\vec{\sigma}_{\alpha\beta}}{2}c_{\mathbf{k}'\beta}$ represent the conduction electron spin density at the impurity site and $\vec{S}$ is the impurity spin. A rigorous proof of the connection between the Anderson and the Kondo model was established by Schrieffer and Wolff[28]. They demonstrated that, in the limit $U\gg\Delta$ and when $\epsilon_d<0$ and $\epsilon_d+U>0$, applying a canonical transformation to the Anderson Hamiltonian it is possible to obtain the Kondo Hamiltonian plus a potential scattering term. The canonical transformation is

$$H_K=e^S H_{AIM}e^{-S} \tag{1.34}$$

with generator

$$S=\left(\sum_{\mathbf{k}\sigma}\frac{V_{kd}}{\epsilon_{\mathbf{k}}-\epsilon_d-U}n_{d-\sigma}c^\dagger_{\mathbf{k}\sigma}d_\sigma+\sum_{\mathbf{k}\sigma}\frac{V_{kd}}{\epsilon_{\mathbf{k}}-\epsilon_d}(1-n_{d-\sigma})c^\dagger_{\mathbf{k}\sigma}d_\sigma\right)+h.c. \tag{1.35}$$

The couplings of the two models can be related via

$$J_K = |V_{\mathbf{k}d}|^2 \frac{U}{\epsilon_d(\epsilon_d + U)} < 0 \tag{1.36}$$

implying that the coupling is always antiferromagnetic.

This mapping between Kondo and Anderson models demonstrates once more that in the latter the impurity may behave as a magnetic moment in a suitable range of parameters.

The same relation was also interesting in view of the discovery of a striking phenomenon, the resistance minimum in metals with magnetic impurities: very small amount of magnetic impurities (Fe, Mn, Cr) in a non-magnetic host (Cu, Ag, Au, Al) causes a resistivity minimum at low temperature and eventually a saturation at $T = 0$.

In 1964 Kondo[29] provided an explanation for this phenomenon calculating the third order correction to the resistivity due to the presence of the impurity in the $s-d$ model. The result was that the resistivity is

$$R \sim 2\pi\rho_0 c J_K^2 \left[1 + 4J_K\rho_0 \ln\left(\frac{T}{D}\right)\right] \tag{1.37}$$

where ρ_0 is the density of states at the Fermi level of the conduction band, c is the concentration of impurity and D is the bandwidth of conduction electrons. It is clear from this formula that in the antiferromagnetic case $J_K < 0$ when the temperature decreases the second term in parenthesis grows, becoming of order 1 for a temperature of the order of the so called Kondo temperature

$$T_K \sim D \exp\left(\frac{1}{2J_K\rho_0}\right). \tag{1.38}$$

This result is limited to high temperatures, since for temperatures of the order of T_K the perturbation expansion breaks down, but it already points to a qualitative change in the physics of the Kondo model at low temperature. The emergence of logarithmic terms in perturbation theory and the non-analytic expression of the Kondo temperature is the hallmark of an intrinsically non-perturbative problem.

The solution to this puzzle came with the contributions of Anderson and Wilson. The first introduced the idea of scaling[30] of the Kondo coupling J_K: the process of lowering the temperature is equivalent to replacing the original problem with a

new one with a rescaled coupling. The antiferromagnetic case can be interpreted in terms of an effective coupling scaling to infinity at zero temperature. In this way the impurity forms a singlet with conduction electrons and gives a unitary contribution to the resistivity. Establishing a correspondence between the Kondo problem and the statistical mechanics of appropriate Ising chains[31–34], Anderson was able to guess correctly the low temperature behavior.

Once accepted that the low temperature physics is described by the strong coupling $J_K \to -\infty$ theory, the difficult task is to connect the high-temperature and the low-temperature regimes. This was done by Wilson with the help of a numerical solution of the Kondo problem[35]. Wilson provided the most striking proof that below T_K the Kondo impurity is screened by the conduction electrons and the ground state is a total singlet.

The technique introduced by Wilson, the numerical renormalization group (NRG), became a cornerstone and was later used to solve many other impurity models. In this thesis we employed mainly the NRG to analyze our impurity models. A more detailed description of this method is deferred to Chapter 2.

After the solution of the Kondo problem, NRG was applied to the AIM by Krishnamurthy et al.[36, 37]. The picture that emerged confirmed the validity of the Schrieffer-Wolff transformation and can be summarized by the renormalization group flow of the symmetric AIM between the different fixed points in the phase space. At high temperature the impurity is essentially a free orbital; when the temperature drops below U the system flows to the so called local moment fixed point, in which the impurity is singly occupied and behaves as a spin-$1/2$ but is decoupled from the conduction band resembling the Kondo model for weak antiferromagnetic coupling; eventually when $T \ll T_K \ll U$ the fixed point is that in which the impurity is completely screened and leaves behind a phase shift $\delta = \pi/2$ for the conduction electrons.

1.4 Non-Fermi liquid behavior

In this Section we briefly introduce those impurity models that present a non-Fermi liquid fixed point in the phase diagram. The first two, the overscreened Kondo model and the two-impurity Kondo model, will be deeply connected with the models we are going to study in this thesis. For the sake of completeness we cite also the pseudogap models, even if they will not be relevant for this thesis.

1.4.1 Over-screened Kondo models

The ordinary Kondo model can be generalized to impurity spin higher than $1/2$ and to an arbitrary number of conduction band channels. The Hamiltonian of the model can be written as

$$H_K = \sum_{\mathbf{k}a\alpha} \epsilon_{\mathbf{k}} c^\dagger_{\mathbf{k}a\alpha} c_{\mathbf{k}a\alpha} - J_K \vec{s}_a \cdot \vec{S} \tag{1.39}$$

where now the electron operator carries an additional index $a = 1, \ldots, k$ representing the channel, $\vec{s}_a = \sum_{\mathbf{k}\mathbf{k}'} c^\dagger_{\mathbf{k}a\alpha} \frac{\vec{\sigma}_{\alpha\beta}}{2} c_{\mathbf{k}'a\beta}$ represent the conduction electron channel-a spin density at the impurity site and $\vec{S}$ is the impurity spin operator. The class of models obtained in this way can be divided into three classes according to the value S of the spin of the impurity and to the number k of conduction channels.

If $k = 2S$ the model is called perfectly screened because the k conduction channels, each carrying a spin $1/2$, are able to compensate the impurity spin exactly. In the strong coupling $J_K \to -\infty$ limit the conduction electrons in each channel are antiferromagnetically oriented in a neighborhood of the impurity such as to screen the impurity. Since the net spin of the conduction electrons is equal to the impurity spin, the low temperature ground state of the model is a non degenerate singlet. This model is the direct generalization of the ordinary Kondo model to higher spin and the physics is practically the same.

If $k < 2S$ the model is underscreened because now there are not enough conduction channels to screen completely the impurity. In this case the strong coupling limit corresponds to the reduction of the impurity spin from S to $S - k/2$, due to the screening of the impurity by the available channels, and the low temperature ground state is degenerate and corresponds to a decoupled spin-$S - k/2$ impurity.

Eventually, if $k > 2S$ the model is called overscreened. The peculiarity of this model is that both the weak and the strong coupling fixed point are unstable and the stable low energy fixed point is at intermediate coupling and has non-Fermi liquid properties. That the strong coupling fixed point is unstable can be seen following a naïve argument due to Nozières and Blandin[13]. Consider the simple case $S = 1/2$ $k = 2$ with the impurity spin polarized along the z direction. At strong coupling, if the impurity spin is $\uparrow$, two conduction electrons (one per channel) are trapped at the impurity site with spin polarization opposite to that of the impurity ($\downarrow$). The impurity in this regime can be seen as an effective spin-$1/2$ with down polarization. The impurity site becomes inaccessible to the remaining conduction electrons except for virtual

processes. Since the conduction electrons at the impurity site are already polarized downward, the only virtual processes allowed by the Pauli principle are those involving the up conduction electrons. By second order perturbation theory the energy of up electrons is this lowered while that of down electrons is unaffected. Considering that the effective polarization of the impurity in the strong coupling regime is pointing downward the effective interaction corresponds to an antiferromagnetic Kondo coupling between the effective impurity and conduction electrons. This is a relevant perturbation and the fixed point is hence unstable.

It is very important to note that the low temperature non-Fermi liquid fixed point is unstable with respect to anisotropies in the couplings. For instance in the above mentioned $S = 1/2$ $k = 2$ case, as soon as one of the channels is coupled to the impurity more strongly than the other, the low temperature stable fixed point is again a Fermi liquid in which the strongly coupled channel screens the impurity while the other is decoupled.

The first to suggest the existence of this non-Fermi liquid intermediate coupling fixed point were Nozières and Blandin[13]. They were able to demonstrate its existence in the case of a large number of conduction channels calculating perturbatively the β-function. Later the problem was solved also numerically by NRG[38] and analytically by Bethe-Ansatz[39–41] and conformal field theory[42–44].

1.4.2 Two impurity Kondo model

This model describes two spin-$1/2$ impurities embedded in a metal. The impurities are sitting at two different positions in space $\mathbf{r}_1$ and $\mathbf{r}_2$ at a distance R one from the other. The Hamiltonian of the model is

$$H = \sum_{\mathbf{k}\sigma} \epsilon_{\mathbf{k}} c^{\dagger}_{\mathbf{k}\sigma} c_{\mathbf{k}\sigma} + J \left[\vec{s}(\mathbf{r}_1) \cdot \vec{S}_1 + \vec{s}(\mathbf{r}_2) \cdot \vec{S}_2 \right] + K \vec{S}_1 \cdot \vec{S}_2 \qquad (1.40)$$

where $\vec{S}_{1,2}$ are the two impurity spins and $\vec{s}(\mathbf{r})$ is the conduction electron spin density operator at position $\mathbf{r}$. The coupling J is the usual Kondo coupling between the impurities and the conduction electrons, while K is the Ruderman-Kittel-Kasuya-Yosida (RKKY) coupling between the impurities. The RKKY coupling is added explicitly here but is also generated by the Kondo term in second order perturbation theory. When antiferromagnetic, the RKKY coupling tends to favor a singlet configuration of the two impurities. This tendency is in contrast with the Kondo effect that tries

to optimize the energy through the screening of the impurity spins by the conduction electrons.

This model was initially analyzed by Jones and Varma using NRG for ferromagnetic RKKY coupling[14]. Later an unstable fixed point with non-Fermi liquid properties was found in the antiferromagnetic RKKY region[15, 16] for $-K \sim T_K$. The complete description of the UFP was found by Affleck and Ludwig[17] using conformal field theory techniques and by Sire, Varma and Krishnamurthy[45] and by Gan[46] using bosonization.

The fixed point separates a phase in which the two impurities are Kondo-screened by the conduction electrons from a phase in which the impurities form a singlet and are decoupled from the conduction electrons. The UFP exists only if the system is particle-hole symmetric and this can be seen from a simple argument[47]. Due to particle-hole symmetry the phase shift of the conduction electrons can be only 0 or $\pi/2$. In the Kondo screened phase the phase shift is $\pi/2$ as in the usual Kondo effect, while in the unscreened phase the phase shift is 0 because the impurities are decoupled from the conduction band. This implies that between these two phases there must be a phase transition, either first or second order. In the latter case the corresponding fixed point must be a point in which the phase shift is not defined, i.e. a non-Fermi liquid fixed point.

1.4.3 Pseudogap models

This class of models is a generalization of the ordinary Kondo and Anderson model to the case in which the conduction band density of states vanishes at the Fermi level with a power-law behavior. The motivation for considering such a generalization comes from the observation that the conduction electrons that contribute to the Kondo screening of the impurity are those that lie close to the Fermi level. It is interesting to ask what happens if we consider a conduction band with a density of states $\rho(\epsilon) \sim \epsilon^r$ where $r > 0$ and the energy is measured with respect to the Fermi level. In this case, as the temperature is lowered, the conduction band has less and less electrons at disposal to screen the impurity. For instance in the case of the Kondo model defined in (1.33), it turns out that if $0 < r < 1/2$ the Kondo effect takes place only for a coupling $J_K < J_K^c$ where $|J_K^c| \sim r$ identifies an unstable non-Fermi liquid fixed point. Above this value of the coupling the system flows to weak coupling. On the other hand, for

$r > 1/2$ the strong coupling fixed point is never reachable and the system always flow to weak coupling. Once again the presence of a symmetry breaking (here a potential scattering that breaks particle-hole symmetry) changes the picture substantially.

The problem was originally studied by Withoff and Fradkin[48]. For a more exhaustive review see Ref. [49] and references therein.

Chapter 2

Numerical and analytical methods

The importance of impurity models is twofold: on one hand they are interesting as theoretical models per se, showing different unusual behaviors; on the other hand they are simpler than lattice models but they still retain many of their physical properties. For these reasons a great variety of techniques has been developed in order to solve these models. Each technique has its advantages and its drawback and very often it is the combinations of different techniques that give the most sensible results.

A real breakthrough in this field is the solution of the Kondo model obtained by Wilson in the early seventies[35]. To tackle the Kondo problem Wilson developed a numerical technique, the NRG, able to link the high and low temperature regimes in a non perturbative way. The NRG technique is the main numerical tool we employed in this work and will be described in detail in the next Section.

After the Wilson solution other analytical techniques were developed that were able to give an essentially exact solution of the Kondo problem: this is the case of the Bethe Ansatz[50] which gives the analytically exact solution of the static and thermodynamic properties of the model and of bosonization.

In the eighties the development of Conformal Filed Theory (CFT) brought a fresh impulse in the physics community and consequences arrived also in the field of impurity models. Cardy's work on Boundary CFT started a development that culminated with Affleck and Ludwig theory of the Kondo model. This theory is able to describe the fixed points of an impurity model based on the assumption of its conformal invariance and symmetry properties. The major success achieved by this method was the solution of the over-screened and of the two-impurity Kondo models. We used

this technique as a counterpart of NRG, given its possibility to extract the finite size properties of the model which can be directly compared with the spectrum obtained numerically.

2.1 Numerical Renormalization Group

The basic idea behind the Wilson approach to the Kondo model is that there is no clear separation of energy scales in the problem and this implies that an infinite number of energy scales should be treated on equal footing. In order to overcome the problem, Wilson introduced a rephrasing of the model in a way suitable for a renormalization treatment: instead of treating the conduction electron band as a continuum of energies, he introduced an artificial logarithmic discretization of the band. This mapping allows to treat each (logarithmic) energy scale as a perturbation of the preceding one and to obtain a scaling recursion for the Hamiltonian of the model.

Let us start from the simpler case of the original Anderson model[36, 37] (generalizations to more complicated models are straightforward)

$$H = \sum_{\mathbf{k}\sigma} \epsilon_{\mathbf{k}} c^{\dagger}_{\mathbf{k}\sigma} c_{\mathbf{k}\sigma} + \sum_{\mathbf{k}\sigma} \frac{V_{\mathbf{k}d}}{\sqrt{\Omega_0}} \left(c^{\dagger}_{\mathbf{k}\sigma} d_{\sigma} + d^{\dagger}_{\sigma} c_{\mathbf{k}\sigma} \right) + \epsilon_d n_d + U n_{d\uparrow} n_{d\downarrow}. \tag{2.1}$$

Moving to a continuum representation, assuming isotropic dispersion relation and hybridization with the impurity and decomposing the conduction electron operators in spherical harmonics centered at the impurity site, one obtain an equivalent description in which only s-wave hybridize with the impurity:

$$\begin{aligned} H &= \sum_{\sigma} \sum_{lm} \int dk\, \epsilon_k c^{\dagger}_{klm\sigma} c_{klm\sigma} \\ &\quad + \sqrt{\frac{1}{2\pi^2}} \sum_{\sigma} \int dk\, k\, V_{kd} \left(c^{\dagger}_{k00\sigma} d_{\sigma} + d^{\dagger}_{\sigma} c_{k00\sigma} \right) \\ &\quad + \epsilon_d n_d + U n_{d\uparrow} n_{d\downarrow} \end{aligned} \tag{2.2}$$

where $c^{\dagger}_{klm\sigma}$ creates an electron with momentum k and spin σ in an l-wave configuration with azimuthal number m around the impurity. Since the impurity hybridize only with $c_{k00\sigma}$, the $l \neq 0$ and $m \neq 0$ components can be dropped and in the following the orbital and azimuthal indexes will be omitted.

The next step is to move to a representation in the energy space substituting $c^\dagger_{k\sigma} = \sqrt{\frac{d\epsilon_k}{dk}}\, c^\dagger_{\epsilon\sigma}$. To simplify the notation we can consider the case in which the energies of the band, measured with respect to the chemical potential, range from $-D$ to D, but generalizations to non-symmetrical bands are again straightforward.

In this simplified case, after a trivial rescaling of variables, the Hamiltonian becomes

$$H = D\int_{-1}^{1} d\epsilon\, \epsilon\, c^\dagger_{\epsilon\sigma} c_{\epsilon\sigma} + \int_{-1}^{1} d\epsilon \sqrt{\frac{D\Delta(D\epsilon)}{\pi}} \left(c^\dagger_{\epsilon\sigma} d_\sigma + d^\dagger_\sigma c_{\epsilon\sigma}\right) + \epsilon_d n_d + U n_{d\uparrow} n_{d\downarrow} \quad (2.3)$$

where $\Delta(\epsilon) = \pi V^2(\epsilon)\rho(\epsilon)$ is the hybridization function, $\rho(\epsilon)$ is the density of states of the conduction band and summation over repeated spin indices is implied from now on.

If one is not interested in particular cases like pseudogap models, where the density of states has a power-law behavior close to the Fermi energy $\rho(\epsilon) \sim \epsilon^r$, the energy dependence of the hybridization function can be neglected and $\Delta(\epsilon)$ replaced by its value Δ_0 at the Fermi energy. Another important application where the energy dependence of Δ is fundamental is DMFT where it enters the self-consistent equations for the effective Weiss field.

It is worth noticing now that under very weak assumptions we obtained a one-dimensional description of the original model. The possibility to map the problem to one dimension is what allows the use of techniques like bosonization, Bethe Ansatz or conformal field theory in impurity models.

To solve the problem numerically it is instead more convenient to transform the Hamiltonian in a tight-binding chain model

$$\begin{aligned} H &= D\sum_{n=0}^{\infty} \left[e_n f^\dagger_{n\sigma} f_{n\sigma} + t_n \left(f^\dagger_{n\sigma} f_{n+1,\sigma} + h.c.\right)\right] \\ &\quad + \sqrt{\frac{2D\Delta_0}{\pi}} \left(f^\dagger_{0\sigma} d_\sigma + d^\dagger_\sigma f_{0\sigma}\right) \\ &\quad + \epsilon_d n_d + U n_{d\uparrow} n_{d\downarrow} \end{aligned} \quad (2.4)$$

using a Lanczos tridiagonalization procedure where the coefficients e_n and t_n and the states f_n (called "shells" because they roughly correspond to conduction electrons in spherical shells of increasing radius around the impurity) are determined via the recursive relations:

$$e_n = \langle f_{n\sigma}| \int_{-1}^{1} d\epsilon\, \epsilon\, c^\dagger_{\epsilon\sigma} c_{\epsilon\sigma} |f_{n\sigma}\rangle \quad (2.5)$$

$$t_n|f_{n+1,\sigma}\rangle = \left(\int_{-1}^{1} d\epsilon\, \epsilon\, c^{\dagger}_{\epsilon\sigma} c_{\epsilon\sigma} - e_n\right)|f_{n\sigma}\rangle - t_{n-1}|f_{n-1,\sigma}\rangle \tag{2.6}$$

$$\langle f_{n+1,\sigma}|f_{n+1,\sigma}\rangle = 1. \tag{2.7}$$

In the simplified case in which the hybridization function is symmetric, $\Delta(-\epsilon) = \Delta(\epsilon)$, it can be easily shown that all the coefficients e_n vanish.

Here f_0 is the linear combination of conduction electrons that couples directly to the impurity:

$$f_{0\sigma} = \frac{1}{\sqrt{2}} \int_{-1}^{1} d\epsilon\, c_{\epsilon\sigma}. \tag{2.8}$$

It is maximally *delocalized* in momentum space and hence it is maximally *localized* at the impurity site in position space.

The crucial point is that in the Hamiltonian obtained after this transformation the coefficients t_n converge to a finite value for large n, thus making any finite-length chain approximation useless. Here comes Wilson's intuition about the energy scales.

Introducing a discretization of the conduction band $[-1, 1]$ in intervals $[\Lambda^{-n-1}, \Lambda^{-n}]$ and $[-\Lambda^{-n}, -\Lambda^{-n-1}]$, where $\Lambda > 1$ is a parameter and $n = 0, 1, \ldots, \infty$, it is possible to obtain a formulation of the problem in which the hopping amplitudes along the chain decay like $t_n \sim \Lambda^{-n/2}$. Indeed replacing the conduction band states in each interval by a single state,

$$a_{n\sigma} = (\Lambda^{n/2}/\sqrt{1-\Lambda^{-1}}) \int_{\Lambda^{-n-1}}^{\Lambda^{-n}} d\varepsilon\, c_{\varepsilon\sigma} \tag{2.9}$$

$$b_{n\sigma} = (\Lambda^{n/2}/\sqrt{1-\Lambda^{-1}}) \int_{-\Lambda^{-n}}^{-\Lambda^{-n-1}} d\varepsilon\, c_{\varepsilon\sigma} \tag{2.10}$$

for positive and negative energy respectively, and repeating the Lanczos construction, the resulting Hamiltonian describes a chain with hopping decreasing exponentially with n.

The main difference between a logarithmic discretization and a linear one is that the former has a poorer resolution in the high energy region but allows to capture energy scales arbitrarily close to the Fermi level and this feature is essential in problems like the Kondo model where logarithmic scales play a crucial role.

The parameter that controls this approximation is Λ: $\Lambda \to 1$ corresponds to the original continuum limit, while $\Lambda > 1$ is an approximation of the original problem but provides a separation of energy scales.

If we now consider chains of finite length N, the smallest energy scale of the system is of order $\Lambda^{-N/2}$, hence the next term in the Hamiltonian, which is of order $\Lambda^{-(N+1)/2}$, can be treated as a "perturbation". Even if this argument is not rigorous, it gives an idea of why the method works.

Hence to solve the problem we can proceed iteratively. We first define the Hamiltonian of the length N system

$$\begin{aligned} H_N &= \Lambda^{(N-1)/2}\Bigg\{ \sum_{n=0}^{\infty} \Lambda^{-n/2}\xi_n \left(f^{\dagger}_{n\sigma} f_{n+1,\sigma} h.c. \right) \\ &\quad +\tilde{\Delta}_0^{1/2} \left(f^{\dagger}_{0\sigma} d_{\sigma} + d^{\dagger}_{\sigma} f_{0\sigma} \right) \\ &\quad +\tilde{\varepsilon}_d n_d + \tilde{U} n_{d\uparrow} n_{d\downarrow} \Bigg\} \end{aligned} \tag{2.11}$$

where $\tilde{\Delta}_0 = C_\Lambda^2(2D\Delta_0/\pi)$, $\tilde{\varepsilon}_d = C_\Lambda \varepsilon_d/D$,$\tilde{U} = C_\Lambda U/D$, $C_\Lambda = 2/(1+\Lambda^{-1})$ and ξ_n are coefficients of order 1. The Hamiltonian is rescaled by the factor $\Lambda^{(N-1)/2}$ in order to have the lowest energy excitations always of order 1. In this way it will be easier to follow the evolution of the low-lying levels and the original Hamiltonian will be recovered in the limit

$$H = \lim_{N\to\infty} C_\Lambda^{-1} D \Lambda^{-(N-1)/2} H_N. \tag{2.12}$$

We derive a simple recursive relation between H_N and H_{N+1}:

$$H_{N+1} = T(H_N) = \Lambda^{1/2} H_N + \xi_N \left(f^{\dagger}_{N\sigma} f_{N+1,\sigma} + h.c. \right). \tag{2.13}$$

This relation represents the renormalization group transformation and ensures that the knowledge of the eigenvalues and eigenvectors of H_N and of the matrix elements $\langle | f^{\dagger}_{N\sigma} | \rangle_N$ is enough to solve the H_{N+1} problem.

In practice the method starts diagonalizing the Hamiltonian H_0 of the system built up with the impurity and the first shell f_0; then H_1, involving also f_1, is constructed from the eigenvalues and eigenvectors of H_0 and is again diagonalized; then the procedure is iterated.

The Hilbert space of the system grows at each iteration by a factor 4 and after few steps becomes too large to be handled entirely. To proceed we focus our attention on the low energy part of the spectrum and truncate the high energy part retaining only a fixed number of states in each diagonalization. In this way we retain the spectrum

relevant for the low temperature properties and, at the same time, we can keep the computational cost of each iteration fixed. This procedure is justified by the fact that matrix elements between high energy and low energy states are small due to the exponential decay of the hopping along the chain, implying that high energy states do not influence the low energy behavior. This exponential decay is in turn governed by the value of Λ.

The choice of Λ is indeed a compromise: for a value close to 1 the model described is more similar to the original model but the computational effort needed to describe it faithfully grows rapidly because a larger number of states must be retained; for a large value of Λ the decay of the hopping along the chain is faster, hence the number of states needed for a good description decreases but on the other hand the approximation of replacing states in an energy interval $[\Lambda^{-n-1}, \Lambda^{-n}]$ by just one state is worse. In practice Λ is typically chosen to lie between 2 and 3.

In order to reduce substantially the computational effort it is fundamental to exploit all the possible symmetries of the problem. Keeping track of the quantum numbers of the states it is possible to reduce the Hamiltonian to a block diagonal form and diagonalize smaller matrices. Typical examples of symmetries exploited are the global charge $U(1)$ and spin $SU(2)$.

The outcome of each iteration is a set of energy levels representing the ground state and low-lying excitations of the system. Analyzing the evolution of these levels with the length of the chain it is possible to identify the flow of the system between various fixed points. Indeed, when the system is close to a fixed point, the Hamiltonian is left almost invariant under the renormalization group transformation (2.13), and the spectrum extracted from the numerical calculation remains constant from iteration to iteration.[1]

Usually the fixed point can be inferred by analyzing its spectrum and assuming that the fixed point itself correspond to a modification of the boundary conditions of the original system. This is the case for the Kondo and the Anderson models, where all the fixed points can be described in terms of the corresponding Hamiltonians in which the original parameters involving the impurity are sent either to 0 or to $\pm\infty$.

[1] Due to the intrinsic differences between chains with even and odd number of sites, the fixed points in these two cases are in general different. Hence the spectrum remains constant from even (odd) iteration to even (odd) iteration. Formally the fixed point is a property of the transformation T^2, being rather a limiting cycle for T.

This will not be the case for other models, like for instance the two-impurity Kondo model, where some fixed points correspond to non-trivial boundary conditions that cannot be defined in terms of the original fermionic degrees of freedom and require a more general definition of boundary condition.

A useful and simple criterion to discriminate between a Fermi liquid fixed point and a non-Fermi liquid one is the spacing of the lowest lying excitations. Indeed in a Fermi liquid the low energy spectrum can be described by quasiparticles with well defined energies. This means that the spacing of the lowest levels must be uniform, corresponding to the energy necessary to add a quasiparticle, and that the spectrum contains levels whose energy is an integer multiple of the quasiparticle energy. On the other hand, the spectrum of a system at a non-Fermi liquid fixed point does not possess in general this peculiar feature.

As we saw, at the N-th iteration the lowest energy scale is $\sim \Lambda^{-N/2}$ and the energies of the states kept lie in a range close to this value (typically between $\sim 10\Lambda^{-N/2}$ and $\sim 0.1\Lambda^{-N/2}$). Then it is natural interpret N as related to the temperature. The relation between N and the temperature of the system is $T \sim \Lambda^{-N/2}$. This relation implies that as the length of the chain grows the system flows to the low temperature fixed point.

2.1.1 Effective Hamiltonian description

During the renormalization group flow the system goes from one fixed point to another but is never exactly *at* a fixed point (unless artificially tuned to lie on it). The presence of relevant (or marginally relevant) operators close to an unstable fixed point drives the system far away from it, hence if the system is not precisely at the fixed point the spectrum is always slightly different from that of the fixed point and the differences grow as the system is driven out of that fixed point. Close to a stable fixed point instead there are irrelevant (or marginally irrelevant) operators that fade away asymptotically but for any finite point along the renormalization group flow (corresponding to a finite length N of the Wilson chain) produce again a deviation from the fixed point spectrum.

If a fixed point can be described by Fermi liquid theory, Wilson provided a simple and effective way to describe the behavior of the system in the vicinity of this fixed point. Describing the system by the fixed point Hamiltonian plus a term containing

the most relevant operators and fitting the deviation of the spectrum from the fixed point values it is possible to extract the magnitude of the operators and describe the system in terms of an effective Hamiltonian

$$H_N = H_N^* + \Lambda^{(N-1)/2} \delta H_N \tag{2.14}$$

where H_N^* represents the fixed point Hamiltonian and δH_N the deviation due to relevant or irrelevant operators.

From this description it is possible to extract susceptibilities and the so called Wilson ratios (the ratio between the change in the susceptibility and the change in the specific heat due to the impurity) for conserved quantities. For non-conserved quantities, scattering amplitudes can be accessed and related to the corresponding susceptibility using Fermi liquid theory.

2.1.2 Spectral functions

The spectral properties of the impurity in the case of the Anderson model are an essential feature in connection with DMFT and in general can provide further insight in the properties of the model.

NRG allows to calculate the spectral function of the impurity simply retaining memory of the matrix elements of the $d_\sigma^\dagger$ operator between the states during the various iterations[51, 52]. Indeed the spectral function can be written using Lehmann representation as

$$A_\sigma(\omega) = \frac{1}{Z} \sum_{m,n} \left| \langle m | d_\sigma^\dagger | n \rangle \right|^2 \delta(\omega - (E_n - E_m)) \left(e^{-\beta E_n} + e^{-\beta E_m} \right). \tag{2.15}$$

Calculating the impurity spectral function in this way we obtain a set of delta peaks at each iteration whose position is cut-off on the low energy side by the typical energy scale of the iteration and on the high energy side by the truncation procedure: at iteration N the lowest energy scale is $\sim \Lambda^{-N/2}$ hence the energy position of the peaks will be larger (in absolute value) of some fraction of this typical value; on the other hand the number of states retained is limited by the computational cost and the highest energy states will be typically within $\sim 10\Lambda^{-N/2}$.

In order to get a smooth function we have to combine the spectral weight from different iterations and broaden the delta peaks. The set of peaks obtained at iteration

N is added to the spectral weight from the previous iterations in the energy region where the two sets don't overlap, while in the overlapping region the two sets are combined with a linear function as weighting factor.

To obtain a continuous curve the delta peaks are then substituted by smooth gaussian functions on a logarithmic scale:

$$\delta(\omega - \omega_{nm}) \to \frac{e^{-b^2/4}}{b\,\omega_{nm}\,\sqrt{\pi}} \exp\left[-\frac{(\ln\omega - \ln\omega_{nm})^2}{b^2}\right] \tag{2.16}$$

where $\omega_{nm} = E_n - E_m$ and b is a broadening parameter. b must be chosen appropriately: if b is too small the resulting $A(\omega)$ has artificial oscillations due to the discretized nature of the spectrum; if it is too large the features like the Hubbard bands and the Kondo resonance result suppressed. Typical values for b are 0.5 for $\Lambda = 2$ and 0.7 for $\Lambda = 3$.

2.1.3 Observable averages

To gain further information on the properties of the system it is useful to calculate the low temperature average of some impurity quantities like spin or angular momentum in case of complex impurities.

In order to obtain this averages we employed a very simple approach. Instead of calculating step by step the matrix elements of the interesting quantity among the states, as in the case of the spectral function, we used the Hellmann-Feynman theorem that relates the average of a perturbation to the derivative of the ground state energy with respect to the strength of the perturbation itself.

Consider a system with Hamiltonian $H = H_0 + \lambda V$ with ground state energy E, and let $|\psi_0\rangle$ be the ground state of H_0. Then

$$\langle\psi_0|V|\psi_0\rangle \simeq \frac{\partial E}{\partial \lambda}. \tag{2.17}$$

To make use of this property we made some runs with an impurity Hamiltonian containing a term proportional to the operator to be averaged and then numerically differentiate the ground state energy with respect to the corresponding coupling constant. The result proved to be very reliable and effective.

2.2 Conformal field theory

In this Section we want to give just a brief survey of some development of conformal field theory related to impurity problems that will be useful in the analysis of our models, without any claim of being exhaustive due to the vastness of the topic[17, 18, 42, 43, 53–60].

There are two properties common to many impurity problems that allow the application of conformal field theory techniques. The first is that the spectrum of the conduction band is and remains gapless, since a single impurity can not open a bulk gap. Secondly, the problem, even if formulated in d dimensions, can be effectively reduced to a 1-dimensional problem.

These two conditions imply that the physical behavior can be described by a suitable $(1+1)$-conformal field theory. In this representation the role of the coordinates of the two-dimensional plane is played by the time and the space coordinate of the original model, $\vec{r} = (t, x)$, $t \in [-\infty, \infty]$, $x > 0$. The impurity becomes a perturbation acting on the boundary $(t, x = 0)$ of the plane. Since the bulk spectrum has to remain gapless, even in the presence of the impurity, this implies that the latter transforms in the scaling limit, namely at a fixed point, into an effective *conformally invariant boundary condition* which substitutes the one in the absence of impurity. This means that at a fixed point, not only the bulk is conformally invariant, but also the impurity is replaced by a boundary condition that is conformally invariant.

In the simple Kondo model the two fixed points, corresponding to $J_K = 0$ and to $J_K = -\infty$, can be described by two simple boundary conditions. Let us consider a one-dimensional version of the Kondo model in the form of a tight-binding chain with the impurity interacting with the first site in the spirit of Eq. (2.4)

$$H = t \sum_{i=0}^{\infty} \left(c^{\dagger}_{i\sigma} c_{i+1\sigma} + h.c. \right) - J_K \vec{S} \cdot c^{\dagger}_{0\sigma} \frac{\vec{\sigma}}{2} c_{0\sigma}. \tag{2.18}$$

In the limit $J_K \to 0$ the impurity is absent and site 0 is equivalent to all other sites. In the opposite limit $J_K \to -\infty$ the first site is locked to form a singlet with the impurity and the bulk electrons cannot access site 0, hence the system becomes equivalent to a chain with one less site. In both cases the impurity disappears from the description of the fixed point and is replaced by a boundary condition.

In a general impurity problem, the physics in the bulk, far from the impurity, is described by a scale-invariant behavior independent on the boundary condition.

However the critical behavior may still be affected, in a universal way, by the presence of the boundary. Consider, for example, a two-point Green's function: in the limit in which the two points are far from the boundary compared to their relative distance, the behavior is that of the bulk, independent on the boundary; if the relative distance between the points is larger that their distance from the boundary, the critical behavior is influenced by the boundary condition.

In general, to each bulk universality class correspond several boundary universality classes. An arbitrary boundary condition should renormalize to one of these at each fixed point.

Provided the assumption of conformal invariance of the boundary at a fixed point is satisfied, an arbitrary conformal transformation is of the form: $z \to w(z)$ where $z = \tau + ix$, τ being the imaginary time, and $w(z)$ an analytic function. Since this transformation must leave the boundary invariant, its Taylor expansion must be of the form

$$w(z) = \sum_{n=1}^{\infty} a_n z^n \tag{2.19}$$

where the coefficients a_n must be real, contrary to the general bulk case in which the a_n can be complex. This means that of the full conformal group, only "half" remains in the presence of the conformally invariant boundary condition. Nevertheless the number of generators of the conformal group in presence of the boundary is still infinite and the theory is still integrable.

From the real time, Hamiltonian viewpoint, the boundary relates left and right movers, i.e. incoming, $\psi_L \sim e^{-ik(x+vt)}$, and outgoing, $\psi_R \sim e^{ik(x-vt)}$, scattering components, and imposes a constraint on the left and right component of the energy-momentum tensor (T and $\bar{T}$ respectively). This condition can be interpreted as the vanishing of the momentum density at the boundary (no current flowing through the boundary)

$$T(t,0) = \bar{T}(t,0). \tag{2.20}$$

Since T is a function of $t+x$ only and $\bar{T}$ is a function of $t-x$ only, Eq. (2.20) implies that $\bar{T}$ can be interpreted as the analytic continuation of T to the negative x-axis

$$T(t,x) \equiv \bar{T}(t,-x) \qquad \text{for } x < 0. \tag{2.21}$$

Thus we can map the model into one defined in terms of left-movers only but living on the entire real axis. This identification of left and right-movers leads to a

modification of Green's functions near the boundary. Indeed an arbitrary operator O consists of a left and a right component

$$O(t,x) = O_L(t+x)\bar{O}_R(t-x). \tag{2.22}$$

Close to the boundary, where left and right are related, (2.22) becomes

$$O(x) = O_L(x)O_L(-x). \tag{2.23}$$

This is similar to the method of image charges in electrostatics and implies that the operator acquire a non vanishing expectation value near the boundary

$$\langle O(x)\rangle \to \langle O_L(x)O_L(-x)\rangle = \frac{C}{(2ix)^\eta}. \tag{2.24}$$

The presence of the boundary can be in general characterized by the operator product expansion (OPE)

$$O(x) \to O_L(x)O_L(-x) \to \sum_j \frac{C_j}{(2ix)^{\eta_j}} O_j(0) \tag{2.25}$$

where the operators O_j correspond to the left-moving Hilbert space of the bulk primary operators and exponents η_j are the associated scaling dimensions. The dependence on the boundary condition enters only in the OPE coefficients C_j.

To find all the possible conformally invariant boundary conditions of a problem, Cardy[56] developed a general theory that relates boundary conditions to *boundary states*. Consider the system defined on a cylinder of circumference β in the τ (imaginary time) directions and length l in the x (space) direction. Denoting by H^l_{AB} the Hamiltonian for the system with *boundary conditions* A and B at the two ends, the partition function is

$$Z_{AB} = \mathrm{Tr} e^{-\beta H^l_{AB}}. \tag{2.26}$$

On the other hand, making a modular transformation, we can interchange space and time, and interpret l as the time interval and β as the spatial length of the system. Now the system becomes periodic in space and it propagates in time for an interval l between *state* $|B\rangle$ at time 0 and *state* $|A\rangle$ at time l. The Hamiltonian can be denoted by H^β_P, where P stands for periodic, and the partition function transforms into the propagation amplitude from state $|B\rangle$ to state $|A\rangle$ in the time l

$$Z_{AB} = \langle A|e^{-lH^\beta_P}|B\rangle. \tag{2.27}$$

$|A\rangle$ and $|B\rangle$ are called boundary states and are in one-to-one correspondence with boundary conditions.

Let us consider the first, time-periodic, cylindrical configuration with boundary conditions A and B. Given that condition (2.20) must be satisfied at both ends of the cylinder, and that it is possible to identify the right-moving part with the analytic continuation of the left-moving one, the system can be viewed as composed by only left-movers defined periodically on a torus of length $2l$.

To the energy-momentum tensor T are associated the conformal towers. Each conformal tower, generated by the application of the generators of the Virasoro algebra to a highest weight state, is in one-to-one correspondence with a primary field of the theory. The Hilbert space is built up as a sum of conformal towers but, while the conformal towers are independent on the boundary conditions imposed, which conformal towers occur in the spectrum does depend on the boundary conditions.

For each conformal tower in the theory we can define the character

$$\chi_i(q) \equiv \sum_\alpha e^{-\beta E^i_\alpha(2l)} \tag{2.28}$$

where $q = e^{-\pi\beta/l}$ and $E^i_\alpha(2l)$ are the energies in the i-th conformal tower for the system with length $2l$

$$E^i_\alpha(2l) = \frac{\pi}{l}(x^i + n_\alpha) - \frac{\pi c}{24l} \tag{2.29}$$

where x^i is the (left) scaling dimension of the i-th primary operator, n_α is an integer, c is the conformal anomaly and we set the Fermi velocity equal to one.

The partition function can be expanded in terms of the characters

$$Z_{AB} = \sum_i n^i_{AB}\chi_i(q) \tag{2.30}$$

where n^i_{AB} are non-negative integer multiplicities. These numbers represent the spectrum of the system with boundary conditions A and B and all the dependence on the boundary condition is encoded in them.

Let us now focus our attention to the second geometry, where the space-periodic system evolves from boundary state $|A\rangle$ to boundary state $|B\rangle$. These states must satisfy the condition

$$\left[T(x) - \bar{T}(x)\right]|A\rangle = 0 \qquad (\forall x) \tag{2.31}$$

and this condition implies that $|A\rangle$ is a linear combination of Ishibashi states[61, 62]

$$|i\rangle \equiv \sum_{\alpha} |i;\alpha\rangle \otimes \overline{|i;\alpha\rangle} \tag{2.32}$$

where α labels the states in the i-th conformal tower. State $|A\rangle$ may be written as

$$|A\rangle = \sum_{i} |i\rangle\langle i,0|A\rangle \tag{2.33}$$

where i labels the conformal towers and $|i,0\rangle \equiv |i;0\rangle \otimes \overline{|i;0\rangle}$.

Using this expression for the boundary states we can rewrite (2.27) as

$$Z_{AB} = \sum_{i} \langle A|i,0\rangle\langle i,0|B\rangle\langle i|e^{-lH_P^{\beta}}|i\rangle. \tag{2.34}$$

From the definition of the Ishibashi states we have that

$$\langle i|e^{-lH_P^{\beta}}|i\rangle = \sum_{\alpha} e^{-2lE_{\alpha}^{i}(\beta)} = \chi_i(\tilde{q}) \tag{2.35}$$

where E_{α}^{i} is given in (2.29) and $\tilde{q} = e^{-4\pi l/\beta}$.

We can now equate the two expressions (2.30) and (2.34) for the partition function

$$Z_{AB} = \sum_{i} n_{AB}^{i}\chi_i(q) = \sum_{i} \langle A|i,0\rangle\langle i,0|B\rangle\chi_i(\tilde{q}) \tag{2.36}$$

and using the modular transformation of characters

$$\chi_i(q) = \sum_{j} S_i^j \chi_j(\tilde{q}) \tag{2.37}$$

where S_i^j is the modular S-matrix, we obtain a relation between the multiplicities n_{AB}^{i} and the matrix elements $\langle i,0|A\rangle$ of the boundary states

$$\sum_{j} S_j^i n_{AB}^{j} = \langle A|i,0\rangle\langle i,0|B\rangle. \tag{2.38}$$

This relation characterizes the possible boundary conditions of a problem but still does not provide a systematic way to find all of them. Fortunately, there is a construction that allows to generate from a known boundary condition a new boundary condition satisfying (2.38). Given a system with boundary states $|A\rangle$ and $|B\rangle$ with spectrum n_{AB}^{j} and given a primary operator ϕ_i, a new boundary state $|A,i\rangle$ can be

obtained by *fusion* of the state $|A\rangle$ with the operator ϕ_i. The spectrum of the system with the new boundary condition is related to the old one by

$$n^j_{(A,i)B} = N^j_{ik} n^k_{AB} \tag{2.39}$$

where N^j_{ik} are the fusion rule coefficients obtained by the OPE. These coefficients represent the number of times that the primary operator j appears in the OPE of operators i and k, and in the minimal models they can assume only the values 0 or 1. On the other hand the matrix elements of the new boundary states are given by

$$\langle A, i|j, 0\rangle = \frac{S^j_i}{S^j_0}\langle A|j, 0\rangle \tag{2.40}$$

where the index 0 in the modular S-matrix refers to the identity operator.

It is easy to show that the new boundary condition satisfies relation (2.38). Using the Verlinde formula[63] to relate the modular S-matrix to the fusion rule coefficients

$$\sum_j S^k_j N^j_{il} = \frac{S^k_i S^k_l}{S^k_0}, \tag{2.41}$$

we obtain that, with the new boundary condition, the right hand side of (2.38) becomes

$$\langle A, i|k, 0\rangle\langle k, 0|B\rangle = \frac{S^k_i}{S^k_0}\langle A|k, 0\rangle\langle k, 0|B\rangle \tag{2.42}$$

while the left hand side becomes

$$\begin{aligned} \sum_j S^k_j n^j_{(A,i)B} &= \sum_{jl} S^k_j N^j_{il} n^l_{AB} \\ &= \sum_l \frac{S^k_i}{S^k_0} S^k_l n^l_{AB}. \end{aligned} \tag{2.43}$$

This construction suggest that in order to find all the conformally invariant boundary conditions of a model we can start from a known boundary condition and generate all the other conditions by fusion with the primary operators of the model.

In practice, in impurity models one is usually able to find by inspection a simple boundary condition like for instance the one corresponding to free fermions. Then, once the spectrum of that boundary condition is known, all the other conditions can be generated by fusion. The problem is that this procedure does not tell us what is the

new boundary condition generated by the fusion, hence one has to resort to physical intuitions or comparison with other methods to identify the new fixed point.

In general one starts identifying the total symmetry of the bulk system. This will be also the symmetry recovered by the system far from the boundary in presence of the boundary condition. From that symmetry, one extracts those symmetries that will survive after the insertion of the impurity at the boundary and then tries, starting from some simple boundary condition, to "guess" what is the effect of fusion with the various operators.

A simple example is the ordinary Kondo model. In that case the symmetries are the $SU(2)$ associated with the spin and the $U(1)$ corresponding to the charge. Starting from free boundary conditions on conduction electrons, corresponding to a non interacting impurity, we want to obtain the strong coupling fixed point. Since the Kondo interaction involves only the spin degrees of freedom it is obvious to "guess" that the fusion must be done with an operator in the spin sector of the theory. Indeed, fusion with the operator corresponding to the spin of the impurity generates the spectrum of free fermions with a $\pi/2$ phase shift corresponding to the strong coupling fixed point.

2.2.1 Finite size spectrum and operator content

The bridge between CFT and NRG analysis is provided by the finite size spectrum. As we saw in the previous Section, NRG produces the energy spectrum of the lowest energy levels and the same quantity can be calculated by CFT. Indeed in the CFT description there is a relation between finite-size spectrum and scaling dimensions of operators. The energy of the i-th highest weight state is given by

$$E_i = \frac{\pi}{l} x^i \tag{2.44}$$

where l is the length of the system, x^i is the scaling dimension of the field and we omitted the term containing the conformal anomaly that depends on the geometry. The other states in the i-th conformal tower differ in energy form the highest weight state for integer multiples of π/l.

Suppose that the multiplicities n^i_{ff} of some trivial boundary condition f are known. These multiplicities tell us which conformal towers are present in the spectrum and hence determine completely the spectrum itself with that boundary condition. If we now obtain a new boundary condition A by fusion with operator a, the spectrum of

the new system is encoded in the multiplicities n^i_{Af} determined through the fusion rules of operators i with operator a.

At the same time it is also possible to extract the operator content of the theory with a definite boundary condition simply by "double fusion". It can be shown that the operator content of the system in the semi-infinite plane geometry in presence of boundary condition A is related to the finite size spectrum on a strip with boundary condition A on both sides. Thus the allowed operators in presence of boundary condition A can be obtained by the operators in presence of boundary condition f fusing with operator a twice.

2.2.2 Scattering matrix

In the presence of a boundary condition, as we have seen previously, the left and right components of the fields are no more independent.

For instance in the free fermion case the Green's function $\langle \psi^\dagger_L(z_1)\psi_R(\bar{z}_2)\rangle$ is zero in the bulk while close to the boundary it becomes

$$\langle \psi^\dagger_L(z_1)\psi_R(\bar{z}_2)\rangle = \frac{e^{i2\delta}}{z_1 - \bar{z}_2} \tag{2.45}$$

where δ is a phase shift and depends on the boundary conditions imposed to the free fermions: $\psi_R(z) = e^{i2\delta}\psi_L(z)$.

For an arbitrary conformally invariant boundary condition, (2.45) can be written

$$\langle \psi^\dagger_L(z_1)\psi_R(\bar{z}_2)\rangle = \frac{S_{(1)}}{z_1 - \bar{z}_2} \tag{2.46}$$

where $S_{(1)}$ is a complex number that depends on the boundary condition and represent the scattering matrix S at zero energy restricted to the single-particle subspace.

If Fermi liquid theory holds, then $|S_{(1)}| = 1$, meaning that on the Fermi surface multi-particle scattering vanish. In general $|S_{(1)}| \leq 1$. In particular an absolute value of $S_{(1)}$ smaller than one implies that the fixed point has non-Fermi liquid character.

In CFT the value of $S_{(1)}$ in presence of a boundary condition A can be calculated by the general relation

$$\langle \phi^i_L(z_1)\bar{\phi}^i_R(\bar{z}_2)\rangle = \frac{\langle i, 0|A\rangle}{\langle I, 0|A\rangle}\frac{1}{(z_1 - \bar{z}_2)^{2x_i}} \tag{2.47}$$

where ϕ^i is a primary field with scaling dimension x_i and I is the identity operator.

Suppose that the primary field ϕ is the electron operator, and f denotes its quantum numbers, then in the presence of trivial free fermion boundary conditions $|F\rangle$ we have the relation

$$S_{(1)} = 1 = \langle f, 0|F\rangle / \langle I, 0|F\rangle. \tag{2.48}$$

If we now obtain a new boundary condition $|A\rangle$ by fusion with operator ϕ^a, $S_{(1)}$ with the new boundary condition is given by

$$S_{(1)} = \frac{\langle f, 0|A\rangle / \langle f, 0|F\rangle}{\langle I, 0|A\rangle / \langle I, 0|F\rangle}. \tag{2.49}$$

These matrix elements can be calculated using the relations (2.38), (2.39) and (2.41). Indeed we have

$$\sum_j S_j^f n_{FA}^j = \langle F|f, 0\rangle\langle f, 0|A\rangle \tag{2.50}$$

where S_j^f is the modular S-matrix and should not be confused with the *scattering* S matrix of which $S_{(1)}$ is the single-particle component. We now substitute the relation

$$n_{FA}^j = N_{ak}^j n_{FF}^k \tag{2.51}$$

into (2.50) to obtain

$$\sum_j S_j^f N_{ak}^j n_{FF}^k = \langle F|f, 0\rangle\langle f, 0|A\rangle. \tag{2.52}$$

Then we use (2.41) to arrive at the expression

$$(S_a^f / S_0^f) \sum_j S_k^f n_{FF}^k = \langle F|f, 0\rangle\langle f, 0|A\rangle. \tag{2.53}$$

Since

$$\sum_j S_k^f n_{FF}^k = \langle F|f, 0\rangle\langle f, 0|F\rangle, \tag{2.54}$$

the final simplification gives

$$\langle f, 0|A\rangle / \langle f, 0|F\rangle = S_a^f / S_0^f \tag{2.55}$$

and the expression for the scattering matrix $S_{(1)}$ becomes

$$S_{(1)} = \frac{S_a^f / S_0^f}{S_a^0 / S_0^0}. \tag{2.56}$$

These relations allow the calculation of the scattering matrix for an arbitrary boundary condition obtained by fusion from the free fermion boundary condition, requiring only the knowledge of the modular S-matrix of the theory.

The scattering matrix can then be related, using Fermi liquid theory, to some properties of the spectral function of the impurity as we will see in the next Chapters.

2.2.3 Ground state degeneracy

The ground state degeneracy is a universal property of one-dimensional critical quantum systems that depends only on the universality class of the boundary conditions. It can be defined through the zero temperature residual entropy:

$$S(0) = \ln g \tag{2.57}$$

and in general depends on the boundaries of the system: $g = g_A g_B$.

For periodic (free fermion) boundary conditions g must be equal to one since there is no boundary. In general g can be non-integer.

To calculate g we can use the partition function. Indeed if we consider the geometry in which the system is periodic in space and evolves between boundary states $|A\rangle$ and $|B\rangle$, we have that in the limit $l/\beta \to 0$ Eq.(2.27) reduces to

$$Z_{AB} = \langle A|0\rangle\langle 0|B\rangle = g_A g_B. \tag{2.58}$$

Using Eq.(2.38) in the same limit we have

$$g_A g_B = \sum_j S_j^0 n_{AB}^j. \tag{2.59}$$

Suppose now that we want to calculate the ground state degeneracy for a boundary condition A that is obtained from free fermion boundary conditions F by fusion with the primary operator a. First of all we must recall that

$$g_F^2 = 1 = \sum_i n_{FF}^i S_i^0. \tag{2.60}$$

Then using Eq.(2.39), the Verlinde formula Eq.(2.41), and Eq.(2.60), we have that

$$g_A g_F = \sum_i n_{AF}^i S_i^0 \tag{2.61}$$

$$= \sum_{ij} N^i_{ja} n^j_{FF} S^0_i \tag{2.62}$$

$$= \frac{S^0_a}{S^0_0} \sum_j S^0_j n^j_{FF} = \frac{S^0_a}{S^0_0}. \tag{2.63}$$

The ground state degeneracy is found to decrease under renormalization group flow of the system from a less stable to a more stable critical point[59].

Chapter 3

Two-orbital model

In this Chapter we study a two-orbital Anderson impurity model that presents a non-Fermi liquid unstable fixed point similar to the two-impurity Kondo model one. The peculiarity of this particular model is the presence of inverted Hund's rules, fundamental ingredient to provide the competition between the Kondo effect and a multiplet splitting.

We pursue the analysis of this AIM by uncovering the spectral behavior across the non-Fermi liquid fixed point. This is not only interesting for the AIM itself, being one of the few cases where non-Fermi liquid dynamical properties may be accessed, but also in the context of the DMFT mapping. The model is also sufficiently simple to allow for an analytical description of the spectral function which reproduces well the numerical results and provide new physical insight. Actually our model spectral function has been quite useful in guiding the analysis of the DMFT solution presented in Ref. [24].

3.1 The Model Hamiltonian

The AIM Hamiltonian we consider is

$$\begin{aligned} H &= H_U + H_J + H_c + H_{hyb} \\ &= \frac{U}{2}\left(n_d - 2 + \nu\right)^2 + 2J\left[\left(T^x\right)^2 + \left(T^y\right)^2\right] \\ &\quad + \sum_{\mathbf{k}a\alpha} \epsilon_{\mathbf{k}}\, c^\dagger_{\mathbf{k}a\alpha} c_{\mathbf{k}a\alpha} + \sum_{\mathbf{k}a\alpha} V_d \left(c^\dagger_{\mathbf{k}a\alpha} d_{a\alpha} + d^\dagger_{a\alpha} c_{\mathbf{k}a\alpha}\right). \end{aligned} \tag{3.1}$$

Here $c^\dagger_{\mathbf{k}a\alpha}$ creates a conduction electron in the band $a = 1, 2$ with momentum $\mathbf{k}$, spin α and energy $\epsilon_{\mathbf{k}}$, measured with respect to the chemical potential. $d^\dagger_{a\alpha}$ is the creation operator of an electron with spin α in the impurity orbital $a = 1, 2$, while $n_d = \sum_{a\alpha} d^\dagger_{a\alpha} d_{a\alpha}$ is the impurity occupation number. We have defined the orbital pseudo-spin operators

$$T^i = \frac{1}{2} \sum_\alpha \sum_{a=1,2} d^\dagger_{a\alpha} \tau^i_{ab} d_{b\alpha}, \tag{3.2}$$

where $i = x, y, z$ and τ^i's are the Pauli matrices in the orbital space.

We further assume that the conduction band density of states is symmetric with respect to the chemical potential, set equal to zero, so that the behavior of the Hamiltonian under a particle-hole symmetry transformation is controlled by the parameter ν in (3.1). For the time being we will take $\nu = 0$, which implies that the Hamiltonian is particle-hole symmetric. Afterwards we will release this constraint.

The model without the impurity exchange coupling J is $SU(4)$ invariant. A finite J lowers the $SU(4)$ symmetry down to $SU(2)_{spin} \times O(2)_{orbit}$. In this case the total charge, the total spin and the total z-component of the pseudospin are the only conserved quantities.

It is convenient to start our analysis by the spectrum of the isolated impurity, $V_d = 0$. In this case the impurity eigenstates, $|n, S, S^z, T, T^z\rangle$, can be labeled by the occupation number n, the spin S, pseudospin T and their z-components, S^z and T^z, respectively, with energies

$$E(n, S, S^z, T, T^z) = \frac{U}{2}(n-2)^2 + 2J\left[T(T+1) - (T^z)^2\right]. \tag{3.3}$$

We assume $U \gg |J|$, so that the impurity ground state with $\nu = 0$ has $n = 2$. In this case the only configurations allowed by Pauli principle are a spin-triplet pseudo-spin-singlet, $S = 1$ and $T = 0$,

$$\begin{aligned} |2, 1, +1, 0, 0\rangle &= d^\dagger_{1\uparrow} d^\dagger_{2\uparrow} |0\rangle, \\ |2, 1, 0, 0, 0\rangle &= \tfrac{1}{\sqrt{2}} \left(d^\dagger_{1\uparrow} d^\dagger_{2\downarrow} - d^\dagger_{2\uparrow} d^\dagger_{1\downarrow} \right) |0\rangle, \\ |2, 1, -1, 0, 0\rangle &= d^\dagger_{1\downarrow} d^\dagger_{2\downarrow} |0\rangle, \end{aligned} \tag{3.4}$$

and a spin-singlet pseudo-spin-triplet, $S = 0$ and $T = 1$. The latter is split by J into a singlet with $T^z = 0$,

$$|2, 0, 0, 1, 0\rangle = \frac{1}{\sqrt{2}} \left(d^\dagger_{1\uparrow} d^\dagger_{2\downarrow} + d^\dagger_{2\uparrow} d^\dagger_{1\downarrow} \right) |0\rangle, \tag{3.5}$$

and a doublet with $T^z = \pm 1$,

$$\begin{aligned} |2,0,0,1,+1\rangle &= d^\dagger_{1\uparrow} d^\dagger_{1\downarrow} |0\rangle, \\ |2,0,0,1,-1\rangle &= d^\dagger_{2\uparrow} d^\dagger_{2\downarrow} |0\rangle. \end{aligned} \tag{3.6}$$

If $J > 0$, the lowest energy configuration is the spin-triplet, $S = 1$ and $T = 0$, which corresponds to the conventional Hund's rules. On the contrary, for $J < 0$, the isolated impurity ground state is the singlet (3.5) with quantum numbers $S = 0$, $T = 1$ and $T^z = 0$.

A finite hybridization, $V_d \neq 0$, induces valence fluctuations within the impurity, which are controlled by the energy scale (hybridization width)

$$\Delta_0 = \pi \, V_d^2 \, \rho_c, \tag{3.7}$$

with ρ_c the conduction electron density of states (DOS) at the chemical potential per spin and band. These fluctuations are suppressed by a strong repulsion $U \gg \Delta_0$, which we assume throughout this work. Although all our calculations refer to the AIM (3.1), it is more insightful to discuss some physical properties in terms of the effective Kondo model which describes the low-energy behavior when $U \gg \Delta_0$:

$$H_{eff} = H_J + H_c + H_K, \tag{3.8}$$

where H_J and H_c have been defined in (3.1) and the Kondo exchange

$$H_K = J_K \left[\vec{S} \cdot \vec{\mathcal{S}} + \vec{T} \cdot \vec{\mathcal{T}} + 4 \sum_{i,j=x,y,z} W_{ij} \, \mathcal{W}_{ij} \right], \tag{3.9}$$

with

$$J_K = 2V_d^2/U. \tag{3.10}$$

Here $\vec{S}$, defined by

$$\vec{S} = \frac{1}{2} \sum_a \sum_{\alpha\beta} d^\dagger_{a\alpha} \, \vec{\sigma}_{\alpha\beta} \, d_{a\beta},$$

$\vec{T}$, which we introduced in Eq. (3.2), and W_{ij},

$$W_{ij} = \frac{1}{4} \sum_{ab} \sum_{\alpha\beta} d^\dagger_{a\alpha} \, \tau^i_{ab} \, \sigma^j_{\alpha\beta} \, d_{b\beta},$$

are impurity spin, pseudo-spin and spin-orbital operators, respectively, while $\vec{\mathcal{S}}$, $\vec{\mathcal{T}}$ and $\mathcal{W}_{ij}$ are the corresponding conduction electron density operators at the impurity

site. The impurity operators in (3.9) act only in the subspace with two electrons occupying the d-orbitals, which, as we showed, includes six states. The Kondo model (3.8) contains two competing mechanisms which tend to freeze the left-over impurity degrees of freedom: (*i*) the Kondo exchange, with its associated energy scale, the Kondo temperature T_K; (*ii*) the intra-impurity exchange splitting J. As we already mentioned, the Kondo exchange (3.9) gains energy by letting the impurity tunnel coherently among all available six configurations, but it is hampered by J which instead tends to trap the impurity into a well defined state.

If $J \gg T_K > 0$, the positive exchange splitting dominates and the impurity is essentially frozen into the lowest energy spin-triplet configuration. The Kondo exchange projected onto the triplet sub-space (3.4) is simply $H_K = J_K \vec{S}\cdot\vec{\mathcal{S}}$, describing a standard $S = 1$ two-channel Kondo model. This is known to be perfectly screened at low energy[13, 53], yielding a scattering phase shift $\delta = \pi/2$ in each spin and orbital channel.

On the contrary, if $J \ll -T_K < 0$, the impurity gets trapped into the $S = 0$, $T = 1$ and $T^z = 0$ configuration, Eq. (3.5). Since (3.5) is non degenerate, the Kondo exchange is ineffective, so that asymptotically the impurity decouples from the conduction bath. This implies a low energy phase shift $\delta = 0$. The main question which we want to address is how the model moves across the two limiting cases.

It is easy to recognize in this behavior a parallel with the two $S = 1/2$ impurity Kondo model (2IKM) in the presence of a direct exchange between the impurity spins[14–18]. In that case, if the two spins are strongly ferromagnetically coupled, the model reduces to an $S = 1$ two-channel Kondo model, while, if they are strongly antiferromagnetically coupled, the two spins bind together into a singlet and decouple from the conduction electrons, exactly as in our model. The two channels correspond in the 2IKM to the symmetric and antisymmetric combinations of the even and odd scattering channels with respect to the midpoint between the impurities. It was demonstrated by Ref. [18] that, provided a peculiar particle-hole symmetry holds, the non-Fermi liquid unstable fixed point (UFP) found by Ref. [14–16] separates the Kondo screened and unscreened regimes. In particular it was shown that while a particle-hole symmetry breaking term

$$\delta H_{p-h} = -\mu_d \sum_{a\alpha} d^\dagger_{a\alpha} d_{a\alpha} - \sum_{\mathbf{k},a\alpha} \mu_{\mathbf{k}}\, c^\dagger_{\mathbf{k}a\alpha} c_{\mathbf{k}a\alpha}, \tag{3.11}$$

does not wash out the UFP, the latter is instead destabilized by the perturbation

$$\begin{aligned}\delta H_{rel} = -h_d \sum_{\alpha} d^{\dagger}_{1\alpha} d_{2\alpha} + H.c. \\ - \sum_{\mathbf{k},\alpha} h_{\mathbf{k}}\, c^{\dagger}_{\mathbf{k}1\alpha} c_{\mathbf{k}2\alpha} + H.c.\,. \end{aligned} \tag{3.12}$$

Translated into our two-orbital language, the dangerous symmetry which needs to be preserved is just the $O(2)_{orbit}$ orbital symmetry. Therefore, unlike in the 2IKM, where the two scattering channels are generically non degenerate, in our case the instability towards $O(2)_{orbit}$ symmetry breaking does correspond to a physical instability. Hence, if orbital symmetry is unbroken, we do expect to find an UFP in our model, with similar properties as in the 2IKM. We notice that, in spite of the analogies, our model has a larger impurity Hilbert space than the 2IKM. In fact the $S = 0$, $T = 1$ and $T^z = \pm 1$ doublet of Eq. (3.6) is absent in the 2IKM, where it would correspond to doubly occupied impurities (the labels 1 and 2 for the d-orbitals translate in the 2IKM into the two one-orbital impurities). Yet we can perturb our Hamiltonian by adding to H of (3.1) the term

$$H_G = G\ (T^z)^2\,, \tag{3.13}$$

with $G > 0$, which raises the energy of the doublet. If $G \gg T_K$, the doublet effectively decouples from the low energy sector, and our model should become equivalent to the 2IKM. In Section 3.2 we show that indeed by increasing G our UFP smoothly transforms into the 2IKM one.

3.2 NRG analysis

We restrict our analysis to large values of U, where valence fluctuations on the impurity are substantially suppressed. Here, as we discussed, the AIM effectively behaves like the Kondo model (3.8). We fix both U and Δ_0 and span the phase space by varying the exchange parameter J.

Following Section 2.1 we introduce the log-discretized Hamiltonian H_N of the system made up with the impurity and $N + 1$ sites:

$$H_N \;=\; \Lambda^{(N-1)/2} \left\{ \sum_{n=0}^{N-1} \Lambda^{-n/2} \xi_n \left(f^{\dagger}_{na\alpha} f_{(n+1)a\alpha} + f^{\dagger}_{(n+1)a\alpha} f_{na\alpha} \right) \right.$$

$$+\tilde{\Delta}_0^{1/2}\left(f_{0a\alpha}^{\dagger}d_{a\alpha}+d_{a\alpha}^{\dagger}f_{0a\alpha}\right)$$
$$+\frac{\tilde{U}}{2}\left(n_d-2+\nu\right)^2+2\tilde{J}\left[\left(T^x\right)^2+\left(T^y\right)^2\right]\Bigg\}. \tag{3.14}$$

Here $\tilde{U}=C_\Lambda\,U$, $\tilde{J}=C_\Lambda\,J$, $\tilde{\Delta}_0=C_\Lambda^2\,\frac{2\Delta_0}{\pi}$, see (3.7), where $C_\Lambda=\left(\frac{2\Lambda}{1+\Lambda}\right)$ and all energies are measured in units of half the conduction bandwidth. ν for the time being is set to 0.

The symmetries exploited in the calculations correspond to the group $U(1)_{charge}\times SU(2)_{spin}\times U(1)_{orbit}$. The three conserved quantities are the charge Q, corresponding to half the deviation of the number of particles from the half-filled condition, the magnitude of the spin S and the z-component of the orbital momentum T_z. The reason to define the charge in this way is that it can be seen as the z-component of a vector. In some impurity problems this vector, called hypercharge, is a conserved quantity and in general in CFT approach this symmetry can be used as a building block to decompose the symmetry group of the bulk system.

3.2.1 Phase diagram

First of all we identify the fixed points by analyzing the low energy spectra (with N typically up to one hundred). Since the conventional size-dependence of the level spacing is absorbed by the factor $\Lambda^{(N-1)/2}$ in front of (3.14), the low-lying energy levels flow to constant values whenever the model is close to a fixed point. Fig. 3.1 shows that there are two different asymptotic regimes separated by a critical value $J^*<0$. In order to facilitate the interpretation of that figure, we recall that the ground state of a particle-hole symmetric free-chain with $N+1$ sites is unique if N is odd and degenerate if N is even.

For $J>J^*$ the low energy spectrum of a chain with *even* number, $N+1$, of sites flows towards that of a free chain with an *odd* number of sites and viceversa. This is evident in the right panel of Fig. 3.1 where the ground state of the chain with odd N (even number of sites) becomes asymptotically degenerate as for a chain with even N (odd number of sites). Apart from the ground state degeneracy, also the low-lying spectrum, i.e. degeneracy and quantum numbers of the levels as well as the level spacings, coincides with that of a free chain. As usual, this is as if the first site of the chain were locked to form a spin and orbital singlet with the impurity, hence

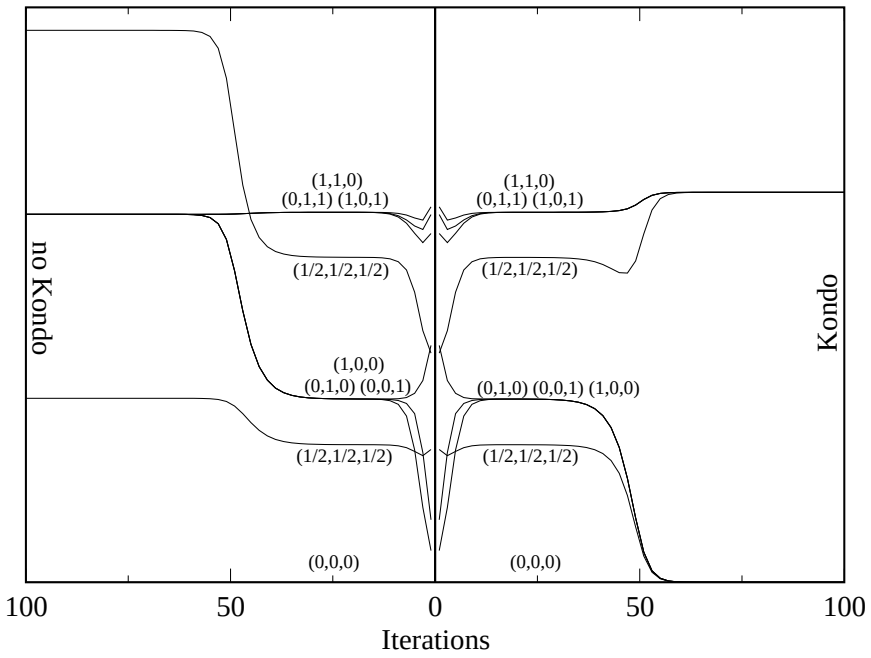

Figure 3.1: Lowest energy levels versus the chain size N. The left/right panels correspond to a deviation $\delta J/J^* = \pm 4 \cdot 10^{-3}$ from the fixed point value J^*. The levels are labeled by the quantum numbers (Q, T^z, S). [$\Lambda = 3$, $J = -0.05057425$ (left) -0.05057375 (right), $J_K = 0.05$]

becoming inaccessible to the conduction electrons which thus acquire a $\pi/2$ phase shift per spin and conduction channel. It is a conventional Kondo screened phase.

For $J < J^*$ the situation is reversed: the low energy spectrum of an odd (even) chain flows to that of an odd (even) free chain. Indeed, as shown in the left panel of Fig. 3.1, the ground state with N odd remains non-degenerate for large N. This case corresponds to an unscreened phase with the impurity asymptotically decoupled from the conduction bath. The phase shift is consequently $\delta = 0$.

In between the Kondo screened and unscreened phases we do find a non-trivial fixed point, as it is visible in the intermediate cross-over region of the spectrum, see Fig. 3.1. The peculiar non-Fermi liquid character of this intermediate coupling unstable fixed point (UFP) is clear by the non-uniform spacing of the low energy levels. A careful analysis of the UFP spectrum reveals that it is just the same as that one found in the particle-hole-symmetric 2IKM[18]. In Table 3.1 we compare the energies E of

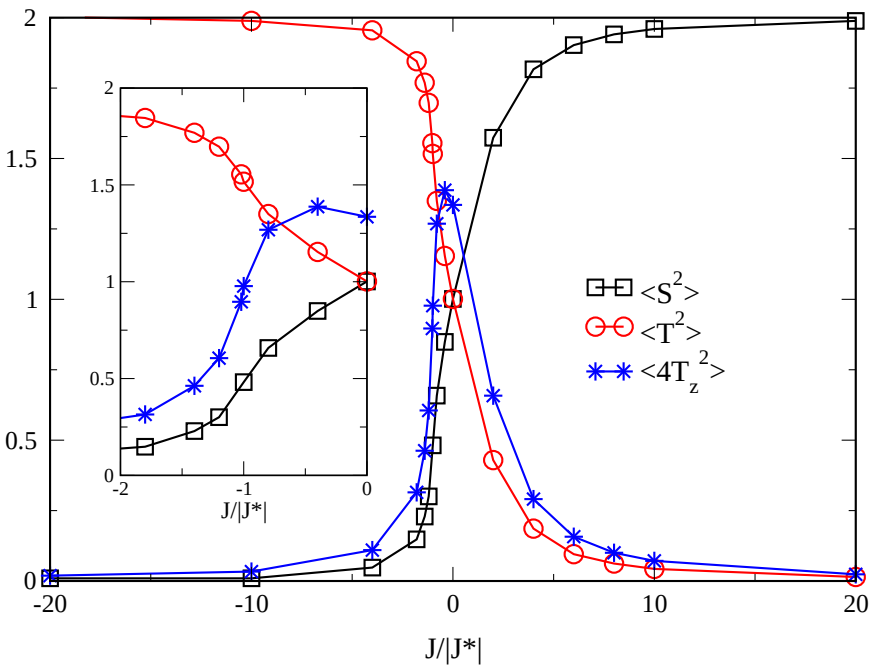

Figure 3.2: Average impurity quantum numbers as function of $J/|J^*|$. In the inset the behavior around the UFP is shown in detail. Notice that the average of $(T^z)^2$ is multiplied by 4 to make it more visible. [$\Lambda = 3$, $J_K = 0.05$]

the lowest-lying levels of the Wilson chain at the UFP, as obtained by NRG, with the prediction x of Conformal Field Theory for the 2IKM[18]. The agreement is a clear evidence that the UFP is indeed the same in both models.

3.2.2 Calculation of $\langle \vec{S}^2 \rangle$, $\langle \vec{T}^2 \rangle$ and $\langle T_z^2 \rangle$ and interpretation in terms of density matrix

Additional information are provided by the average values of the impurity spin, $\langle \vec{S}^2 \rangle$, pseudospin, $\langle \vec{T}^2 \rangle$, and its z-component, $\langle (T^z)^2 \rangle$.

These quantities are shown in Figure 3.2. For large positive J the impurity freezes into the $S = 1$ $T = 0$ configuration, while for J negative and large the preferred configuration is the singlet with $T = 1$ $T^z = 0$. At the $SU(4)$-symmetric point $J = 0$ where spin and pseudospin are equivalent the averages mirror this additional degeneracy being $\langle \vec{S}^2 \rangle = \langle \vec{T}^2 \rangle = 1$. Eventually at the UFP the values are $\langle \vec{S}^2 \rangle = 1/2$,

Table 3.1: Energies E of the low energy levels and their degeneracy Deg at the unstable fixed point. The levels are labeled by the quantum numbers Q, half of the deviation of the number of electrons with respect to the half filled state, S, total spin, and T^z, total z-component of the pseudo-spin. The value x is the prediction of Conformal Field Theory for the two-impurity Kondo model[18]. Notice the anomaly of the member within the $(1/2, 1/2, 1/2)$ multiplets identified by a *, which was also found in Ref. [18]. There an explanation for the discrepancy was proposed.

Q	T^z	S	x	E	Deg
0	0	0	0	0.00000	1
$\frac{1}{2}$	$\frac{1}{2}$	$\frac{1}{2}$	$\frac{3}{8}$	0.37260	8
0	0	1	$\frac{1}{2}$	0.49615	3
0	1	0	$\frac{1}{2}$	0.49583	2
1	0	0	$\frac{1}{2}$	0.49631	2
$\frac{1}{2}$	$\frac{1}{2}$	$\frac{1}{2}$	$\frac{7}{8}$	0.88021	8
0	0	0	1	0.99714	1
				1.00216	1
				1.00311	1
0	0	1	1	1.00279	3
0	1	1	1	1.00248	6
1	0	1	1	1.00295	6
1	1	0	1	1.00264	4
$\frac{1}{2}$	$\frac{1}{2}$	$\frac{1}{2}$	$1+\frac{3}{8}$	1.38880	8
				1.38945	8
				1.51556*	8
$\frac{1}{2}$	$\frac{1}{2}$	$\frac{3}{2}$	$1+\frac{3}{8}$	1.38924	16
$\frac{1}{2}$	$\frac{3}{2}$	$\frac{1}{2}$	$1+\frac{3}{8}$	1.38859	8
$\frac{3}{2}$	$\frac{1}{2}$	$\frac{1}{2}$	$1+\frac{3}{8}$	1.38957	8
0	0	0	$1+\frac{1}{2}$	1.55944	1
0	0	1	$1+\frac{1}{2}$	1.50195	3
				1.55863	3
				1.55983	3
				1.60582	3
0	1	0	$1+\frac{1}{2}$	1.50141	2
				1.55943	2
				1.60467	2
0	1	1	$1+\frac{1}{2}$	1.55904	6
1	0	0	$1+\frac{1}{2}$	1.50222	2
				1.55883	2
				1.60636	2
1	0	1	$1+\frac{1}{2}$	1.55964	6
1	1	1	$1+\frac{1}{2}$	1.55923	12

$\langle \vec{T}^2 \rangle = 3/2$ and $\langle T_z^2 \rangle = 1/4$.

It is possible to give an interpretation of these results in terms of the impurity density matrix. By symmetry, the impurity density matrix is diagonal in the six two-electron configurations. The diagonal elements represent the occupation probabilities $P(S, S^z, T, T^z)$ of states with quantum numbers S, S^z, T and T^z. In the large U-limit, where impurity configurations with $n \neq 2$ have negligible weight, we can write

$$\begin{aligned} P(0,0,1,0) &= \cos^2\theta, \\ P(0,0,1,+1) &= P(0,0,1,-1) = \tfrac{1}{2}\sin^2\theta\,\sin^2\phi, \\ P(1,+1,0,0) &= P(1,0,0,0) = P(1,-1,0,0) = \tfrac{1}{3}\sin^2\theta\,\cos^2\phi, \end{aligned} \tag{3.15}$$

from which we derive that

$$\begin{aligned} \langle \vec{S}^2 \rangle &= 2\sin^2\theta\,\cos^2\phi, \\ \langle \vec{T}^2 \rangle &= 2\left(\cos^2\theta + \sin^2\theta\,\sin^2\phi\right), \\ \langle (T^z)^2 \rangle &= \sin^2\theta\,\sin^2\phi. \end{aligned} \tag{3.16}$$

In Fig. 3.3 we plot the angles θ and ϕ as obtained through (3.16) by the average values calculated numerically. The UFP is characterized by $\theta = \phi = \pi/4$, namely by the value 1/2 of the occupation probability of the singlet state (3.5). The precise value of the other occupation probabilities, in other words of ϕ, are instead not relevant, apart from the obvious fact that their sum should be 1/2 too. In fact, if we add the term (3.13) with $G > 0$, we do find the same UFP, which locations now depends also on G, which is still identified by $P(0,0,1,0) = 1/2$, *i.e.* $\theta = \pi/4$, although the weight of the spin-triplet is enhanced with respect to the doublet (3.6), $\phi < \pi/4$. For large G we do recover the 2IKM values $\theta = \pi/4$ and $\phi = 0$, see Fig. 3.4. This represents another confirmation of the fact that the two UFP's are indeed the same.

3.2.3 Fermi liquid effective Hamiltonian description

As we said the low energy spectrum both in the Kondo screened and unscreened phases flows to that of free chains, with one less site in the former case. Hence in both cases the low energy stable fixed point Hamiltonian is very simple and allows for a Fermi liquid description.

In the Kondo phase the fixed point Hamiltonian

$$H_N^* = \Lambda^{(N-1)/2} \sum_{n=1}^{N-1} \Lambda^{-n/2} \xi_n \left(f_{na\alpha}^\dagger f_{(n+1)a\alpha} + f_{(n+1)a\alpha}^\dagger f_{na\alpha} \right) \tag{3.17}$$

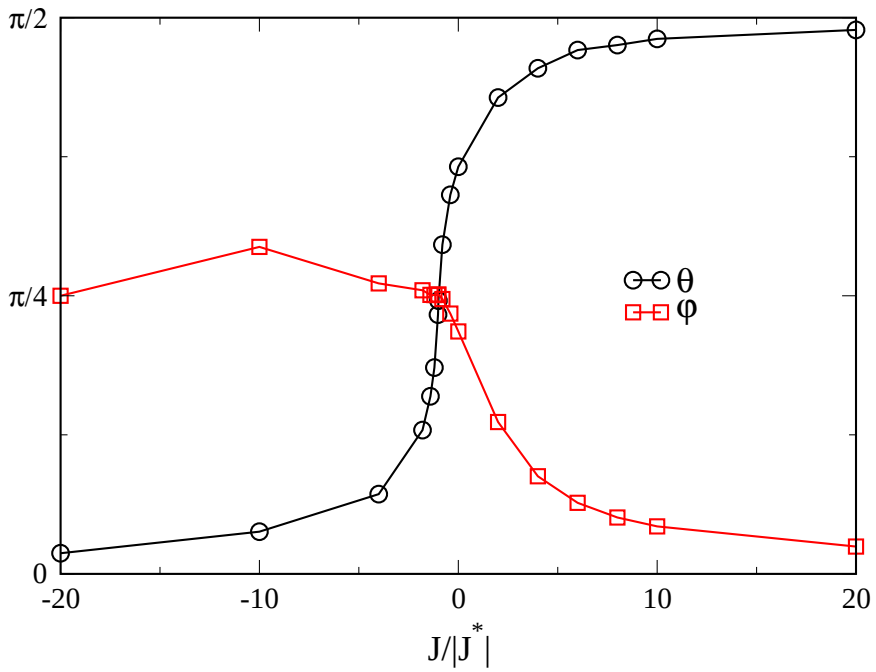

Figure 3.3: The angles θ and ϕ as defined through Eq. (3.16). Notice that the fixed point is identified by $\theta = \phi = \pi/4$. [$\Lambda = 3$, $J_K = 0.05$]

is that of two decoupled non-interacting chains with site 0 removed from both; in the unscreened phase the fixed point Hamiltonian

$$H_N^* = \Lambda^{(N-1)/2} \sum_{n=0}^{N-1} \Lambda^{-n/2} \xi_n \left(f_{na\alpha}^\dagger f_{(n+1)a\alpha} + f_{(n+1)a\alpha}^\dagger f_{na\alpha} \right) \tag{3.18}$$

is that of two decoupled non-interacting chains with all the original sites, being this the only difference with the previous case. Due to this similarity it is possible to use the same description for the odd-N fixed point in the Kondo phase and for the even-N one in the unscreened phase (and viceversa).

As seen in Section 2.1.1, the flow towards the asymptotic spectrum can be described by the fixed point Hamiltonian (free chains) plus a term containing the most relevant operators allowed by the symmetries of the problem. In this particular case the most relevant operators can be at most marginally irrelevant in the renormalization group sense, being both fixed points stable. In reality they are irrelevant and in particular they amount to local perturbation terms[35, 36] acting on the first available

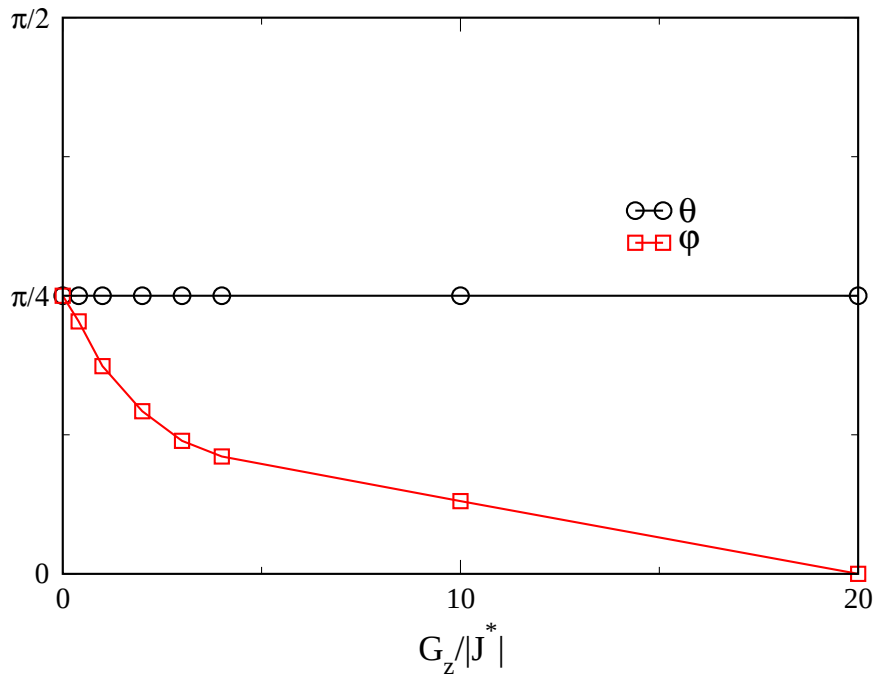

Figure 3.4: The UFP values of θ and ϕ along the path parameterized by the coupling G from our to the 2IKM model. [$\Lambda = 3$, $J_K = 0.05$]

site, denoted as site 0, of the conduction chain, which is actually the second site in the Kondo screened phase.

The most general possible local term allowed by the symmetry can be written as

$$\begin{aligned}\delta H &= -t_* \sum_{a\alpha} \left(f^\dagger_{0a\alpha} f_{1a\alpha} + H.c. \right) + \frac{U_*}{2} \left(n_0 - 2 \right)^2 \\ &\quad + J_{S*} \vec{\mathcal{S}}_0 \cdot \vec{\mathcal{S}}_0 + J_{T*} \vec{\mathcal{T}}_0 \cdot \vec{\mathcal{T}}_0 - 2 \left(J_{S*} + J_{T*} \right) \left(\mathcal{T}^z_0 \right)^2 . \end{aligned} \tag{3.19}$$

We choose this particular form because it has the advantage that the energy of the center of gravity of each multiplet with given number of particles n_0 is just $U_*(n_0 - 2)^2/2$.

In principle there are infinitely many other terms allowed by symmetry, but, as we will see, they are less relevant than these.

Let us concentrate on the odd-N fixed point in the Kondo phase. The Hamiltonian (3.17) can be easily diagonalized numerically to obtain a set of eigenvalues and eigenvectors. Due to particle-hole symmetry the spectrum is symmetric with respect

to the Fermi energy and, since both chains have now an odd number of sites there are two eigenvalues equal to zero. Thus the ground state of the fixed point Hamiltonian is 16-fold degenerate.

In the large-N limit the lowest eigenvalues converge to limiting values that depend on Λ. For instance for $\Lambda = 2$ these values are:

$$\begin{array}{cc} \text{Eigenvalue} & \text{Associated operators} \\ \hat{\eta}_0 = 0 & g^\dagger_{0a\alpha} \\ \hat{\eta}_1 = 1.2963854 & g^\dagger_{1a\alpha}, h^\dagger_{1a\alpha} \\ \hat{\eta}_2 = 2.8259658 & g^\dagger_{2a\alpha}, h^\dagger_{2a\alpha} \\ \hat{\eta}_3 = 5.6568515 & g^\dagger_{3a\alpha}, h^\dagger_{3a\alpha} \end{array} \tag{3.20}$$

where operators $g^\dagger_{ia\alpha}$ create particles in orbital a with spin α while $h^\dagger_{ia\alpha}$ create holes (annihilate particles) in orbital a with spin α.

The strategy now is to express the operators in (3.19) in terms of the eigenvectors of the fixed point Hamiltonian g_i, h_i and calculate to first order in perturbation theory the change in energy due to such terms. The discrepancy between any finite-N spectrum and that of the fixed point can then be fitted using (3.19) with suitable parameters. This procedure gives the values for the effective couplings U_*, t_*, J_{S*} and J_{T*} that in turn will allow us to extract the Wilson ratios and scattering amplitudes.

A subtlety arises at this point: due to the error introduced by the truncation procedure in the calculation, the spectrum obtained numerically never approaches exactly the fixed point spectrum of (3.17). This problem is solved using as limiting spectrum the one obtained for very large N, where the contribution of the irrelevant operators is eventually negligible.

The relations between the operators f_0 and f_1 appearing in (3.19) and the operators g_i and h_i are

$$f_{0a\mu} = \Lambda^{-(N-1)/4} \left(\hat{\alpha}_{00} g_{0a\mu} + \sum_{j=1}^{(N-1)/2} \hat{\alpha}_{0j} \left(g_{ja\mu} + h^\dagger_{ja\mu} \right) \right) \tag{3.21}$$

$$f_{1a\mu} = \Lambda^{-3(N-1)/4} \left(\sum_{j=1}^{(N-1)/2} \hat{\alpha}_{1j} \left(g_{ja\mu} - h^\dagger_{ja\mu} \right) \right) \tag{3.22}$$

where the coefficients $\hat{\alpha}_{nj}$ are extracted from the diagonalization of (3.17).

Incidentally we notice that the part of the effective Hamiltonian that contains the irrelevant operators scales like

$$\Lambda^{(N-1)/2}\delta H \sim \Lambda^{-(N-1)/2} \tag{3.23}$$

due to the Λ factors in (3.21) and (3.22). The relation between f_3 and (g_i, h_i) is similar to (3.21) but the prefactor is $\Lambda^{-5(N-1)/4}$ and similarly for higher f_n. Hence any operator involving f_n with $n > 1$ is less relevant than those in (3.19).

To proceed we need to classify the states in the spectrum in terms of g_i and h_i operators. Since the effective couplings to be fitted are just 4 we can use the lowest energy states involving only operators g_0, g_1 and h_1.

To build the full Hilbert space $\mathcal{H}$ it is easier to build first the Hilbert space, $\mathcal{H}_{(1)}$, of a single chain and then divide it in subspaces of given charge and spin. Indicating a subspace as (Q, S) we have the following decomposition:

$$\begin{aligned}\mathcal{H}_{(1)} &= (0,3/2) \oplus [8 \times (0,1/2)] \oplus [3 \times (\pm 1/2, 1)] \\ &\quad \oplus [6 \times (\pm 1/2, 0)] \oplus [3 \times (\pm 1, 1/2)] \oplus (\pm 3/2, 0).\end{aligned} \tag{3.24}$$

Now we compose the states of the first and second chain to construct states of the full system with given charge and spin. For instance the subspace with $Q = 0$ and $S = 0$ of the full system of two chains is given in terms of subspaces of the single chains by (the subscript indicates the chain)

$$\begin{aligned}(0,0) &= (-3/2,0)_1 \otimes (3/2,0)_2 \bigoplus (3/2,0)_1 \otimes (-3/2,0)_2 \\ &\quad \bigoplus 9 \times [(-1,1/2)_1 \otimes (1,1/2)_2]_{S=0} \bigoplus 9 \times [(1,1/2)_1 \otimes (-1,1/2)_2]_{S=0} \\ &\quad \bigoplus 36 \times (-1/2,0)_1 \otimes (1/2,0)_2 \bigoplus 36 \times (1/2,0)_1 \otimes (-1/2,0)_2 \\ &\quad \bigoplus 9 \times [(-1/2,1)_1 \otimes (1/2,1)_2]_{S=0} \bigoplus 9 \times [(1/2,1)_1 \otimes (-1/2,1)_2]_{S=0} \\ &\quad \bigoplus 64 \times [(0,1/2)_1 \otimes (0,1/2)_2]_{S=0} \bigoplus [(0,3/2)_1 \otimes (0,3/2)_2]_{S=0}\end{aligned} \tag{3.25}$$

and similarly for the other subspaces.

We can restrict our analysis to those states that contain at most one operator of the first excited level (g_1 or h_1) since the number of states obtained in this way is more than enough to study the low energy properties of the system. In Table 3.2 is shown as an example a summary of the lowest energy states for the $(Q = 0, S = 0)$ subspace. We analyze only subspaces with $Q \geq 0$ and $T^z \geq 0$ since, due to the

Table 3.2: States in the $Q = 0$ $S = 0$ subspace employed to fit the couplings of the effective Hamiltonian. These states are a subset of the states contained in the subspace. Notice that $h^\dagger_{a\uparrow}$ lowers the charge by 1 and the z component of the spin by $1/2$

$Q = 0, S = 0$		
Subspace$_1$ $\otimes$ Subspace$_2$	State	T^z
$E = 0$		
$(-1/2, 0)_1 \otimes (1/2, 0)_2$	$g^\dagger_{02\uparrow} g^\dagger_{02\downarrow}$	-1/2
$(1/2, 0)_1 \otimes (-1/2, 0)_2$	$g^\dagger_{01\uparrow} g^\dagger_{01\downarrow}$	+1/2
$(0, 1/2)_1 \otimes (0, 1/2)_2$	$\frac{1}{\sqrt{2}} \left(g^\dagger_{01\uparrow} g^\dagger_{02\downarrow} - g^\dagger_{01\downarrow} g^\dagger_{02\uparrow} \right)$	0
$E = \hat{\eta}_1$		
$(-1/2, 0)_1 \otimes (1/2, 0)_2$	$\frac{1}{\sqrt{2}} \left(g^\dagger_{02\uparrow} g^\dagger_{12\downarrow} - g^\dagger_{02\downarrow} g^\dagger_{12\uparrow} \right)$	-1/2
$(-1/2, 0)_1 \otimes (1/2, 0)_2$	$\frac{1}{\sqrt{2}} \left(g^\dagger_{01\uparrow} h^\dagger_{11\uparrow} + g^\dagger_{01\downarrow} h^\dagger_{11\downarrow} \right) g^\dagger_{02\uparrow} g^\dagger_{02\downarrow}$	-1/2
$(1/2, 0)_1 \otimes (-1/2, 0)_2$	$\frac{1}{\sqrt{2}} \left(g^\dagger_{01\uparrow} g^\dagger_{11\downarrow} - g^\dagger_{01\downarrow} g^\dagger_{11\uparrow} \right)$	+1/2
$(1/2, 0)_1 \otimes (-1/2, 0)_2$	$\frac{1}{\sqrt{2}} \left(g^\dagger_{02\uparrow} h^\dagger_{12\uparrow} + g^\dagger_{02\downarrow} h^\dagger_{12\downarrow} \right) g^\dagger_{01\uparrow} g^\dagger_{01\downarrow}$	+1/2
$[(0, 1/2)_1 \otimes (0, 1/2)_2]_{S=0}$	$\frac{1}{\sqrt{2}} \left(g^\dagger_{01\uparrow} g^\dagger_{12\downarrow} - g^\dagger_{01\downarrow} g^\dagger_{12\uparrow} \right)$	0
$[(0, 1/2)_1 \otimes (0, 1/2)_2]_{S=0}$	$\frac{1}{\sqrt{2}} \left(g^\dagger_{11\uparrow} g^\dagger_{02\downarrow} - g^\dagger_{11\downarrow} g^\dagger_{02\uparrow} \right)$	0
$[(0, 1/2)_1 \otimes (0, 1/2)_2]_{S=0}$	$\frac{1}{\sqrt{2}} \left(g^\dagger_{01\uparrow} g^\dagger_{02\uparrow} g^\dagger_{02\downarrow} h^\dagger_{12\uparrow} + g^\dagger_{01\downarrow} g^\dagger_{02\uparrow} g^\dagger_{02\downarrow} h^\dagger_{12\downarrow} \right)$	0
$[(0, 1/2)_1 \otimes (0, 1/2)_2]_{S=0}$	$\frac{1}{\sqrt{2}} \left(g^\dagger_{01\uparrow} g^\dagger_{01\downarrow} h^\dagger_{11\uparrow} g^\dagger_{02\uparrow} + g^\dagger_{01\uparrow} g^\dagger_{01\downarrow} h^\dagger_{11\downarrow} g^\dagger_{02\downarrow} \right)$	0

particle-hole symmetry and to the $O(2)_{orb}$ symmetry, subspaces with Q and $-Q$ or with T^z and $-T^z$ are degenerate. Once identified the relevant states we calculate the matrix elements of (3.19) using a Fortran program due to the large number of states involved and the lengthy expression of (3.19) in terms of g_0, g_1 and h_1.

The last step consists in fitting the difference between the spectrum of a finite-N iteration and the asymptotic one in terms of the parameters of the effective Hamiltonian.

To obtain the same information in the unscreened phase we apply the same procedure for N even.

The result is shown in Fig. 3.5. Upon approaching the UFP on both sides, we find

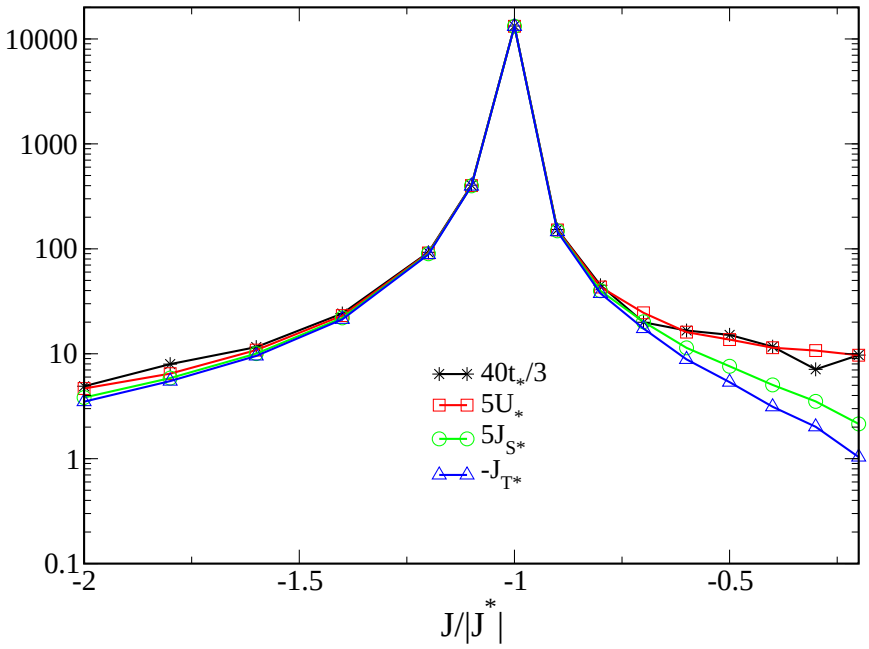

Figure 3.5: J dependence of the effective couplings in Eq. (3.19) around the UFP. Notice that the couplings have been properly rescaled to show the common behavior approaching the UFP. [$\Lambda = 3$, $J_K = 0.05$]

that $U_* \sim J_{S*} = \gamma \to +\infty$, $J_{T*} \sim -5\gamma \to -\infty$ and $t_* \sim 3\gamma/8 \to +\infty$.

The behavior of t_* implies a divergence of the impurity contribution to the specific heat coefficient. Namely if δC_V is the variation of the specific heat with respect to its value C_V in the absence of the impurity, then

$$\frac{\delta C_V}{C_V} \sim \rho_c \, t_* \to \infty.$$

The knowledge of the couplings of the effective Hamiltonian allows the calculation of Wilson ratios and scattering amplitudes. In Appendix A we will introduce a Fermi liquid theory that provide the natural framework to analyze these results.

3.2.4 Entropy and energy scales

The physics around and right at the UFP has been uncovered by Conformal Field Theory and bosonization[17, 18, 45, 46, 64]. Due to the existence of two energy scales, the Kondo temperature T_K and the exchange splitting, J, the quenching of the

impurity degrees of freedom takes place in two steps. First, around an energy scale $T_+ \sim \max(T_K, |J|)$, most of the $\ln 6$ entropy of the two-electron impurity multiplets is removed, leaving behind a residual entropy $\ln\sqrt{2}$ which gets quenched only below a lower energy scale $T_- \sim 1/\gamma$. The latter depends quadratically upon the deviation from the UFP, namely $T_- \sim |J - J^*|^2/T_+$. The entropy has a low energy linear behavior, $S(T) \sim T/T_-$, followed above T_- by another linear one, $S(T) - \ln\sqrt{2} \sim T/T_+$[18, 46]. At the fixed point, $T_- = 0$, there is a finite residual entropy $S(0) = \ln\sqrt{2}$ and $S(T) - S(0) \sim T/T_+$.

3.2.5 Impurity spectral function

The impurity density of states (DOS), $\rho(\epsilon)$, is defined through

$$\rho(\epsilon) = -\frac{1}{2\pi} \lim_{\eta\to 0} \left[G(\epsilon + i\eta) - G(\epsilon - i\eta)\right], \tag{3.26}$$

where $G(i\epsilon_n)$ is the impurity Green's function in Matsubara frequencies, which, by symmetry, is diagonal in spin and orbital indices, and independent upon them. In general

$$G(i\epsilon_n)^{-1} = i\epsilon_n - \Delta(i\epsilon_n) - \Sigma(i\epsilon_n) = G_0(i\epsilon_n)^{-1} - \Sigma(i\epsilon_n), \tag{3.27}$$

where $G_0(i\epsilon_n)$ is the non-interacting, $U = J = 0$, Green's function,

$$\Delta(i\epsilon_n) = V_d^2 \sum_{\mathbf{k}} \frac{1}{i\epsilon_n - \epsilon_{\mathbf{k}}}, \tag{3.28}$$

is the hybridization function, and $\Sigma(i\epsilon_n)$ the impurity self-energy. Let us suppose to follow the behavior of the DOS as the interaction is switched on. We will imagine to increase slowly both U and $|J|$ at fixed $U/|J| \gg 1$ with $J < 0$. When U is small, one can show by perturbation theory that

$$\mathcal{I}m\Sigma(\epsilon) \sim \epsilon^2,$$

which is the standard result that the quasiparticle decay rate vanishes faster than the frequency. Therefore at the chemical potential, $\epsilon = 0$, the impurity DOS is not affected by a weak interaction, since

$$\rho(0) = -\frac{1}{\pi} \lim_{\eta\to 0} \mathcal{I}m\, G(0 + i\eta) = -\frac{1}{\pi} \lim_{\eta\to 0} \mathcal{I}m\, G_0(0 + i\eta) = \frac{1}{\pi\Delta_0} = \rho_0, \tag{3.29}$$

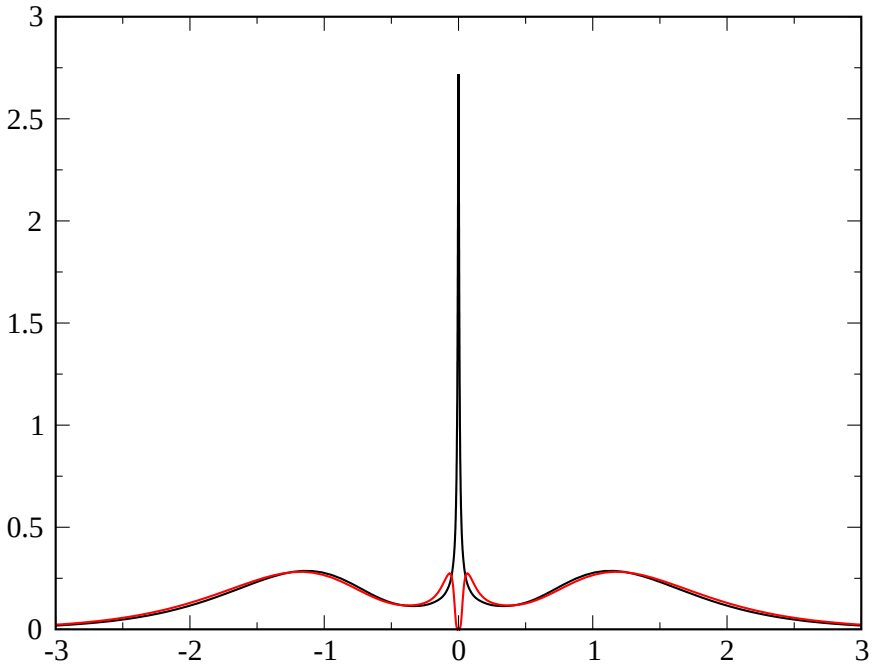

Figure 3.6: Impurity DOS in the presence of particle-hole symmetry across the fixed point. The temperature is set by the length of the chain; it is practically zero. In black the DOS's well inside the Kondo screened phase $(J/J^* = 0)$ and in red the unscreened one $(J/J^* = 5.75)$. Here $U = 2$, $\Delta_0 = U/(6\pi)$ and J_* turns out to be $\simeq -0.0035$, all in units of half the conduction bandwidth. [$\Lambda = 2$]

where $\Delta_0 = -\mathcal{I}m\,\Delta(0 + i\eta)$ was introduced in Eq. (3.7), and ρ_0 denotes the non-interacting DOS at the chemical potential. In a single-orbital AIM, the above result remains valid even when the interaction is very large. In our case we may expect that something non-trivial should instead occur. Indeed, upon increasing U, the AIM enters the Kondo regime, with a Kondo temperature exponentially decreasing with U. Therefore at some critical U_c, when $T_K \sim |J|$, the AIM has to cross the non-Fermi liquid UFP. Namely the UFP of our AIM can also be attained by increasing the interaction strength, signaling a breakdown of the conventional perturbation theory. We now discuss how this criticality shows up in the spectral properties.

In Fig. 3.6 and 3.7 we show the outcome of the numerical calculation in the particle-hole symmetric case.

For $J > J^*$, in the Kondo screened region of the phase space, the DOS presents

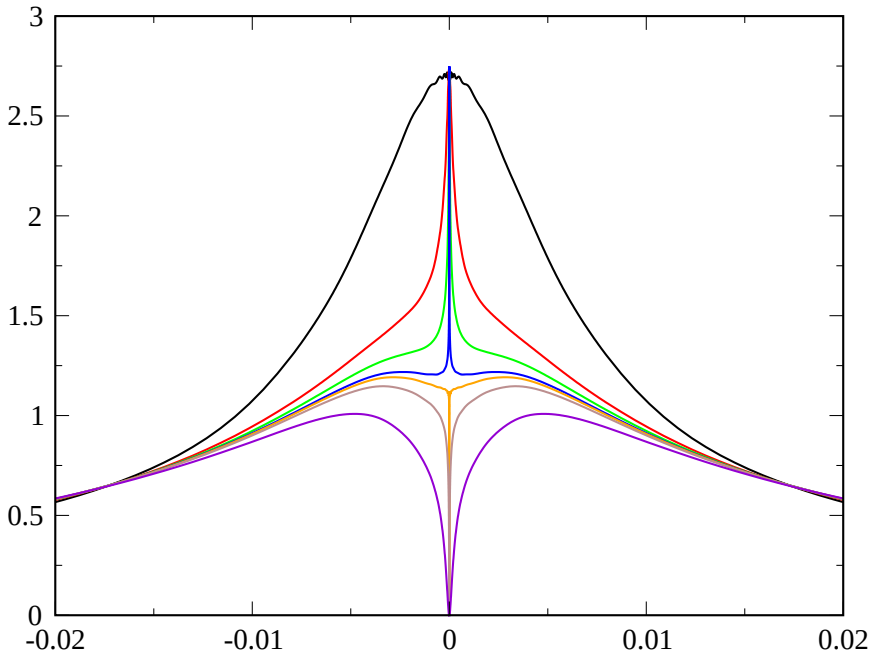

Figure 3.7: Details of the impurity DOS close to the chemical potential across the UFP. (From top to bottom $J/J^* = 0, 0.859, 0.945, 0.988, 1.002, 1.031, 1.146$. The other parameters are the same as in Fig. 3.6) Notice the narrow peak which transforms into a narrow pseudo-gap.

the typical features of a Kondo screened impurity. At an energy of order $\pm U/2$ there are the so-called Hubbard peaks, representing charge fluctuations of the impurity, and the Kondo resonance is pinned at the chemical potential. As predicted by simple perturbation theory, the height at the chemical potential is $\rho(0) = \rho_0$. As the system gets closer to the UFP, the Kondo resonance becomes the sum of two resonances, a broad one that remains almost constant as a function of J and a narrow peak that shrinks progressively approaching the UFP.

In the unscreened region the two Hubbard peaks are still present but now, close to the UFP, the narrow peak transforms into a narrow pseudo-gap within the broad resonance, and $\rho(0) = 0$. Numerically we find that $\rho(\epsilon) \sim \epsilon^2$. As discussed before, this implies that the conventional behavior $\mathcal{I}m\Sigma(\epsilon) \sim \epsilon^2$ breaks down across the UFP.

Exactly at the fixed point, both the narrow peak and the pseudo-gap disappear, leaving aside only the broad resonance. The calculated DOS at the chemical potential

seems to be half of its non-interacting value, see Fig. 3.7. In other words our numerical results point to a DOS at the chemical potential which jumps across the UFP, being $\rho(0) = \rho_0$ everywhere in the Kondo-screened phase, $\rho(0) = 0$ in the unscreened one, and $\rho(0) = \rho_0/2$ right at the UFP.

3.2.6 Modeling of the spectral function

It is possible to infer an analytical expression of the impurity DOS. First of all we notice that the values at the chemical potential in the screened and in the unscreened Kondo regimes are compatible with general scattering theory. In both phases the impurity has disappeared at low energy, either because it has been absorbed by the conduction sea or because J has taken care of quenching the impurity spin and orbital degrees of freedom. This in turns means that what remains at low energy is just a potential scattering felt by the conduction electrons plus a local electron-electron interaction term, as we saw in Section 3.2.3. The on-shell S-matrix at the chemical potential has in general elastic and inelastic contributions (see Ref. [65]). At zero temperature only the former survives. Since we considered just s-wave scattering, the elastic component of the S-matrix is given by:

$$S(0) = 1 - 2\pi i \rho_c T(0) = 1 - 2\,\pi\,\Delta_0\,\rho(0), \tag{3.30}$$

where ρ_c is the conduction electron DOS at the chemical potential per spin and band, and the T-matrix is defined through the conduction electron Green's function $\mathcal{G}$ by

$$\mathcal{G} = \mathcal{G}_0 + \mathcal{G}_0\,T\,\mathcal{G}_0. \tag{3.31}$$

On the other hand the S-matrix is related to the scattering phase shift by

$$S(0) = \mathrm{e}^{2i\delta(0)}. \tag{3.32}$$

In the Kondo screened phase, we know that $\delta(0) = \pi/2$ which, through (3.32) and (3.30) implies $\rho(0) = 1/\pi\Delta_0$, namely its non-interacting value ρ_0. On the other hand, in the unscreened regime $\delta(0) = 0$ hence $\rho(0) = 0$, as we indeed find. It has been proposed that at the non-Fermi liquid fixed point of the over-screened $S = 1/2$ two-channel Kondo model the S-matrix is instead purely inelastic[17, 66, 67]. That would imply a vanishing elastic contribution, $S(0) = 0$ in (3.30), and in turn a DOS at the UFP

$$\rho(0) = \frac{1}{2\pi\Delta_0} = \frac{1}{2}\rho_0, \tag{3.33}$$

which is indeed compatible with our numerical results[68]. Yet there is a difference between the UFP of our model, equivalently of the 2IKM, and the non-Fermi liquid fixed point of the $S = 1/2$ two-channel Kondo model. While in the latter the specific heat has a singular temperature behavior right at the UFP, in our model it has a conventional linear behavior. The singular behavior of the two-channel Kondo model is due to the presence of a leading irrelevant operator at the fixed point with dimension $3/2$. The same operator is not allowed in the 2IKM[18] as well as in our model due to symmetry constraints and hence the specific heat in that case is linear.

For the same reason we do not expect any non-analytic correction to the electron self energy[43] which leads us to a simple ansatz for the low-energy impurity DOS:

$$\rho_{\pm}(\epsilon) = \frac{\rho_0}{2}\left(\frac{T_+^2}{\epsilon^2+T_+^2} \pm \frac{T_-^2}{\epsilon^2+T_-^2}\right), \tag{3.34}$$

where the plus sign refers to the Kondo screened phase and the minus to the unscreened one. The two energy scales have the same meaning as in Section 3.2.4. In particular T_- controls the deviations from the UFP, so that right at the UFP, when $T_- = 0$, the DOS is

$$\rho_*(\epsilon) = \frac{\rho_0}{2}\,\frac{T_+^2}{\epsilon^2+T_+^2}. \tag{3.35}$$

The model-DOS (3.34) also implies a model impurity Green's function in Matsubara frequencies:

$$G_{\pm}(i\epsilon_n) = \frac{1}{2\Delta_0}\left(\frac{T_+}{i\epsilon_n + iT_+\,\mathrm{sign}\epsilon_n} \pm \frac{T_-}{i\epsilon_n + iT_-\,\mathrm{sign}\epsilon_n}\right). \tag{3.36}$$

The fixed point Green's function, $G_*(i\epsilon_n)$, is identified by $T_- = 0$. The impurity self-energy can then be extracted by the relation

$$\Sigma_{\pm}(i\epsilon_n) = i\epsilon_n + i\Delta_0\,\mathrm{sign}\,\epsilon_n - G_{\pm}(i\epsilon_n)^{-1}.$$

In particular, at low frequency we find that

$$i\epsilon_n - \Sigma_+(i\epsilon_n) \simeq i\epsilon_n\,\frac{\Delta_0}{2}\left(\frac{1}{T_+}+\frac{1}{T_-}\right), \tag{3.37}$$

in the Kondo screened phase, hence a standard linear behavior. On the contrary, in the unscreened regime the self-energy is singular

$$i\epsilon_n - \Sigma_-(i\epsilon_n) \simeq -\frac{1}{i\epsilon_n}\,\frac{2\Delta_0 T_+ T_-}{T_+ - T_-}. \tag{3.38}$$

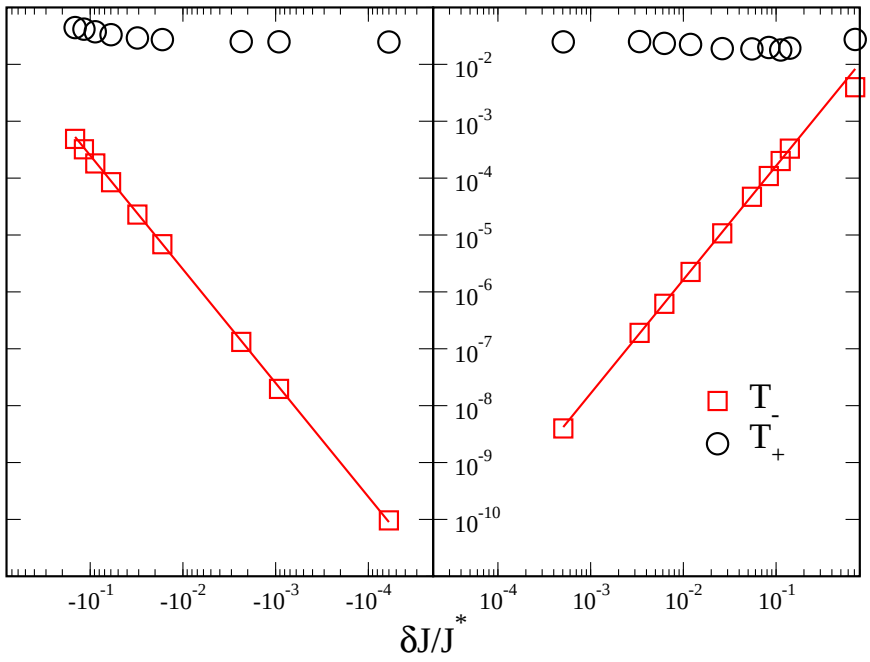

Figure 3.8: Fit values of T_+ and T_- close to the UFP. The lines are quadratic fits, $T_- = A(\delta J)^2$. [$U = 2$, $\Delta_0 = U/(6\pi)$, $J_* \simeq -0.0035$, $\Lambda = 2$]

Finally, at the fixed point the self-energy is finite at zero frequency, being given by

$$i\epsilon_n - \Sigma_*(i\epsilon_n) = i\Delta_0 \frac{T_+ + 2\epsilon_n}{T_+}. \tag{3.39}$$

We have checked that the model-self-energy gives indeed a good representation of the actual numerical results. In Fig. 3.8 we draw the fit values of T_+ and T_- around the UFP.

We can further test the consistency of the approach by invoking the scattering theory which, by the Friedel's sum rule, allows us to identify the scattering phase shifts through:

$$\delta(\epsilon) = \mathrm{Im} \ln G(\epsilon + i0^+). \tag{3.40}$$

By means of our ansatz for the impurity Green's function (3.36) we readily find that the expression of the low-energy phase-shifts is

$$\delta_+(\epsilon) \simeq \frac{\pi}{2} + \frac{\epsilon}{2}\left(\frac{1}{T_+} + \frac{1}{T_-}\right) \equiv \frac{\pi}{2} + \alpha_+\epsilon \tag{3.41}$$

within the Kondo screened regime, and

$$\delta_-(\epsilon) \simeq \epsilon \left(\frac{1}{T_+} + \frac{1}{T_-} \right) \equiv \alpha_- \epsilon, \tag{3.42}$$

in the pseudo-gap unscreened phase, consistent with our starting assumption. Moreover, by the energy dependence of the phase shifts, we can calculate the impurity correction to the specific heat

$$\frac{\delta C_V}{C_V} = \frac{\alpha_\pm}{\pi \rho_c}. \tag{3.43}$$

3.3 Fermi liquid theory

In Appendix A we have presented a Landau Fermi liquid description of a generic AIM which generalizes the conventional theory, as for instance developed by Mihály and Zawadowskii[75], to cases where Kondo screening does not take place, yet the behavior is Fermi liquid like. This is just our case in the unscreened regime where the phase shift at the chemical potential is zero.

In this Section we are going to use this theory to extract some physical properties upon approaching the UFP for convenience from the Kondo screened side.

A suitable generalization of Fermi liquid theory is achieved by the introduction of the quantity

$$\bar{\rho}_* = \int_{-\infty}^{\infty} \frac{d\epsilon}{\pi} \frac{\partial f(\epsilon)}{\partial \epsilon} \operatorname{Im} \left\{ G(\epsilon + i\delta) \left[1 - \left(\frac{\partial \Delta(i\epsilon)}{\partial i\epsilon} \right)_{i\epsilon \to \epsilon + i\delta} - \left(\frac{\partial \Sigma(i\epsilon)}{\partial i\epsilon} \right)_{i\epsilon \to \epsilon + i\delta} \right] \right\}, \tag{3.44}$$

which plays the role of the quasiparticle density of states at the chemical potential and does not vanish both in the Kondo screened and in the unscreened phases, in spite of the fact that in the latter the impurity DOS $\rho(\epsilon)$ is actually zero at $\epsilon = 0$. In the Kondo screened phase, where $\rho(0) \neq 0$ and the self-energy is well behaved,

$$\bar{\rho}_* = \frac{\rho(0)}{Z}, \tag{3.45}$$

where

$$\frac{1}{Z} = 1 - \left(\frac{\partial \Sigma(i\epsilon)}{\partial i\epsilon} \right)_{i\epsilon \to i0^+}, \tag{3.46}$$

is the conventional definition of the quasiparticle residue Z.

An incoming pair can be a spin-triplet orbital-singlet, with a scattering vertex at zero incoming and outgoing frequencies given by

$$\Gamma^1 \rightarrow \Gamma_{1\sigma,2\sigma;2\sigma,1\sigma}\,, \quad \frac{1}{2}\Gamma_{1\sigma,2\,-\sigma;2\,-\sigma,1\sigma} - \frac{1}{2}\Gamma_{1\sigma,2\,-\sigma;1\,-\sigma,2\sigma}\,.$$

Here 1 and 2 label the two orbitals with $T^z = +1/2$ and $T^z = -1/2$, respectively. Alternatively it can be a spin-singlet orbital-triplet with $T^z = 0$, with scattering vertex

$$\Gamma^0_0 \rightarrow \frac{1}{2}\Gamma_{1\sigma,2\,-\sigma;2\,-\sigma,1\sigma} + \frac{1}{2}\Gamma_{1\sigma,2\,-\sigma;1\,-\sigma,2\sigma}\,,$$

or with $T^z = \pm 1$, in which case

$$\Gamma^0_\pm \rightarrow \Gamma_{1\sigma,1\,-\sigma;1\,-\sigma,1\sigma}\,, \quad \Gamma_{2\sigma,2\,-\sigma;2\,-\sigma,2\sigma}\,.$$

In reality it is more convenient to introduce for each scattering vertex the corresponding dimensionless quantity through:

$$\begin{aligned} \mathcal{A}^1 &= Z\,\rho(0)\,\Gamma^1, \\ \mathcal{A}^0_0 &= Z\,\rho(0)\,\Gamma^0_0, \\ \mathcal{A}^0_\pm &= Z\,\rho(0)\,\Gamma^0_\pm, \end{aligned} \tag{3.47}$$

valid in the Kondo screened regime.

As we discuss in Appendix A, only the susceptibilities of conserved quantities can be expressed in terms of the Landau parameters (A.16), which are simply connected to the scattering vertices at zero frequency. Yet we can still define Landau parameters for non-conserved quantities, which, although do not serve to calculate susceptibilities, may provide a qualitative estimate of their magnitude. Therefore we are going to introduce the Landau parameters for the charge, A_C, spin A_S, the z-component of the pseudo-spin $\vec{T}$, $A^{||}_T$, all being related to conserved quantities, but also for the x and y components of $\vec{T}$, $A^{\perp}_T$, as well as for the spin-orbital components, $A^{||}_{ST}$ and $A^{\perp}_{ST}$. In terms of the dimensionless amplitudes (3.47) they can be shown, after some lengthy algebra, to have the following expressions:

$$A_C = \frac{1}{4}\left(6\mathcal{A}^1 + 2\mathcal{A}^0_0 + 4\mathcal{A}^0_\pm\right), \tag{3.48}$$

$$A_S = \frac{1}{4}\left(2\mathcal{A}^1 - 2\mathcal{A}^0_0 - 4\mathcal{A}^0_\pm\right), \tag{3.49}$$

$$A^{||}_T = \frac{1}{4}\left(-6\mathcal{A}^1 - 2\mathcal{A}^0_0 + 4\mathcal{A}^0_\pm\right), \tag{3.50}$$

$$A_T^{\perp} = \frac{1}{4}\left(-6\mathcal{A}^1 + 2\mathcal{A}_0^0\right), \tag{3.51}$$

$$A_{ST}^{||} = \frac{1}{4}\left(-2\mathcal{A}^1 + 2\mathcal{A}_0^0 - 4\mathcal{A}_{\pm}^0\right), \tag{3.52}$$

$$A_{ST}^{\perp} = \frac{1}{4}\left(-2\mathcal{A}^1 - 2\mathcal{A}_0^0\right). \tag{3.53}$$

Let us consider several possible cases.

- If $J = 0$, $SU(4)$ symmetry holds. Then $\mathcal{A}^1 = \mathcal{A}_0^0 = \mathcal{A}_{\pm}^0 = A$, leading to

$$\begin{aligned} A_C &= 3\,A, \\ A_S &= A_T^{||} = A_T^{\perp} = A_{ST}^{||} = A_{ST}^{\perp} = -A. \end{aligned}$$

  In the s-d limit, when the AIM maps onto an $SU(4)$ Kondo model, the charge compressibility in negligible, leading to $3A = 1$. The Wilson ratios for the conserved quantities are defined trough

$$R_i = \frac{\delta\chi^{(i)}}{\chi_0}\frac{C_V}{\delta C_V} = 1 - A_i, \tag{3.54}$$

  where $\delta\chi^{(i)}$ has been defined in (A.8), $\chi_0 = \rho_c$ and C_V are respectively the conduction-electron susceptibility and specific heat in the absence of the impurity, and

$$\delta C_V = \frac{\bar{\rho}_*}{\rho_c}\,C_V,$$

  is the variation of the specific heat due to the impurity. Hence all Wilson ratios have a universal value,

$$R_S = R_T = R_{ST} = 1 + A = 4/3, \tag{3.55}$$

  in agreement with Conformal Field Theory.

- If $J \gg T_K > 0$ the impurity gets frozen in the Kondo limit into a spin S=1. Then both $A_C = 1$ and $A_T^{||} = 1$, which implies

$$\begin{aligned} \mathcal{A}_{\pm}^0 &= 1, \\ \mathcal{A}_0^0 &= -3\,\mathcal{A}^1. \end{aligned}$$

However one expects that, being the spin-triplet an orbital singlet, the $SU(2)$ orbital symmetry gets restored at the fixed point, much in the same way as spin anisotropy is irrelevant at the Kondo fixed point. This further implies that

$$\mathcal{A}_0^0 = -3\mathcal{A}^1 = 1,$$

namely $A_S = -5/3$, with a Wilson ratio $R_S = 8/3$, in agreement with known results.

- Let us now suppose to be close to the UFP within the Kondo screened regime. As usual the charge degrees of freedom are suppressed already below U, so that we can still assume $A_C = 1$.

  Moreover we expect that the spin and the orbital degrees of freedom related to T^z get quenched below T_+. This is suggested by the regular behavior of the susceptibilities associated to S and T_z at the UFP. Indeed, as we have seen, in our UFP it is absent the leading irrelevant operator that generates singular correction to the spin susceptibility in the $S = 1/2$ two-channel Kondo model. The remaining degrees of freedom are freezed only below $T_- \ll T_+$.

  Therefore at very low temperatures $T < T_-$, we can safely assume that

$$T_-\,\delta\chi_S \sim T_-\,\delta\chi_T^{||} \sim \frac{T_-}{T_+} \sim 0,$$

  namely $A_S = A_T^{||} = 1$. As a result we find that

$$\mathcal{A}_\pm^0 = \mathcal{A}^1 = 1, \tag{3.56}$$
$$\mathcal{A}_0^0 = -3. \tag{3.57}$$

  Eq. (3.57) implies a strongly attractive s-wave singlet channel. The other Landau parameters are thus given by

$$A_T^\perp = A_{ST}^{||} = -3, \tag{3.58}$$
$$A_{ST}^\perp = 1. \tag{3.59}$$

  This further proves that the fixed point is equally unstable in the s-wave Cooper channel Γ_0^0, as well as in the T^x, T^y and $\vec{S}\,T^z$ particle-hole channels.

We finally notice that, although the Landau A-parameters would suggest that the susceptibilities in the unstable channels, all of which correspond to non-conserved quantities, diverge as $1/T_{-}$, in reality they only diverge logarithmically[18, 45, 46]. This is not incompatible with Fermi liquid theory, which allows to express in terms of the A-parameters only those response functions related to conserved quantities.

We can now use these Fermi liquid theory predictions to interpret the NRG results of Section 3.2.3. Indeed from the effective Hamiltonian couplings it is possible to extract the scattering amplitudes and compare them with the Fermi liquid theory results.

In Fig 3.9 we plot the Wilson ratios for spin (R_S) and z-component of orbital momentum (R_{T^z}) as obtained from NRG calculations. The first thing to notice is that in the $SU(4)$ regime with $J = 0$ and in the large J limit the results agree with Fermi liquid picture and with know results. Close to the UFP instead both Wilson ratios vanish as expected.

A deeper insight is provided by the scattering amplitudes shown in Fig 3.10. Again the values calculated numerically agree with the Fermi liquid theory prediction in the three cases considered.

The most relevant result is the behavior close to the UFP: in this region

$$\mathcal{A}_0^0 \simeq A_T^{\perp} \simeq A_{ST}^{||} \simeq -3,$$

while all the other A_i's tend to 1, implying vanishing Wilson ratios. The fixed point seems therefore to display a large hidden symmetry, actually an $SO(7)$ as identified by Ref. [18]. The UFP is equally unstable in the s-wave Cooper channel with $S = 0$, $T = 1$ and $T^z = 0$, as well as in the particle-hole $T^{x(y)}$ and $\vec{S}T^z$ channels. All of them correspond to physical instabilities as we anticipated and unlike what happens in the 2IKM. On the contrary any external field in the other channels do not spoil the UFP, in particular in the charge, spin and T^z particle-hole channels, which refer to conserved quantities.

Let us now use our model self-energy to extract some additional information. Through Eq. (3.37), we find that in the Kondo screened regime the expression (A.16) holds with a quasiparticle residue

$$\frac{1}{Z} = \frac{\Delta_0}{2}\left(\frac{1}{T_+} + \frac{1}{T_-}\right). \tag{3.60}$$

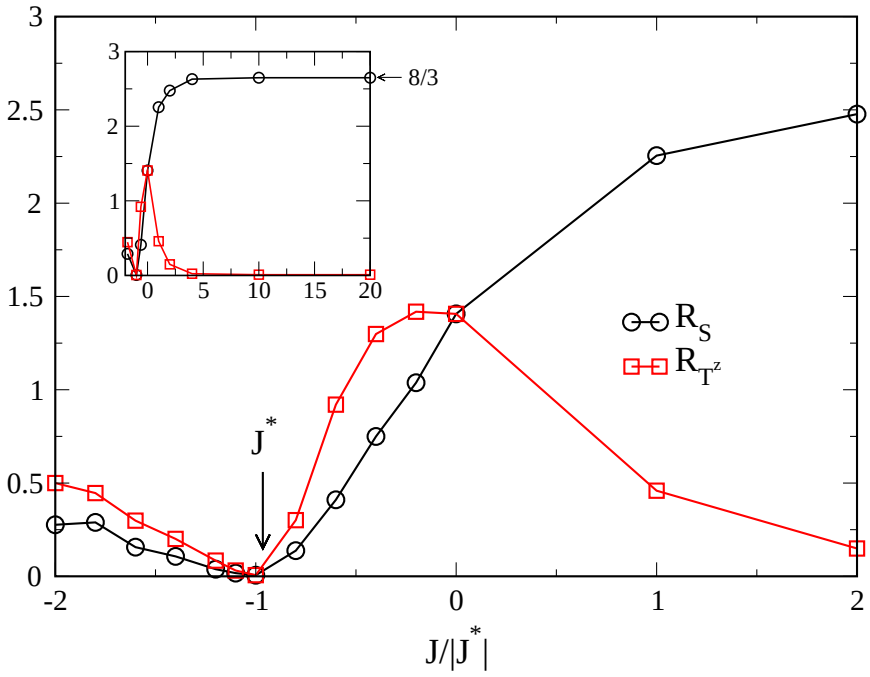

Figure 3.9: Spin (R_S) and z-component of orbital momentum (R_{T^z}) as functions of J. [$\Lambda = 3$, $J_K = 0.05$]

Indeed $Z \sim 2T_-/\Delta_0 \to 0$ upon approaching the unstable fixed point.

On the contrary, the general expression (A.14) has to be used inside the non-Kondo screened pseudo-gap phase. Through Eq. (3.36) for $G_-(i\epsilon_n)$ we find that at low frequency

$$G_-(\epsilon + i\delta)\, G_-(\epsilon - i\delta) \simeq \frac{1}{4\Delta_0^2} \frac{\epsilon^2 \left(T_+ - T_-\right)^2}{T_+^2 T_-^2} \simeq \frac{\pi}{2\Delta_0}\, \rho_-(\epsilon)\, \frac{T_+ - T_-}{T_+ + T_-}.$$

By Eq. (3.38) the quasiparticle DOS at the chemical potential turns out to be finite,

$$\bar{\rho}_* = \frac{1}{\pi} \frac{T_+ + T_-}{T_+ T_-}, \tag{3.61}$$

even though the impurity DOS vanishes. In conclusion, within the pseudo-gap phase the Landau parameters have the following expression

$$A_i \;=\; \frac{\pi}{2} \frac{T_+ T_- \left(T_+ - T_-\right)}{\left(T_+ + T_-\right)^2} \int_{-\infty}^{\infty} d\epsilon\, d\epsilon' \, \frac{\partial f(\epsilon)}{\partial \epsilon}\, \rho(\epsilon)\, \frac{\partial f(\epsilon')}{\partial \epsilon'}\, \rho(\epsilon')$$

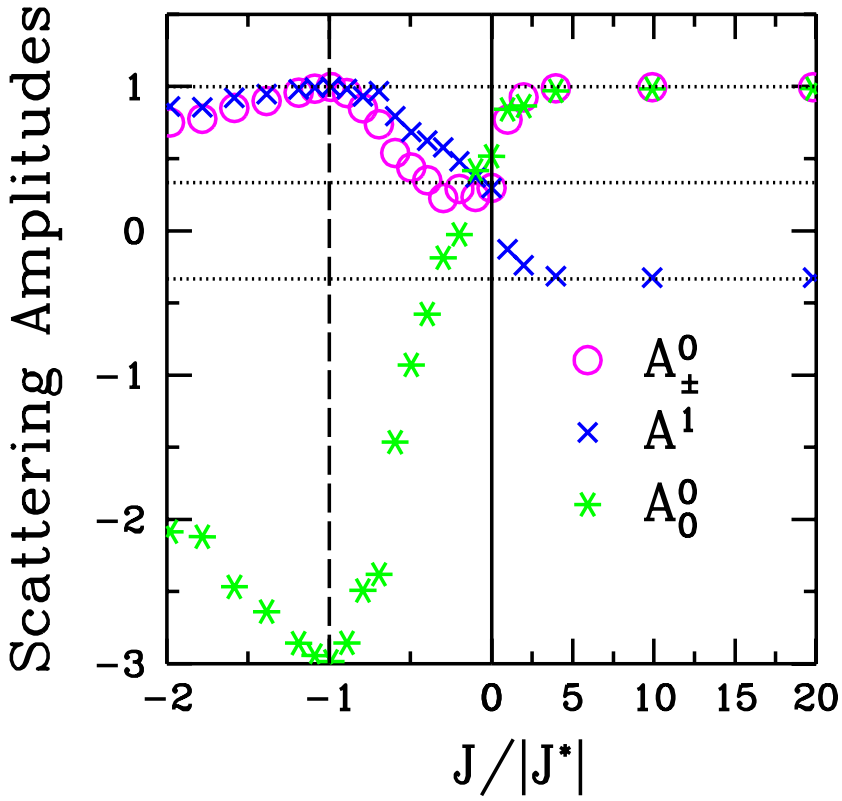

Figure 3.10: The scattering amplitudes in the various particle-particle channels as function of J measured in units of the UFP J^*. [$\Lambda = 3$, $J_K = 0.05$]

$$\sum_{cd;\gamma\delta} \Gamma_{a\alpha,d\delta;c\gamma,b\beta}(\epsilon + i\delta, \epsilon' - i\delta'; \epsilon' + i\delta', \epsilon + i\delta) \left(M^{(i)}\right)^{\gamma\delta}_{cd} \left(M^{(i)}\right)^{\beta\alpha}_{ba}. \tag{3.62}$$

In spite of the anomalous impurity Green's function, the low-energy behavior should still be described within a local Fermi liquid scenario by finite Landau parameters A_i's. Therefore, since the impurity DOS vanishes quadratically in the pseudo-gap phase, then the scattering vertices must display a singular behavior

$$\Gamma(\epsilon, \epsilon'; \epsilon', \epsilon) \sim \frac{1}{(\epsilon + \epsilon')^4},$$

to compensate for the vanishing DOS's and provide finite A's.

3.4 Particle-hole symmetry breaking

In this Section we analyze more in detail various symmetry breaking terms in the particle-hole channel. In particular we are going to consider the three following perturbations to the original Hamiltonian (3.1) with $\nu = 0$:

$$\delta H_{p-h} = \nu\, U\, n_d \equiv \frac{h_{p-h}}{2}\, n_d, \tag{3.63}$$

$$\delta H_z = h_z\, T^z, \tag{3.64}$$

$$\delta H_x = h_x\, T^x. \tag{3.65}$$

The term (3.63) breaks particle-hole symmetry trying to occupy the impurity with $2-\nu$ electrons instead of two, see (3.1). The other terms, (3.64) and (3.65), split the orbital degeneracy. It is convenient to decompose the orbital $O(2)$ symmetry into the continuous $U(1)$ symmetry related to proper rotations around the z-axis, and a discrete Z_2, corresponding to interchanging the two orbitals. Then δH_z breaks the orbital Z_2 while δH_x breaks the orbital $U(1)$. Among them, only the latter, δH_x, is predicted to be relevant and wash out the fixed point, at least according to bosonization[64]. Actually this looks a bit strange result if one invokes naïvely the argument of Ref. [18] to demonstrate the existence of an UFP in the absence of any particle-hole symmetry breaking term. This argument is based on the observation that, when $O(2)_{orbit}$ symmetry holds, the phase shifts in both orbital channels have to be equal, $\delta_1 = \delta_2$. By general particle-hole symmetry, this further implies that $2\delta_1 = 2\delta_2 = 0\ mod(\pi)$. Since for $J \gg T_K > 0$ we know that $\delta_1 = \delta_2 = \pi/2$, while for $J \ll -T_K < 0$, $\delta_1 = \delta_2 = 0$, there must necessarily be a fixed point in between.

Let us assume now that the T^z-term (3.64) is present and follow Ref. [18] to demonstrate that the necessary condition for the existence of an intermediate fixed point does not hold anymore. Since (3.63) is absent, there is still a residual particle-hole symmetry according to which

$$\delta_1 + \delta_2 = 0\ mod(\pi).$$

If $\delta_1 = -\delta_2$ then the two limiting cases, $\delta_1 = \delta_2 = 0$ and $\delta_1 = -\delta_2 = \pi/2$, can be smoothly connected without requiring any critical point in between. This argument thus proves that an intermediate fixed point does not need to exist, yet it does not demonstrate its non-existence. Indeed we know by bosonization and we now show

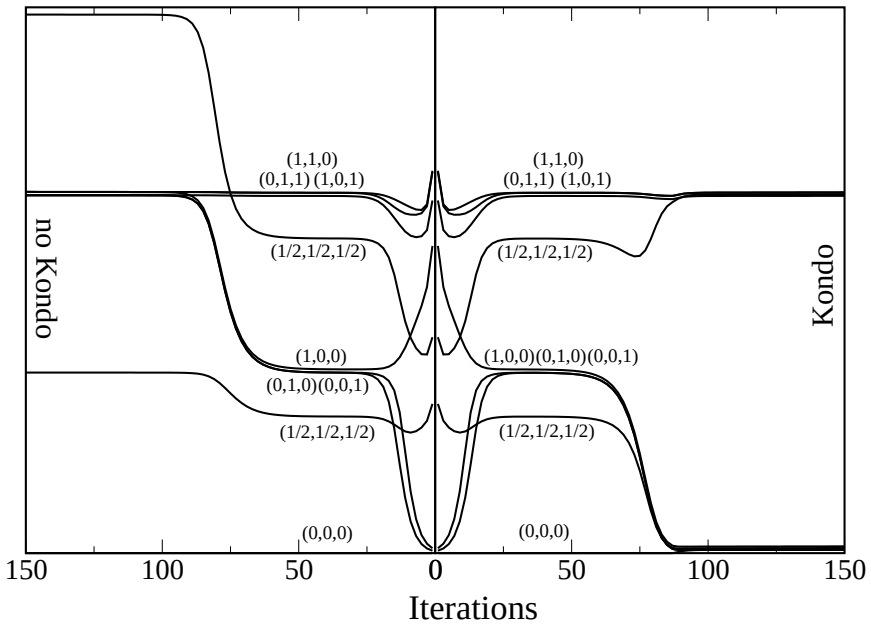

Figure 3.11: Lowest energy levels versus the chain size N in the presence of a finite $\nu = 0.05$. The left/right panels correspond to a deviation $\delta J/J^* = \pm 3 \cdot 10^{-5}$ from the fixed point value J^*. The levels are labeled by the quantum numbers (Q, T^z, S) as in Fig. 3.1. Notice that as a consequence of $\nu \neq 0$ some degeneracies found in the particle-hole symmetric case are lost. [$\Lambda = 2$, $U = 2$, $\Delta_0 = U/(6\pi)$, $J = -0.0035985$ (left), $J = -0.0035984$ (right)]

by NRG that both (3.64) as well as (3.63) do not wash out the UFP. On the contrary a T^x-term (3.65) does destabilize the fixed point, as shown later.

A direct way to prove that a particle-hole symmetry breaking perturbation of the form (3.63) does not spoil the UFP is by analyzing the low energy spectrum. We show in Fig. 3.11 the analogous of Fig. 3.1 in the presence of a finite $\nu = 0.05$ which breaks particle-hole symmetry. In spite of that, we still find evidences of an UFP separating the Kondo screened from the unscreened regimes. Needless to say, this fixed point is identified by the same spectrum we find in the particle-hole symmetric case, as can be realized by comparing the intermediate cross-over region in Fig. 3.11 with that in Fig. 3.1. Yet one might object that this is not a rigorous proof since numerically it is not possible to distinguish a true transition from a sharp cross-over. Even though we did check that upon varying J we can approach as close as we want

the UFP, eventually flowing in either of the two stable fixed points, we have found more convenient to resort to an alternative proof which seems more free of numerical uncertainties.

Let us go back to Eq. (3.30) and try to guess how would it change in the presence of (3.63) and/or (3.64). We have now to introduce an S-matrix for each channel, S_a with $a = 1, 2$, satisfying

$$\mathcal{R}e\, S_a(0) = \cos\, 2\delta_a(0) = 1 - 2\,\pi\,\Delta_0\,\rho_a(0). \tag{3.66}$$

Let us assume that, across the UFP, the zero-frequency phase shifts still jump by $\pi/2$. In other words, if we denote as

$$\delta_{-,a}(0) \equiv \delta_a, \tag{3.67}$$

the phase shift in the unscreened phase, in the Kondo-screened one the phase shift should be

$$\delta_{+,a}(0) = \delta_a + \frac{\pi}{2}.$$

Through (3.66) this would imply a jump of the DOS at the chemical potential given by

$$\rho_{+,a}(0) - \rho_{-,a}(0) = \frac{1}{\pi\Delta_0}\,\cos 2\delta_a = \rho_0\,\cos 2\delta_a. \tag{3.68}$$

The above scenario predicts that although the pseudo-gap in the unscreened phase is partly filled away from particle-hole symmetry, yet the DOS has a finite jump across the UFP. This is indeed confirmed by NRG. In Fig. 3.12 we plot the DOS at fixed $\nu = 0.05$, see Eq. (3.63), across the UFP, clearly showing the jump.

We notice that if only (3.63) is present, then $\delta_1 = \delta_2$ in Eq. (3.67). If (3.63) is absent but (3.64) is present, then $\delta_1 = -\delta_2$, yet the behavior across the UFP is similar, which is the reason why we just show the results with finite ν.

This behavior is also compatible with the NRG result that the charge and T^z Wilson ratios vanish around the UFP. Actually they all suggest that the model can absorb a chemical potential shift, equal or different in the two channels 1 and 2, on a high energy scale, at least of order T_+, without having to modify what takes place at lower energies of order T_-: a kind of Anderson's compensation principle for our conserved quantities. Following these observations, we argue that the DOS for orbital $a = 1, 2$ in the presence of any of the two perturbations, (3.63) and (3.64), assumed to be weak,

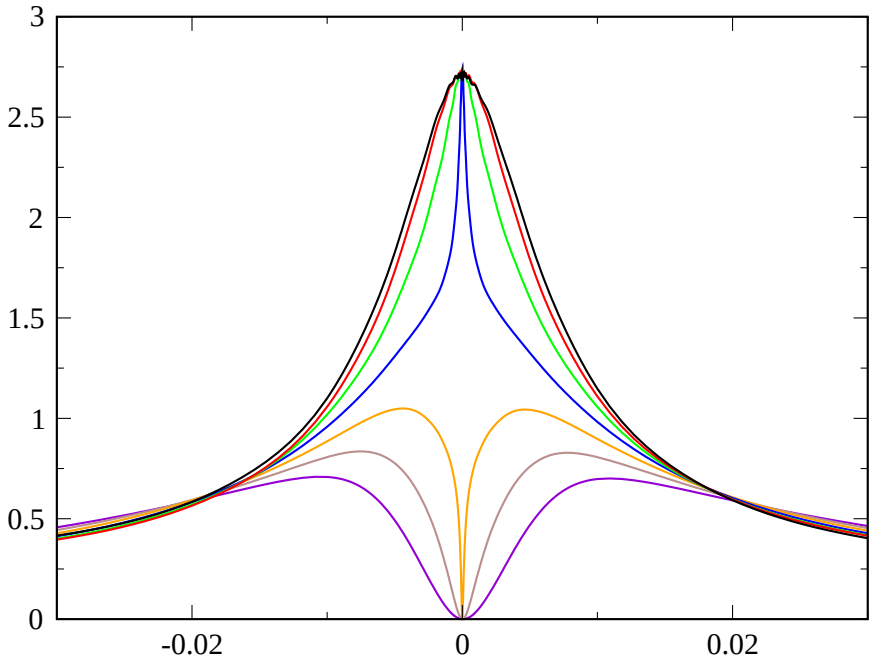

Figure 3.12: Impurity DOS across the UFP in the presence of a finite $\nu = 0.05$ which breaks particle-hole symmetry. From top to bottom $J/J^* = 0, 0.28, 0.57, 0.86, 1.14, 1.43, 1.71$. Notice that the DOS at the chemical potential is always finite, although very small hence not visible in the figure. [$\Lambda = 2$, $U = 2$, $\Delta_0 = U/(6\pi)$, $J^* \sim -0.0035985$]

can be modeled as

$$\rho_{\pm,a}(\epsilon) = \frac{\rho_a}{2}\left[\frac{T_+^2 + \mu_{\pm,a}^2}{(\epsilon + \mu_{\pm,a})^2 + T_+^2} \pm \cos 2\delta_a \, \frac{T_-^2}{\epsilon^2 + T_-^2}\right], \tag{3.69}$$

where again the plus refers to the Kondo screened phase, the minus to the unscreened one, $\rho_a = \rho_{+,a}(0)$ is the value of the DOS at the chemical potential in the screened regime, while

$$\mu_{\pm,a} = \pm T_+ \, \sin 2\delta_a.$$

According to the model DOS (3.69), the narrow peak and pseudo-gap remain pinned at the chemical potential, $\epsilon = 0$, while only the broad resonance moves away from particle-hole symmetry.

Let us now study what happens if, starting from the particle-hole symmetric pseudo-gap phase we move away by increasing ν, keeping all other Hamiltonian pa-

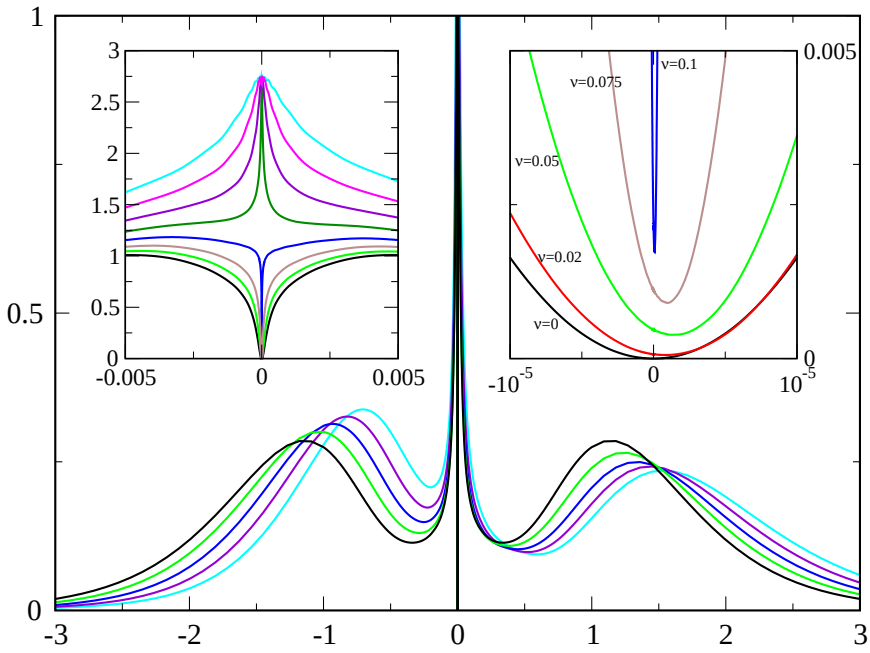

Figure 3.13: Impurity DOS upon increasing the strength of particle-hole symmetry breaking ν starting from the unscreened pseudo-gapped phase ($\nu = 0, 0.05, 0.1$) up to the Kondo screened one ($\nu = 0.15, 0.2$). In the left inset it is shown the low energy part across the UFP (from top to bottom $\nu = 0.2, 0.175, 0.15, 0.125, 0.1, 0.075, 0.05, 0$); notice the analogy with the p-h symmetric case in Fig. 3.6 and 3.7. In the right inset we explicitly show the gradual filling of the pseudo-gap upon increasing ν. [$\Lambda = 2$, $U = 2$, $\Delta_0 = U/(6\pi)$, $J = -0.004$]

rameters fixed. As shown in Fig. 3.13, ν is able to drive the model across the UFP. This result could be foreseen. Indeed ν forces the impurity to accommodate $2 - \nu$ electrons. If $\nu = 1$, the impurity tends to be singly-occupied. Therefore in the Kondo limit it behaves like a spin $S = 1/2$ and pseudo-spin $T = 1/2$ moment, which can be perfectly Kondo-screened and it is moreover stable with respect to little changes of ν with respect to $\nu = 1$. Hence, if the model is at $\nu = 0$ in the pseudo-gap phase, it has to cross a fixed point to reach the large-ν Kondo screened regime. This behavior is quite interesting in connection with DMFT lattice calculations, since it implies that the lattice-model local critical regime, which reflects the single-impurity UFP, may also be attained by doping, as recently confirmed[24].

In conclusion we find that the UFP extends away from the particle-hole symmetric point, $\nu = 0$, giving rise to a whole critical line: $J_*(\nu, \Delta_0, U) < 0$ such that for $J > J_*(\nu, \Delta_0, U)$ complete Kondo screening takes place while for $J < J_*(\nu, \Delta_0, U)$ the impurity is in the unscreened pseudo-gap regime.

Let us briefly discuss the fate of this critical line as particle-hole asymmetry becomes very large. We find that $J_*(\nu, \Delta_0, U)$ decreases by increasing ν, being of order $-T_K$ for $\mu \simeq 0$ and becoming of order $-U$ for large $|\nu|$, thus eventually going outside the region $U \gg |J|, \Delta_0$ we are interested in.

This result can also be physically understood. Let us suppose for instance that the average impurity-occupancy is fixed to be one. Still we keep assuming $U \gg \Delta_0$, thus preventing the occupancy from freely fluctuating around its mean value. We notice that the effective Hubbard repulsion, U_{eff}, acting on the impurity is by definition $U_{eff} \equiv E_0(0) + E_0(2) - 2E_0(1)$, where $E_0(n)$ is the ground-state energy for n-electron configurations.

If $J < 0$, the $n = 2$ ground state has $S = 0$, $T = 1$ and $T_z = 0$, see Eq. (3.5), and we find $U_{eff} = U - 2|J|$. Therefore, if $U \gg |J|$, the impurity effectively behaves like a spin $S = 1/2$ and pseudo-spin $T = 1/2$ moment which, as we said, is Kondo screened. On the contrary, if $J \ll -U$, $U_{eff} \ll 0$ hence the impurity prefers to oscillate between zero and double occupancy to take full advantage of the inverted Hund's rules. In this unconventional mixed-valence regime induced by J, the DOS actually develops a pseudo-gap at the chemical potential. Therefore the critical line transforms for large particle-hole asymmetry into the critical point which separates the local moment from the J-induced mixed valence regime.

A completely different behavior occurs if we introduce instead a T^x perturbation of the form (3.65). Here, as expected, we do not find any jump of the DOS, as clear in Fig. 3.14 where we compare the DOS at the chemical potential in the presence either of (3.63), $h_{p-h} \neq 0$, or (3.65), $h_x \neq 0$. This demonstrates that a perturbation in the particle-hole channel which breaks the orbital $U(1)$ symmetry is relevant at the UFP, unlike (3.63) and (3.64) which instead do not break the $U(1)_{orbit}$ symmetry.

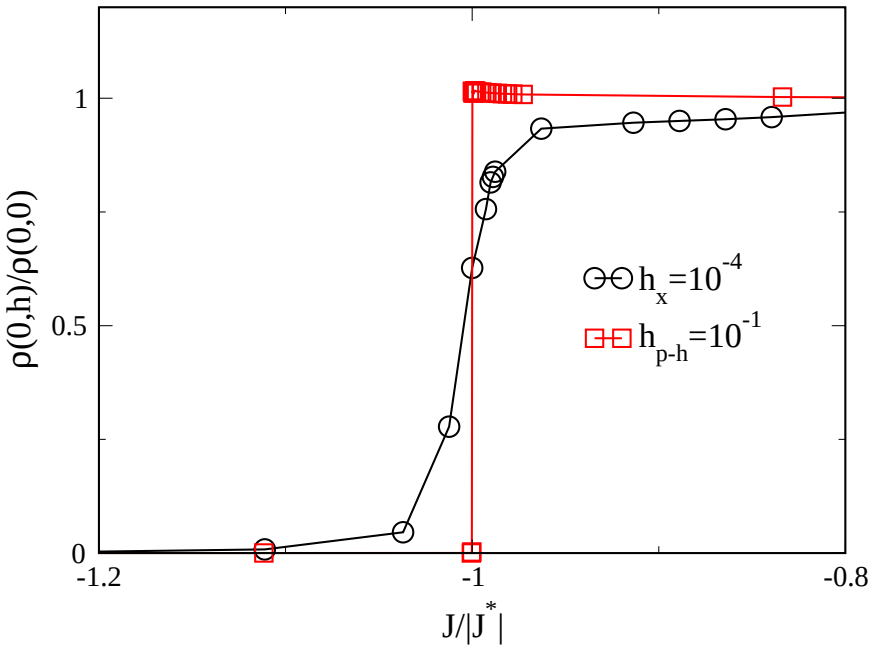

Figure 3.14: Comparison of the DOS values at the chemical potential as function of J either in the presence of a finite particle-hole symmetry breaking h_{p-h}, $\rho(0, h_{p-h})$, or of a T^x symmetry breaking h_x, $\rho(0, h_x)$, normalized to their values at $J = 0$. Notice that h_x, although three order of magnitude smaller than h_{p-h}, washes out the DOS jump contrary to h_{p-h}. [$\Lambda = 2$, $U = 2$, $\Delta_0 = U/(6\pi)$]

3.5 Relevance of the single impurity results in connection with DMFT

Let us now discuss the above results in connection with DMFT. In reality a formal correspondence between single-impurity and lattice models holds strictly only in the limit of large lattice-coordination. Nevertheless we believe that this correspondence, at least close to a Mott transition, may remain valid even beyond that limit, making the single-impurity analysis of much broader interest. Therefore, although inversion of Hund's rules may indeed occur in realistic AIM's or in artificially designed quantum dot devices, here we rather focus on lattice models which map within DMFT into our AIM.

Suppose there is a lattice model which maps in the limit of large lattice-coordination

onto the AIM (3.1) with $J < 0$. If the model is driven towards a Mott metal-insulator transition, the effective AIM is necessarily pushed into a regime in which $T_K \sim |J|$, namely in the critical region around the UFP. As shown in Fig. 3.10, the s-wave scattering amplitude $\mathcal{A}_0^0$ as well as the equally relevant $A_T^{\perp}$ and $A_{ST}^{||}$ are strongly attractive in an entire interval around the UFP. This suggests that the impurity fixed-point instability might transform by DMFT self-consistency into a whole pocket where the model generates spontaneously a bulk symmetry breaking order-parameter along one of the relevant channels. If nesting or Van Hove singularities are absent, it is most likely that the dominant instability will occur in the Cooper channel, the only one which is singular in any dimensions and for any band-structure with a finite density of states at the chemical potential. This has been indeed confirmed by very recent DMFT calculations in Refs. [24, 69].

The other interesting observation is that in the conventional Hund's regime, the Kondo screened phase with $J > 0$, an attraction in the spin-triplet $T = 0$ channel develops, $\mathcal{A}^1 < 0$. In realistic lattice models which map onto the AIM with $J > 0$ in the limit of large lattice-coordination, spin-triplet superconductivity would compete with bulk magnetism. Yet, if magnetism is frustrated, spin-triplet superconductivity might emerge. In particular, since increasing the Hubbard U in the lattice model implies decreasing T_K in the AIM, which is the same as increasing the effective strength of $J > 0$, we should expect that spin-triplet superconductivity is enhanced near the MIT. This has been recently observed by DMFT[69]. However the enhancement of the spin-triplet amplitude is not as dramatic as for the spin-singlet one near the UFP at $J < 0$.

3.5.1 Two-band Hubbard model in the presence of an $e \otimes E$ Jahn-Teller coupling

Let us start by considering a two-band Hubbard model in which each site is Jahn-Teller coupled to a doubly degenerate phonon. The Hamiltonian reads

$$\begin{aligned} H &= -\frac{t}{\sqrt{z}} \sum_{a=1}^{2} \sum_{\sigma} \sum_{<ij>} \left(c_{ai\sigma}^{\dagger} c_{aj\sigma} + H.c. \right) \\ &\quad + \frac{U}{2} \sum_i (n_i - 2)^2 + 2J_H \sum_i \left[(T_i^x)^2 + (T_i^z)^2 \right] \end{aligned}$$

$$+\frac{\omega_0}{2}\sum_i\sum_{a=x,z}\left(q_{ia}^2+p_{ia}^2\right)-g\sum_i\left(q_{ix}\,T_i^x+q_{iy}\,T_i^z\right). \qquad (3.70)$$

Here $-t/\sqrt{z}$ is the hopping matrix element between one site and its z-neighbors and $J_H>0$ is a conventional Hund's exchange. q_{ix} and q_{iz} are the phonon coordinates at site i, p_{ix} and p_{iz} their conjugate momenta, ω_0 the phonon frequency and g the Jahn-Teller coupling. The latter gives rise to a retarded electron-electron interaction whose Fourier transform is

$$g^2\sum_i\frac{\omega_0}{\omega^2-\omega_0^2}\left[T_i^x(\omega)\,T_i^x(-\omega)+T_i^z(\omega)\,T_i^z(-\omega)\right].$$

If the phonon frequency ω_0 is much larger than the quasiparticle bandwidth we can safely neglect the ω-dependence at low energy, so that the phonon-mediated interaction becomes unretarded and given by

$$-\frac{g^2}{\omega_0}\sum_i\left[(T_i^x)^2+(T_i^z)^2\right].$$

Within DMFT the Hamiltonian maps in the limit of large lattice-coordination onto the same AIM model as in Eq. (3.1) upon interchanging the z and y components of $\vec{T}$ and with

$$J=J_H-\frac{g^2}{2\omega_0}, \qquad (3.71)$$

which may be either positive or negative. The case with $J<0$ as well as the starting model realistically including phonons have been recently studied by DMFT[24, 69]. We notice that the superconducting order parameter, in the representation in which the phonon coordinates are x and z, is

$$\langle c^\dagger_{1\mathbf{k}\uparrow}c^\dagger_{1-\mathbf{k}\downarrow}+c^\dagger_{2\mathbf{k}\uparrow}c^\dagger_{2-\mathbf{k}\downarrow}\rangle \qquad (3.72)$$

that does not break time-reversal symmetry if the energies of the band arising from orbital 1 and 2 are not degenerate.

3.5.2 Two-band Hubbard model with single-ion anisotropy

Another realization which may also be physically relevant is the following lattice model:

$$H \;=\; -\frac{t}{\sqrt{z}}\sum_{a=1}^{2}\sum_\sigma\sum_{<ij>}\left(c^\dagger_{ai\sigma}c_{aj\sigma}+H.c.\right)$$

$$+\frac{U}{2}\sum_i (n_i-2)^2 - 2J_H \sum_i \vec{S}_i\cdot\vec{S}_i$$
$$+D\sum_i (S_i^z)^2\,. \tag{3.73}$$

For $J_H > 0$ and $D \neq 0$ this model describes a two-band Hubbard model with conventional Hund's rules, favoring a spin-triplet two-electron configuration, in the presence of a single-ion anisotropy which splits the spin-triplet into a singlet with $S^z = 0$ and a doublet with $S^z = \pm 1$. If $D > 0$, the $S^z = 0$ configuration is favored. Upon interchanging $\vec{S} \leftrightarrow \vec{T}$, this model maps in the $z \to \infty$ limit onto (3.1) with

$$\begin{aligned} J &= -J_H, \\ G &= D - 2J_H. \end{aligned} \tag{3.74}$$

Our analysis suggests that the lattice model with $D > 0$ would still enter a local critical regime before the MIT. Here the tendency towards spontaneous generation of a bulk order parameter should be dramatically enhanced in the particle-hole channels S^x, S^y and $\vec{T}\,S^z$ as well as in the spin-triplet Cooper channel with $S^z = 0$: $c^\dagger_{1\uparrow}\,c^\dagger_{2\downarrow} - c^\dagger_{2\uparrow}\,c^\dagger_{1\downarrow}$.

3.5.3 Two coupled Hubbard planes

Finally let us consider two coupled single-band Hubbard planes described by the Hamiltonian

$$\begin{aligned} H &= -\frac{t}{\sqrt{z}}\sum_{a=1}^{2}\sum_{\sigma}\sum_{<ij>}\left(c^\dagger_{ai\sigma}c_{aj\sigma} + H.c.\right) + \frac{U}{2}\sum_{a,i}\left(n_{ai}-1\right)^2 \\ &\quad + \sum_i J\,\vec{S}_{1i}\cdot\vec{S}_{2i} \;+\; V\,(n_{1i}-1)(n_{2i}-1), \end{aligned} \tag{3.75}$$

where $a = 1, 2$ labels the two planes and $-t/\sqrt{z}$ is the in-plane hopping between one site and its z-neighbors. In the limit $z \to \infty$ the relations between the interaction parameters of the AIM, (3.1) plus (3.13), and those of (3.75) are given in Table 3.3.

In reality it is more interesting to consider the model (3.75) with $J = V = 0$ but in the presence of an inter-plane hopping

$$-t_\perp \sum_{i\sigma}\left(c^\dagger_{1i\sigma}c_{2i\sigma} + H.c.\right). \tag{3.76}$$

Table 3.3: Mapping between the AIM interaction parameters and the two Hubbard plane ones.

AIM	Two Hubbard planes
U	$\frac{1}{2}(U+V)-\frac{1}{8}J$
J	$-\frac{1}{4}J$
G	$U-V+\frac{1}{4}J$

In the limit of large lattice-coordination, this model maps close to the MIT onto a two-orbital AIM with an hybridization width at the chemical potential much smaller than U. Since by the Table 3.3 $G = U$, we can safely project out of the low energy subspace the doublet (3.6). The effective AIM within the impurity subspace which includes the singlet (3.5) and the spin-triplet is

$$\begin{aligned} H_{AIM} &= H_c + J_K \left(\vec{S}_1 + \vec{S}_2\right) \cdot \vec{\mathcal{S}} \\ &\quad + J\, \vec{S}_1 \cdot \vec{S}_2 + J_K \frac{t_\perp}{U} \mathcal{T}^x, \end{aligned} \tag{3.77}$$

where H_c and J_K have been defined in Eqs. (3.1) and (3.10), $\vec{S}_1$ and $\vec{S}_2$ are the impurity spin operators for the singly-occupied orbitals 1 and 2, while $\vec{\mathcal{S}}$ and $\mathcal{T}^x$ are respectively the conduction-electron spin-density operator and x-component of the pseudo-spin density operator, $\vec{\mathcal{T}}$, at the impurity site. The impurity antiferromagnetic exchange, $J = 4t_\perp^2/U$, lowers the energy of the singlet (3.5) with respect to the spin triplet. Therefore J alone might induce an UFP within the phase diagram, just like in our model as well as in the 2IKM. However $t_\perp$ also introduces a $\mathcal{T}^x$ scattering potential at the impurity site, last term in the right hand side of Eq. (3.77), which is known to be relevant at the UFP, as seen in Section 3.4. In this respect $t_\perp$ plays an intriguing role: on one hand it provides a mechanism, the antiferromagnetic exchange J, able to stabilize a non-trivial fixed point, but, in the meantime, it also prevents that fixed point from being reachable. Yet we might wonder whether the critical region around the UFP is completely or only partially washed out. In the latter case we should expect that the physics of the lattice model close to the MIT is still influenced by the UFP, with interesting consequences.

Since the UFP is never reachable, the model always flows to a Fermi liquid fixed

point. In the presence of $t_\perp$ it is more appropriate to introduce the even and odd combinations of the orbitals 1 and 2:

$$\begin{aligned} d_{e\sigma} &= \frac{1}{\sqrt{2}}\left(d_{1\sigma} + d_{2\sigma}\right), \\ d_{o\sigma} &= \frac{1}{\sqrt{2}}\left(d_{1\sigma} - d_{2\sigma}\right), \end{aligned}$$

and correspondingly the even and odd conduction-electron scattering channels. According to what we said in Section 3.4, we expect the phase shifts $\delta_e = -\delta_o$ to be smooth functions of J. If there were no remnant of the UFP, the DOS's should simply show a resonance, the even channel above the chemical potential and the odd channel below it. In reality the behavior of the DOS remains strongly influenced by the UFP, even though never reachable. This is evident in Fig. 3.15, where we draw the DOS of $d_{e\sigma}$, $\rho_e(\epsilon)$, (the odd one is simply obtained by reflection around zero energy) at fixed $t_\perp$ upon varying the hybridization width Δ_0. There is no point at which the DOS jumps at the chemical potential, yet a partly filled asymmetric pseudo-gap remains. In Fig. 3.16 we draw the low-energy difference between the even and odd DOS's, which is also the off-diagonal spectral function $A_{12}(\epsilon)$. $A_{12}(\epsilon)$ shows a low energy feature which has a non-monotonic behavior in Δ_0 and almost develops into a singularity around $\Delta_0 = 0.47$. We think that these results bring to the fore that $t_\perp$ alone is able to drive the model very close to the UFP. In other words the width of the critical region is larger than the energy scale which cut-off the fixed-point singularities, although both are generated by the same $t_\perp$.

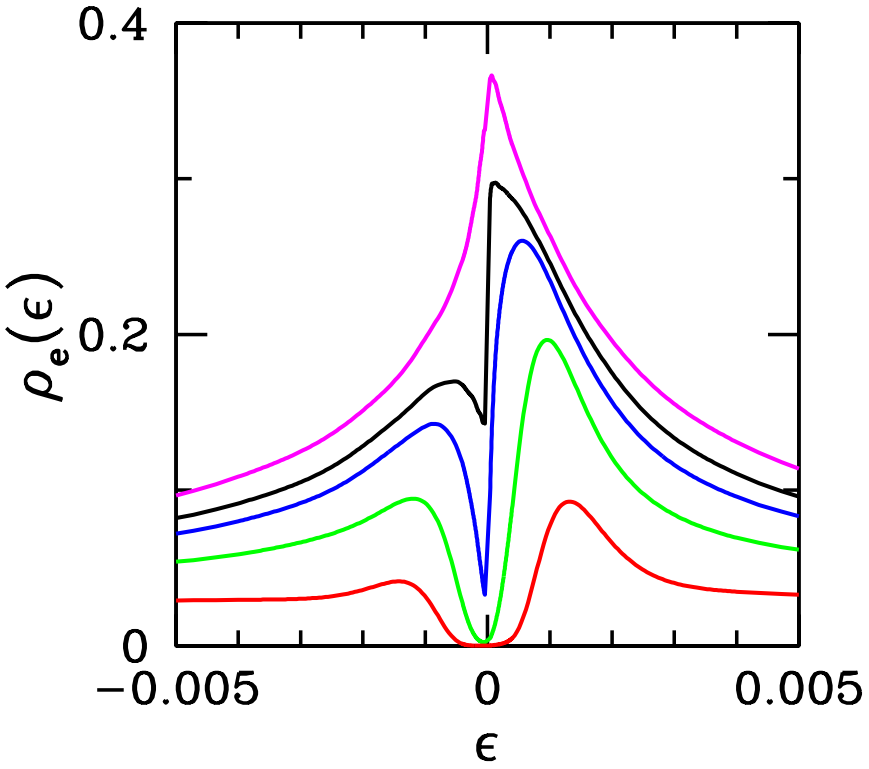

Figure 3.15: Impurity DOS of $d_{e\sigma}$, $\rho_e(\epsilon)$, for the AIM Eq. (3.77). The different curves correspond from the top to the bottom to values of $\Delta_0 = 0.5, 0.47, 0.45, 0.4, 0.3$ with $t_\perp = 0.05$ and $U = 8$. These values correspond to $J_K = 0.08, 0.075, 0.072, 0.064, 0.049$ and $J = 4t_\perp^2/U = 0.00125$. We notice the remnant of an asymmetric pseudo-gap of order J. [$\Lambda = 2$]

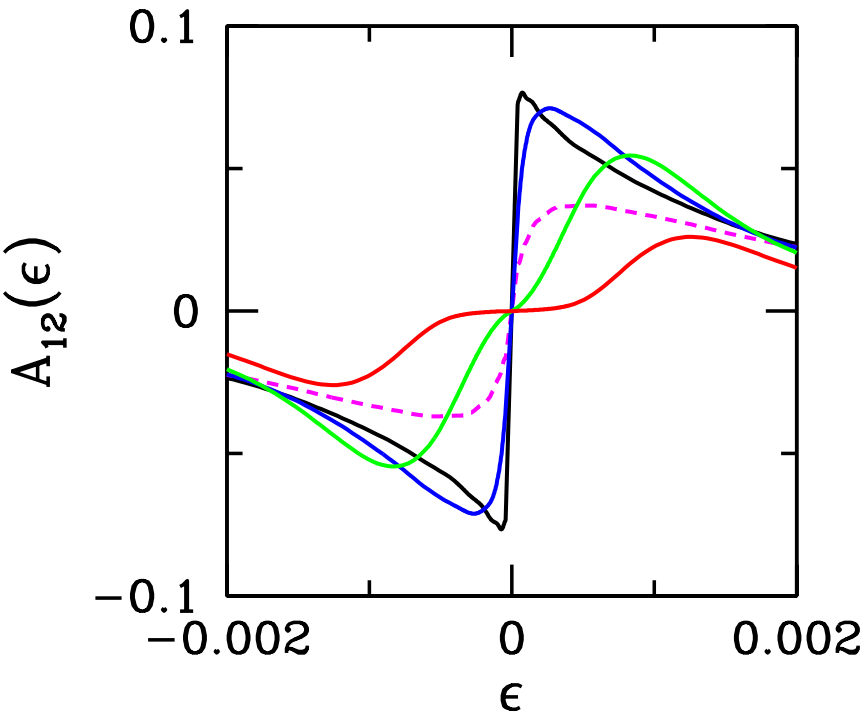

Figure 3.16: Off-diagonal spectral function, $A_{12}(\epsilon)$, with $t_\perp = 0.05$. The different solid curves correspond from the top to the bottom for $\epsilon > 0$ to values of $\Delta_0 = 0.47, 0.45, 0.4, 0.3$, while the dashed curve corresponds to $\Delta_0 = 0.5$. We notice that the low energy feature first moves towards zero energy when Δ_0 increases from 0.3 to 0.47, but from 0.47 to 0.5 it goes back again. Moreover, around $\Delta_0 = 0.47$, $A_{12}(\epsilon)$ is almost singular. [$\Lambda = 2$]

Chapter 4

Three-orbital model

In this Chapter we study another Anderson impurity with a richer and more intriguing phase diagram than that one studied in the previous Chapter. The model is the single-impurity version of the lattice model which has been introduced in Refs. [20, 21] as representative of alkali doped fullerides A_nC_{60} (A=K,Rb,Cs,Na). Fullerenes are molecular conductors made of C_{60} molecules. Each molecule has a threefold degenerate t_{1u} LUMO which hosts the valence electrons of the dopant alkali atoms. According to band structure calculations, A_nC_{60} should be metallic for any $0 < n < 6$. Indeed A_3C_{60} are metals which become superconducting at relatively high temperatures. On the contrary, the only other stable three-dimensional compound, A_4C_{60}, is a non-magnetic insulator.

It has been proposed[20, 21] that the insulating behavior is due to the Mott phenomenon, since the narrow molecular bandwidth, $W \sim 0.5$ eV, is almost three times smaller than the intra-molecule Hubbard repulsion U. The reason why the Mott insulator is non-magnetic, as would derive from Hund's rules, is believed to be the Jahn-Teller effect. Indeed the t_{1u} orbitals are strongly Jahn-Teller coupled to eight fivefold degenerate H_g molecular vibrational modes, which are thought to be the main responsible for superconductivity in the trivalent compounds. Single molecule calculations predict that C_{60}^{-4} has a non-degenerate spin-singlet ground state just because the Hund's rules loose against the Jahn-Teller effect, which in an isolated molecule stays always dynamical. The analysis of Refs. [20, 21] predict that in the Mott insulating phase of A_4C_{60} each C_{60}^{-4} essentially recovers its molecular singlet ground state. Moreover, in accordance with the experimental evidences of no static molecu-

lar distortion, it was argued that the Jahn-Teller effect remains dynamical also in the lattice system.

Accordingly it was later studied by DMFT how the transition into a singlet Mott insulator occurs through a simplified model where the Jahn-Teller effect was forced to stay dynamical by assuming very high vibrational frequencies. In this limit, the so-called anti-adiabatic regime, the Jahn-Teller coupling effectively reduces to a non-retarded electron-electron interaction of the same form as the standard exchange splitting but with opposite sign, thus leading to an inversion of the conventional Hund's rules. Unexpectedly it was found that a superconducting phase intrudes between the metal and the non-magnetic Mott insulator[22], with quite unusual properties[23].

It was actually conjectured[22] that this result might be intimately connected with the Anderson impurity model onto which the lattice model maps by DMFT. Indeed the Anderson impurity includes, besides the Kondo exchange, also a competing intra-impurity screening mechanism, the inverted Hund's coupling, just like the model we studied in Chapter 3. In view of our previous results, which have been confirmed by a DMFT calculation, this conjecture seems very plausible. Indeed we will show that an Anderson impurity model for a C_{60}^{-4} has a very similar phase diagram as the two-orbital model we have previously analyzed. Namely it includes a non Fermi liquid fixed point separating a conventional Kondo screened phase from an unscreened one.

Much more intriguing is what we find for the more interesting case of a C_{60}^{-3} impurity. Here the inverted Hund's coupling is not able to get rid of all the impurity degeneracy, so that the phase diagram still includes an unstable fixed point which separates a Kondo screened phase from a stable non-Fermi liquid phase, analogous of an overscreened Kondo fixed point. This result should have interesting consequences within a DMFT calculation, which has so far not been performed, and might be relevant to explain the properties of superconducting A_3C_{60} compounds.

Due to the higher degeneracy of the model the computational effort needed is much higher and the complexity of some descriptions grows accordingly. For this reason we did not perform an effective Hamiltonian description of the Fermi liquid phases to support the Fermi liquid theory results on the scattering amplitudes as we did in the two-orbital model but nevertheless we present the "guessed" scattering amplitudes.

4.1 The Model Hamiltonian

The model Hamiltonian is

$$\begin{aligned} H &= H_U + H_J + H_c + H_{hyb} \\ &= \frac{U}{2}\left(n_d - n_0\right)^2 - J\left[2\vec{S}\cdot\vec{S} + \frac{1}{2}\vec{T}\cdot\vec{T}\right] \\ &\quad + \sum_{\mathbf{k}a\alpha} \epsilon_{\mathbf{k}}\, c^\dagger_{\mathbf{k}a\alpha} c_{\mathbf{k}a\alpha} \\ &\quad + \sum_{\mathbf{k}a\alpha} V_d \left(c^\dagger_{\mathbf{k}a\alpha} d_{a\alpha} + d^\dagger_{a\alpha} c_{\mathbf{k}a\alpha}\right). \end{aligned} \tag{4.1}$$

where the notation is the same as for Eq. (3.1), with the difference that now the orbital index runs over the three orbitals and represents the corresponding value of the z-components of the orbital momentum $a = -1, 0, 1$. $\vec{S}$ is the total spin of the impurity and $\vec{T}$ is the total orbital angular momentum. Instead of using a parameter ν to control the deviations from the particle-hole symmetry as in Eq. (3.1), we introduce here explicitly a parameter n_0 which represents the average number of electrons on the impurity. The particle-hole symmetric case corresponds to $n_0 = 3$.

The symmetry of the problem in the absence of H_J is $U(1)_{charge} \times SU(6)$ and it is lowered down to $U(1)_{charge} \times SU(2)_{spin} \times SU(2)_{orbit}$ by H_J. Contrary to the two-orbital model, the $SU(2)_{orbit}$ is not broken down.

As previously, the term H_J mimic the Hund's rule or the dynamic Jahn-Teller effect depending in the sign of J. In particular $J > 0$ corresponds to the usual Hund's rule coupling while $J < 0$ derives from a $t_u \otimes H_g$ Jahn-Teller effect.

4.2 Perturbative regimes

Before interpreting the NRG results we try to understand what will be the behavior of the system in the large J limit, where we can use perturbation theory to guess the answer. Due to the complication of the model with three orbitals this task is now more complicated and requires a more systematic approach.

First of all, let us focus on the large U limit, such that the number of electrons on the impurity is fixed by the parameter n_0. We will analyze the cases $n_0 = 3$ (particle-hole symmetry) and $n_0 = 2$ (equivalent also to $n_0 = 4$). It is useful to change the representation of the model to a tight-binding chain similar to the Wilson chain but

without the logarithmic discretization of the band energy. To avoid confusion with the symbol n_0, indicating the average occupation of the impurity, the chain starts with site 1. The procedure is the same as in Eqs. (2.4-2.7) and, if we assume a particle-hole symmetric band, the transformed Hamiltonian is

$$\begin{aligned} H &= \frac{U}{2}\left(n_d - n_0\right)^2 - J\left[2\vec{S}_d\cdot\vec{S}_d + \frac{1}{2}\vec{T}_d\cdot\vec{T}_d\right] \\ &\quad + t\left(c^\dagger_{1,a\alpha}d_{a\alpha} + d^\dagger_{a\alpha}c_{1,a\alpha}\right) \\ &\quad + \sum_{n=1}^{\infty} t_n\,\left(c^\dagger_{n,a\alpha}c_{n+1,a\alpha} + h.c.\right) \end{aligned} \tag{4.2}$$

where we added the subscript d to impurity spin and orbital momentum for clarity.

Once the charge fluctuations are ruled out by the large value of U, we can perform a Schrieffer-Wolff transformation and obtain an effective Kondo-like model

$$\begin{aligned} H_K &= -J\left[2\vec{S}_d\cdot\vec{S}_d + \frac{1}{2}\vec{T}_d\cdot\vec{T}_d\right] \\ &\quad + \frac{4t^2}{U}\sum_{ab}\sum_{\alpha\beta} c^\dagger_{1,a\alpha}c_{1,b\beta}d^\dagger_{b\beta}d_{a\alpha} \\ &\quad - \frac{2t^2}{U}\sum_{a\alpha}\left(c^\dagger_{1,a\alpha}c_{1,a\alpha} + d^\dagger_{a\alpha}d_{a\alpha}\right) \end{aligned} \tag{4.3}$$

$$\begin{aligned} H &= H_K + H_{cond} \\ &= H_K + \sum_{n=1}^{\infty} t_n\,\left(c^\dagger_{n,a\alpha}c_{n+1,a\alpha} + h.c.\right). \end{aligned} \tag{4.4}$$

The Kondo coupling can be written in terms of particle-hole operators with well defined spin and orbital momentum of the impurity and of the first site of the chain. These operators with orbital momentum l and z-component λ and with spin s and z-component σ are defined through

$$\left\{c^\dagger\otimes c\right\}_{l\lambda,s\sigma} = \sum(-1)^{k-1}C^{l\lambda}_{1j,1-k}(-1)^{\beta-1/2}C^{s\sigma}_{1/2\alpha,1/2-\beta}c^\dagger_{j\alpha}c_{k\beta} \tag{4.5}$$

where $C^{c\gamma}_{a\alpha,b\beta}$ are the Clebsh-Gordan coefficients and summation over repeated indices is implied. The adjoint operator satisfies

$$\left(\left\{c^\dagger\otimes c\right\}_{l\lambda,s\sigma}\right)^* = (-1)^{-\lambda}(-1)^{-\sigma}\left\{c^\dagger\otimes c\right\}_{l\lambda,s\sigma} \tag{4.6}$$

and the inverse of relation (4.5) is

$$c^\dagger_{j\alpha}c_{k\beta} = \sum (-1)^{1-k} C^{l\lambda}_{1j,1-k} (-1)^{1/2-\beta} C^{s\sigma}_{1/2\alpha,1/2-\beta} \left\{c^\dagger \otimes c\right\}_{l\lambda,s\sigma}. \qquad (4.7)$$

Making use of these definitions we can rewrite (4.3), apart from a constant, as

$$\begin{aligned} H_K &= \frac{4t^2}{U}\hat{J}_K + \frac{2t^2}{3U}(n_d-3)(n_1-3) \\ &\quad -J\left[2\vec{S}_d\cdot\vec{S}_d + \frac{1}{2}\vec{T}_d\cdot\vec{T}_d\right] \end{aligned} \qquad (4.8)$$

where $n_i = \sum_{a\alpha} c^\dagger_{i,a\alpha}c_{i,a\alpha}$ and

$$\hat{J}_K = \sum_{l=0}^{2}\sum_{\lambda=-l}^{l}\sum_{s=0}^{1}\sum_{\sigma=-s}^{s}(1-\delta_{l0}\delta_{s0})(-1)^{-\lambda-\sigma}\left\{c^\dagger_1\otimes c_1\right\}_{l\lambda,s\sigma}\left\{d^\dagger\otimes d\right\}_{l-\lambda,s-\sigma}. \qquad (4.9)$$

Given this expression for H_K, we can now further assume that $|J| \gg T_K$. Hence the impurity is frozen in the most favorable configuration (for that number of electrons hosted) before the Kondo effect can take place. This implies that the Kondo exchange can only involve the remaining degenerate degrees of freedom. At this stage we have to fix n_0 and the sign of J and find the lowest energy configuration of $\hat{J}_K$ and its degeneracy to guess the behavior of the system in the large $|J|$ regime. To obtain the energy of the various configurations we exploit all the symmetries of the problem classifying the states by the following conserved quantities: number of electrons on the impurity and on the first shell of the chain (represented through the charges Q_d and Q_1 respectively, defined as the deviation of the number of particles from the half-filled condition[1]), total orbital momentum T and corresponding z-component τ, total spin S and corresponding z-component Σ, orbital momentum and spin of the impurity, T_d and S_d, and of the first shell, T_1 and S_1. A generic state is then labeled by

$$\begin{aligned} &|Q_1, Q_d; T, \tau, T_1, T_d; S, \Sigma, S_1, S_d\rangle = \\ &= \sum C^{T\tau}_{T_1\tau_1,T_d\tau_d} C^{S\Sigma}_{S_1\Sigma_1,S_d\Sigma_d} |Q_1; T_1\tau_1; S_1\Sigma_1\rangle |Q_d; T_d\tau_d; S_d\Sigma_d\rangle. \end{aligned} \qquad (4.10)$$

From this expression for the states it is possible to obtain the matrix elements of $\hat{J}_K$

$$\langle Q_1, Q_d; T, \tau, T_1', T_d'; S, \Sigma, S_1', S_d'|\hat{J}_K|Q_1, Q_d; T, \tau, T_1, T_d; S, \Sigma, S_1, S_d\rangle =$$

[1]Notice that in this Chapter we use a definition of the charge that corresponds to twice the charge defined in Chapter 3. In the present case the z-component of the hypercharge vector will be $I_z = Q/2$.

$$= \sum_{(l,s)\neq(0,0)} (-1)^{-T+3T_1+2T_d+T_1'+2T_d'} \begin{Bmatrix} T_d & T_1 & T \\ T_1' & T_d' & l \end{Bmatrix} [(2T_1+1)(2T_d+1)(2T_1'+1)(2T_d'+1)]^{1/4}$$

$$(-1)^{-S+3S_1+2S_d+S_1'+2S_d'} \begin{Bmatrix} S_d & S_1 & S \\ S_1' & S_d' & s \end{Bmatrix} [(2S_1+1)(2S_d+1)(2S_1'+1)(2S_d'+1)]^{1/4}$$

$$\langle Q_1; T_1', S_1' || \left\{ c_1^\dagger \otimes c_1 \right\}_{l,s} || Q_1; T_1, S_1 \rangle \langle Q_d; T_d', S_d' || \left\{ d^\dagger \otimes d \right\}_{l,s} || Q_d; T_d, S_d \rangle \quad (4.11)$$

where the symbols in curly brackets in the second and third rows are the $6j$ symbols and the matrix elements in the last row are called reduced matrix elements and are defined in Appendix B. A detailed derivation of this calculation is presented in that Appendix.

Now we move to analyze the different possible cases.

4.2.1 Three electrons on the impurity

We fix $n_0 = 3$ and consider the limits $J \gg T_K$ and $J \ll -T_K$. If $n_0 = 3$ the Hilbert space $\mathcal{H}_{imp}$ of the impurity contains the following subspaces (T_d, S_d)

$$\mathcal{H}_{imp} = \left(2, \frac{1}{2}\right) \oplus \left(1, \frac{1}{2}\right) \oplus \left(0, \frac{3}{2}\right). \quad (4.12)$$

If $J \gg T_K$, corresponding to the conventional Hund's effect, the impurity is quenched in the states with $S_d = 3/2$ and $T_d = 0$ that minimizes H_J. The only non-vanishing reduced matrix elements of $\hat{J}_K$ between these states are those involving $\left\{ d^\dagger \otimes d \right\}_{0,1}$ and hence H_K reduces to

$$H_K = \frac{8t^2}{3U} \vec{S}_d \cdot \vec{S}_1. \quad (4.13)$$

This means that in this regime the impurity behaves as a spin-$3/2$ local moment antiferromagnetically coupled to the conduction electrons. Since three channels interacting with a spin-$3/2$ realize a perfectly screened Kondo model, we expect a low-energy Kondo screened phase with a phase shift $\delta = \pi/2$ per spin and conduction channel.

Instead if $J \ll -T_K$, corresponding to the inverted Hund's rule, the impurity freezes in the configuration with $S_d = 1/2$ and $T_d = 1$ and the allowed combinations of (l, s) are $(1, 0)$, $(0, 1)$ and $(2, 1)$. To understand what happens in this case we can

assume that $4t^2/U$ is much larger than the conduction bandwidth. Hence we can diagonalize H_K first and treat H_{cond} as a perturbation.

The ground state of H_K for $J \ll -T_K$ can be calculated from the matrix elements of $\hat{J}_K$ and is a total singlet $T = 0, S = 0$. This configuration is realized by screening the impurity using first-site configurations with quantum numbers $T_1 = 1$ and $S_1 = 1/2$. States of the first shell with these quantum numbers can be realized in three different ways, either with one, or with three or finally with five electrons. Let us label the different states by the number of electrons hosted on the first shell:

$$|n_1 = 1\rangle \equiv |Q_1 = -1, Q_d = 0; T = 0, T_1 = 1, T_d = 1; S = 0, S_1 = 1/2, S_d = 1/2\rangle$$

$$|n_1 = 3\rangle \equiv |Q_1 = 0, Q_d = 0; T = 0, T_1 = 1, T_d = 1; S = 0, S_1 = 1/2, S_d = 1/2\rangle$$

$$|n_1 = 5\rangle \equiv |Q_1 = +1, Q_d = 0; T = 0, T_1 = 1, T_d = 1; S = 0, S_1 = 1/2, S_d = 1/2\rangle$$

These states are degenerate in energy and can be viewed as realizing a spin-1 in the charge sector. Indeed we can associate to each state a value of the z-component of a hypercharge-1 vector $\vec{I}$, $|n_1 = 1\rangle = |-1\rangle$, $|n_1 = 3\rangle = |0\rangle$ and $|n_1 = 5\rangle = |+1\rangle$.

This additional degeneracy that remains unscreened must then be screened by the next shell of the chain. Indeed by second order perturbation theory in the hopping t_1 connecting shell 1 to shell 2 we obtain an effective term proportional to

$$\propto \frac{t_1^2}{\frac{4t^2}{U}} \vec{I} \cdot \vec{I}(2) \tag{4.14}$$

where $\vec{I}(2)$ is the hypercharge operator on the second shell, defined by

$$I_z(2) = \frac{1}{2}\left(n_2 - 3\right),$$

$$I^+(2) = c^\dagger_{2,+1\uparrow} c^\dagger_{2,-1\downarrow} + c^\dagger_{2,-1\uparrow} c^\dagger_{2,+1\downarrow} - c^\dagger_{2,0\uparrow} c^\dagger_{2,0\downarrow},$$

$$I^-(2) = \left(I^+(2)\right)^\dagger.$$

The procedure can be summarized in this way. Given the hierarchy of energy scales $U \gg |J| \gg 4t^2/U \gg t_1$, the first effect that takes place is the quenching of charge fluctuations due to the large Coulomb repulsion. After that, the interaction J selects the ground state of the impurity and then the H_K term forces the first shell of conduction electrons to screen the remaining degrees of freedom. The last effect is the screening of the left-over degrees of freedom by the remaining conduction electrons.

The low-energy effective Hamiltonian (4.14) corresponds to a Kondo Hamiltonian in the charge sector and in particular to a spin-1 three-channel Kondo model, hence an over-screened model. From this we can expect that, if the description is correct, the low energy *stable* fixed point of the model has non-Fermi liquid character.

The procedure we employed to guess the result is not general but, as we will see, it captures the essential physics of the model and what we find by NRG is indeed a non-Fermi liquid stable phase in the negative J region in the particle-hole symmetric case.

In addition, we can argue along the line of the two-orbital model and infer the presence of at least one unstable fixed point separating the two regions of Kondo screening and non-Fermi liquid. This UFP is again a non-Fermi liquid fixed point as in the two-orbital model.

The last issue we can discuss in this preliminary and naïve approach is the stability against particle-hole symmetry breaking of this non-Fermi liquid phase. A particle-hole symmetry breaking removes the degeneracy between the states $|n_1 = 1\rangle$, $|n_1 = 3\rangle$ and $|n_1 = 5\rangle$ and may correspond to adding two kind of terms. The first is proportional to

$$I_z \tag{4.15}$$

and is the analog of a local magnetic field acting on the impurity in the spin language. The second term is proportional to

$$I_z^2. \tag{4.16}$$

It is known from [44] that, while a perturbation like (4.16) is not relevant near the non-Fermi liquid fixed point of the multi-channel Kondo model, a magnetic field like (4.15) is relevant and destroys the non-Fermi liquid nature of the system. From this we can conclude that the non-Fermi liquid phase, if present, would be unstable with respect to particle-hole symmetry breaking and would eventually flow to a Fermi liquid fixed point. Yet we still expect that an UFP separates the two different Fermi liquid fixed points.

4.2.2 Two electrons on the impurity

Let us consider now the cases in which the impurity hosts two electrons and $J \gg T_K$ or $J \ll -T_K$. The impurity Hilbert space contains the subspaces (T_d, S_d)

$$\mathcal{H}_{imp} = (0,0) \oplus (2,0) \oplus (1,1)\,. \tag{4.17}$$

The simpler case is when $J \ll -T_K$, since the impurity is locked by J in the total singlet configuration with $S_d = 0$ and $T_d = 0$. Hence the Kondo coupling is completely ineffective, there are no allowed combinations of (l, s) that give non-zero matrix elements for $\hat{J}_K$. The Kondo effect cannot take place and only the potential scattering

$$-\frac{2t^2}{3U}(n_1 - 3) \tag{4.18}$$

remains.

On the other hand, when $J \gg T_K$ the impurity is forced in the configuration with $S_d = 1$ and $T_d = 1$ and all the combinations (l, s) are allowed. We can argue along the lines of the case $n_0 = 3$, $J \ll -T_K$, diagonalize H_K first and then treat the conduction Hamiltonian as a perturbation. Once again the ground state of H_K is a total singlet that can be realized with two different configurations of the first shell electrons, namely using two or four electrons. These two configurations can be interpreted as a hyperspin-1/2 in the hypercharge sector and this suggest that the effective problem can be interpreted as a hyperspin-$1/2$ three-channel Kondo model. As in the $n_0 = 3$, $J \ll -T_K$ case, this model is over-screened but now there is also a potential scattering term $-2t^2/3U(n_1 - 3)$ that breaks explicitly the particle-hole symmetry. As we have seen, this term corresponds to a local magnetic field applied to the impurity and spoils completely the non-Fermi liquid fixed point of the over-screened Kondo model. Thus we expect that the stable low energy fixed point is again Fermi liquid-like.

The different properties of the two phases found for $J \ll -T_K$ and $J \gg T_K$ suggests that there can be an UFP in between. If the UFP occurring in the three-electron case is not spoiled by the particle-hole symmetry breaking it is reasonable to argue that there is a line of fixed points connecting those at $n_0 = 3$ and $n_0 = 2$.

4.3 Analysis of the three electrons case

The NRG analysis of the three-orbital model is similar to that performed in the two-orbital model. The discretized Hamiltonian of the length N system is

$$\begin{aligned} H_N &= \Lambda^{(N-1)/2}\Bigg\{ \sum_{n=0}^{N-1} \Lambda^{-n/2}\xi_n \left(f^\dagger_{na\alpha} f_{(n+1)a\alpha} + f^\dagger_{(n+1)a\alpha} f_{na\alpha} \right) \\ &\quad + \tilde{\Delta}_0^{1/2} \left(f^\dagger_{0a\alpha} d_{a\alpha} + d^\dagger_{a\alpha} f_{0a\alpha} \right) \\ &\quad + \frac{\tilde{U}}{2} \left(n_d - n_0 \right)^2 - \tilde{J} \left[2\vec{S}\cdot\vec{S} + \frac{1}{2}\vec{T}\cdot\vec{T} \right] \Bigg\}. \end{aligned} \tag{4.19}$$

Here $\tilde{U} = C_\Lambda\, U$, $\tilde{J} = C_\Lambda\, J$, $\tilde{\Delta}_0 = C_\Lambda^2 \frac{2\Delta_0}{\pi}$, $C_\Lambda = \left(\frac{2\Lambda}{1+\Lambda}\right)$ and the unit of energy is half the conduction bandwidth. We restrict ourselves to the large U limit and, fixing Δ_0, we span the phase diagram varying J.

The outcome of the analysis can be summarized by Fig. 4.1, where the spectrum of the system for odd N is plotted as a function of the length of the Wilson chain. The phase space is divided in two regions separated by a critical value $J^* < 0$. In Fig. 4.1 the left panel corresponds to a value J smaller than J^* but close to it. Conversely, the right panel describes the spectrum of the system close to the critical value with J larger than J^*. It is immediately clear that the asymptotic behavior of the system is completely different in the two phases.

For $J > J^*$ the asymptotic low temperature spectrum is that of a free chain with a $\pi/2$ phase shift. This is the signature of the Kondo effect: the first shell screens the impurity and becomes inaccessible to the conduction electrons. This is clear from the large degeneracy of the ground state of the odd N chain (that has an even number of sites). This asymptotic behavior characterizes the system for every $J > J^*$ and confirms the analysis based on the perturbative large J regime.

The phase we found for $J < J^*$ is immediately recognizable as a non-Fermi liquid due to the non-uniform spacing of the levels. In this regime the naïve analysis of the previous Section predicts that the fixed point should resemble that of an over-screened Kondo model with hypercharge replacing the spin. Indeed this is the case, further supporting our preliminary analysis.

As in the two-orbital case, for J close to J^* there is a crossover region in which the system is close to an unstable fixed point. Also in this case the fixed point has

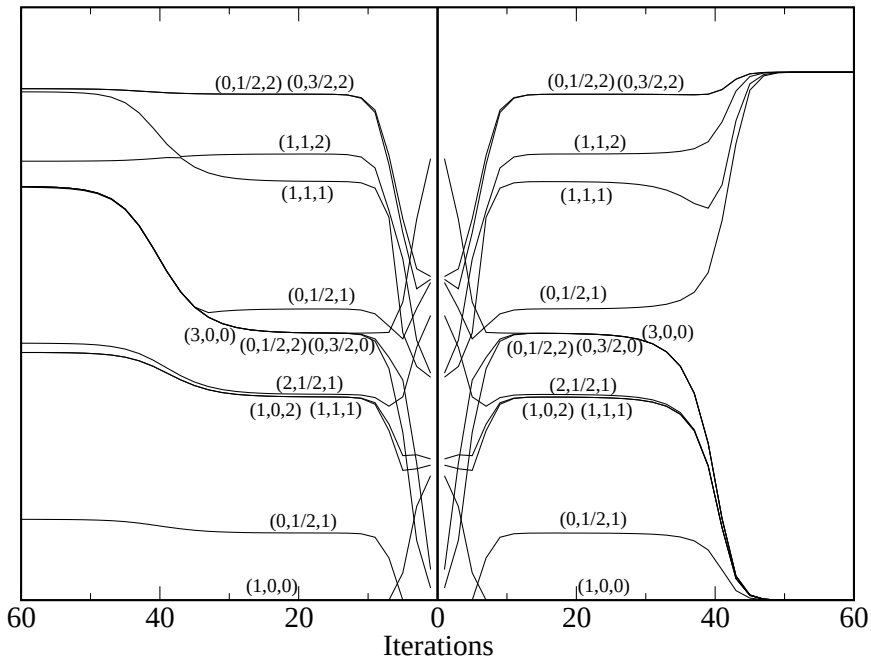

Figure 4.1: Lowest energy levels versus the chain size N (odd). The levels are labeled by the quantum numbers (Q, S, T). The left/right panels correspond to a deviation $\delta J/J^* = \pm 2 \cdot 10^{-4}$ from the fixed point value J^*. [$\Lambda = 5$, $U = 2$, $\Delta_0 = U/(6\pi)$, $J = -0.03366$ (left), $J = -0.033655$ (right)]

non-Fermi liquid properties but it is also clearly different from the *stable* fixed point found for $J < J^*$.

From the NRG spectra we cannot extract more information, mainly due to the presence of the non-Fermi liquid fixed points. Hence we resort to CFT to describe the fixed point of this model. As we have seen, the power of CFT consists in the possibility of describing non-Fermi liquid fixed point in a rather natural way. To employ this technique we have to identify the relevant symmetries of the model. The symmetries of the Kondo model (4.4) onto which the model (4.1) transforms in the large U limit correspond to the usual three sectors: charge, spin and orbital momentum. The first sector is described by a $U(1)$ theory with conformal anomaly $c = 1$. The spin sector symmetry corresponds to $SU(2)_3$ where the subscript indicates the Kac-Moody level and is described by a theory with conformal anomaly $c = 9/5$. The orbital sector is described by an $SU(2)_8$ theory with $c = 12/5$.

Since the conformal anomaly is an invariant of the theory, the sum of the building block theories corresponding to the various symmetries must add up to the value of the original theory. In this case the conformal anomaly of the full theory is $c = 6$ corresponding to a theory with six complex fermions. The sum of the conformal anomaly of the theories in which we decomposed the original problem is less than 6, hence we are missing some part of the description. The difference in the conformal anomaly is equal to $4/5$, meaning that the missing part is a minimal model.

A conformal anomaly $c = 4/5$ corresponds to the minimal model $\mathcal{M}(6, 5)$ whose Kac table is

3	13/8	2/3	1/8	0
7/5	21/40	1/15	1/40	2/5
2/5	1/40	1/15	21/40	7/5
0	1/8	2/3	13/8	3

There are two theories with $c = 4/5$. One is the tetracritical Ising model that corresponds to the diagonal theory of $\mathcal{M}(6, 5)$. The other is the three-state Potts model. This theory has an additional symmetry connected with an extended W-algebra and its primary fields form a subset of the primary fields of the $\mathcal{M}(6, 5)$ model[57, 70–72].

To decide which of the two is the correct theory we can notice that the symmetry of the free fermion system, i.e. the system where the impurity is absent, is $SO(12)$ or, equivalently, $U(6)$. In order to describe this system in the presence of the impurity we can decompose the total symmetry group into a product of lower symmetry groups. For instance, the $U(6)$ group can be decomposed into $SU(2)_{3,spin} \times SU(2)_{3,hypercharge} \times SU(2)_{8,orbit}$. The conformal anomaly of both the descriptions correctly adds up to 6. This procedure is called "conformal embedding".

This symmetry would survive after the introduction of the impurity if the Coulomb term $U/2(n_d - 3)^2 = 2UI_{z,d}^2$ would not be present. Indeed the Coulomb term lowers the hypercharge symmetry to the $U(1)$ subgroup. We can thus further decompose the hypercharge symmetry into the product of the $U(1)$ subgroup and of the coset

$$\frac{SU(2)_3}{U(1)} = Z_3 \tag{4.20}$$

which is the Potts model.

We briefly summarize the operators in each of the theories together with their scaling dimension

- In presence of three conduction channels the $U(1)$ theory has six primary fields corresponding to charges $Q = 0, \ldots, 5$ and dimensions $x_Q = Q^2/12$.

- The $SU(2)_3$ spin theory has, apart from the identity, three primary fields $\phi^S_{j_S}$ with quantum numbers $j_S = 1/2, 1, 3/2$ and dimensions

$$x_{j_S} = \frac{j_S(j_S+1)}{5} = \frac{3}{20}, \frac{2}{5}, \frac{3}{4} \tag{4.21}$$

  respectively.

- The $SU(2)_8$ orbital sector has the identity and other four primary fields $\phi^T_{j_T}$ with quantum numbers $j_T = 1, 2, 3, 4$ and dimensions

$$x_{j_T} = \frac{j_T(j_T+1)}{10} = \frac{1}{5}, \frac{3}{5}, \frac{6}{5}, 2 \tag{4.22}$$

  respectively.

- The primary operators of the Potts sector are listed here with their scaling dimensions

ϕ_P	x_P
I	0
W	3
ϵ	2/5
ϵ'	7/5
σ	1/15
$\bar{\sigma}$	1/15
Z	2/3
$\bar{Z}$	2/3

  The primary fields of the model correspond to fields in the odd columns of the Kac table of $\mathcal{M}(6,5)$. Notice that there are two operators (σ and Z) that appear twice because they are related by charge conjugation. Furthermore operators whose dimensions differ by integers belong to the same conformal tower. This is the case for ϵ and ϵ' and for I and W.

The fusion rules for the $SU(2)_k$ primary fields are

$$\phi_j \phi_{j'} = \sum_{l=|j-j'|}^{\min(j+j',k-j-j')} \phi_l. \tag{4.23}$$

For the Potts model we will need the fusion rules of the primary fields not only among themselves but also with operators in the $\mathcal{M}(6,5)$ Kac table that are not contained in the theory (those lying in the even columns). Hence we list all the fusion rules of all the fields in the $\mathcal{M}(6,5)$ table. The operators in the even columns are indicated by their scaling dimension.

$$\begin{aligned}
\frac{1}{8} \times \frac{1}{8} &= I + Z \\
\frac{1}{8} \times Z &= \frac{1}{8} + \frac{13}{8} \\
\frac{1}{8} \times \frac{13}{8} &= Z + W \\
\frac{1}{8} \times W &= \frac{13}{8} \\
\frac{1}{8} \times \epsilon &= \frac{1}{40} \\
\frac{1}{8} \times \frac{1}{40} &= \epsilon + \sigma \\
\frac{1}{8} \times \sigma &= \frac{1}{40} + \frac{21}{40} \\
\frac{1}{8} \times \frac{21}{40} &= \sigma + \epsilon' \\
\frac{1}{8} \times \epsilon' &= \frac{21}{40}
\end{aligned}$$

$$\begin{aligned}
Z \times Z &= \bar{Z} \\
Z \times \bar{Z} &= I + W \\
Z \times \frac{13}{8} &= \frac{1}{8} + \frac{13}{8} \\
Z \times W &= Z \\
Z \times \epsilon &= \sigma \\
Z \times \frac{1}{40} &= \frac{1}{40} + \frac{21}{40}
\end{aligned}$$

$$
\begin{aligned}
Z \times \sigma &= \bar{\sigma} \\
Z \times \bar{\sigma} &= \epsilon + \epsilon' \\
Z \times \frac{21}{40} &= \frac{1}{40} + \frac{21}{40} \\
Z \times \epsilon' &= \sigma
\end{aligned}
$$

$$
\begin{aligned}
\frac{13}{8} \times \frac{13}{8} &= I + Z \\
\frac{13}{8} \times W &= \frac{1}{8} \\
\frac{13}{8} \times \epsilon &= \frac{21}{40} \\
\frac{13}{8} \times \frac{1}{40} &= \sigma + \epsilon' \\
\frac{13}{8} \times \sigma &= \frac{1}{40} + \frac{21}{40} \\
\frac{13}{8} \times \frac{21}{40} &= \epsilon + \sigma \\
\frac{13}{8} \times \epsilon' &= \frac{1}{40}
\end{aligned}
$$

$$
\begin{aligned}
W \times W &= I \\
W \times \epsilon &= \epsilon' \\
W \times \frac{1}{40} &= \frac{21}{40} \\
W \times \sigma &= \sigma \\
W \times \frac{21}{40} &= \frac{1}{40} \\
W \times \epsilon' &= \epsilon
\end{aligned}
$$

$$
\begin{aligned}
\epsilon \times \epsilon &= I + \epsilon' \\
\epsilon \times \frac{1}{40} &= \frac{1}{8} + \frac{21}{40} \\
\epsilon \times \sigma &= \sigma + Z \\
\epsilon \times \frac{21}{40} &= \frac{1}{40} + \frac{13}{8} \\
\epsilon \times \epsilon' &= \epsilon + W
\end{aligned}
$$

$$
\frac{1}{40} \times \frac{1}{40} = I + \sigma + \epsilon' + Z
$$

$$
\begin{aligned}
\frac{1}{40}\times\sigma &= \frac{1}{8}+\frac{13}{8}+\frac{1}{40}+\frac{21}{40}\\
\frac{1}{40}\times\frac{21}{40} &= \sigma+\epsilon+Z+W\\
\frac{1}{40}\times\epsilon' &= \frac{1}{40}+\frac{13}{8}
\end{aligned}
$$

$$
\begin{aligned}
\sigma\times\sigma &= \bar{\sigma}+\bar{Z}\\
\sigma\times\bar{\sigma} &= I+\epsilon+\epsilon'+W\\
\sigma\times\frac{21}{40} &= \frac{1}{8}+\frac{13}{8}+\frac{1}{40}+\frac{21}{40}\\
\sigma\times\epsilon' &= \sigma+Z
\end{aligned}
$$

$$
\begin{aligned}
\frac{21}{40}\times\frac{21}{40} &= I+\sigma+\epsilon'+Z\\
\frac{21}{40}\times\epsilon' &= \frac{1}{8}+\frac{21}{40}
\end{aligned}
$$

$$
\epsilon'\times\epsilon' = I+\epsilon'
$$

Now that we identified the relevant symmetries we have to find a simple boundary condition. The natural choice corresponds to the chain used in the Wilson NRG when the impurity is decoupled. That system has open boundary conditions at the two end of the chain and, if the Fermi level lies between two energy levels, it has a non-degenerate ground state. Imposing these boundary conditions, the spectrum of the free fermions can be easily obtained. In Table 4.1 we list the primary fields appearing in the spectrum up to charge 3, the remaining can be obtained using particle-hole symmetry. In the case of the free fermion boundary conditions the spectrum of the system coincides with the scaling dimension of the allowed operators of the theory, hence the same table lists both the operator content and the spectrum. These primary fields correspond to the non-vanishing multiplicities n^i_{FF} in the partition function of the system with free boundary conditions. Notice that, in general, not all the possible combinations of operators in the different sectors appear. This is due to the already mentioned conformal embedding. Indeed the free fermion system is described by a theory with larger symmetry (in this case the full symmetry is $SO(12)$), hence if we want to describe it with a lower symmetry group in general we have to impose

Table 4.1: Spectrum of free fermions with open boundary conditions.

Q	S	T	Z_3	x
0	0	0	I	0
0	0	2	ϵ	1
0	0	4	I	2
0	1	1	ϵ	1
0	1	2	I	1
0	1	3	ϵ	2
1	1/2	1	σ	1/2
1	1/2	2	Z	3/2
1	1/2	3	σ	3/2
1	3/2	0	Z	3/2
1	3/2	2	σ	3/2
1	3/2	4	Z	7/2

Q	S	T	Z_3	x
2	0	0	Z	1
2	0	2	σ	1
2	0	4	Z	3
2	1	1	σ	1
2	1	2	Z	2
2	1	3	σ	2
3	1/2	1	ϵ	3/2
3	1/2	2	I	3/2
3	1/2	3	ϵ	5/2
3	3/2	0	I	3/2
3	3/2	2	ϵ	5/2
3	3/2	4	I	7/2

additional constraints, known as "gluing conditions"[42, 53], on the possible combinations of fields of the lower symmetry group to select those combinations that respect the higher symmetry.

To obtain the spectrum at the Kondo screened fixed point, where the impurity behaves as a spin-$3/2$, we guess that we have to perform a fusion with the operator in the spin sector $\phi^S_{3/2}$. This "guess" is motivated by the observation that the strong coupling fixed point of the Kondo model is obtained by fusion with the spin operator S, where S is the spin of the impurity. This fusion corresponds to the absorption of the impurity by the conduction electrons and the generation of the $\pi/2$ phase shift that is characteristic of the strong coupling fixed point of the Kondo model. The spectrum obtained by the fusion (again up to charge 3) is shown in Table 4.2. Notice that in this case the ground state is degenerate. This spectrum reproduces precisely the asymptotic spectrum found by NRG for $J > J^*$. The allowed operators of the theory at this fixed point are obtained by double fusion with $\phi^S_{3/2}$. The result of the second fusion with $\phi^S_{3/2}$ gives an operator content described by the same table that gives the spectrum of free fermions, Table 4.1. This was expected because the system is still described by a Fermi liquid.

Table 4.2: Spectrum at the Kondo screened fixed point for $n_0 = 3$.

Q	S	T	Z_3	$x - 3/4$
0	1/2	1	ϵ	0
0	1/2	2	I	0
0	1/2	3	ϵ	1
0	3/2	0	I	0
0	3/2	2	ϵ	1
0	3/2	4	I	2
1	0	0	Z	0
1	0	2	σ	0
1	0	4	Z	2
1	1	1	σ	0
1	1	2	Z	1
1	1	3	σ	1

Q	S	T	Z_3	$x - 3/4$
2	1/2	1	σ	0
2	1/2	2	Z	1
2	1/2	3	σ	1
2	3/2	0	Z	1
2	3/2	2	σ	1
2	3/2	4	Z	3
3	0	0	I	0
3	0	2	ϵ	1
3	0	4	I	2
3	1	1	ϵ	1
3	1	2	I	1
3	1	3	ϵ	2

Following our simple perturbative analysis, to obtain the boundary condition corresponding to the non-Fermi liquid stable phase at $J < J^*$ we should fuse the spectrum of the free fermions with an operator with $S = 1/2$ and $L = 1$. We encounter a technical problem in this procedure because in the fusion process with two primary fields belonging to two different sectors, the spin and the orbital, we are not sure to properly account for the Pauli principle and we could not find in the literature any work facing this unusual situation. Indeed in this way we obtain states that are not compatible with the statistics. To overcome the problem we can use the Kondo boundary condition as the reference state and start the fusion process from there. Physically this corresponds to applying a phase shift $\pi/2$ to the conduction channel, hence removing from it one state. This decoupled state is then settled in the optimal configuration that minimizes H_K. After that, the effective interaction felt by the conduction electrons tends to screen the hypercharge degrees of freedom associated with the three degenerate charge configurations. This process would correspond to fusion with an operator $I = 1$ in the hypercharge sector but hypercharge is not a symmetry of the theory, being broken by the Coulomb term. Nevertheless we can notice that if we decompose the hypercharge symmetry $SU(2)_3$ into $U(1) \times Z_3$, the operator $I = 1$

corresponds either to $Q = 0, Z_3 = \epsilon$ or to $Q = 2, Z_3 = \sigma$. Hence we choose to fuse with ϵ in the Z_3 sector.

The result of the fusion is summarized in Table 4.3. For the lowest energy states the CFT prediction is compared with the (suitably normalized) energy levels obtained by NRG (for higher energy states the large degeneracy of the levels makes this comparison too complicated).

The agreement is fairly good, considered also the great computational effort of the calculation. We can also compute the allowed operators to check the stability of the fixed point. These are obtained fusing the operator content of the Kondo fixed point twice with operator ϵ. The most relevant operators (those with dimension up to $7/5$) are listed in Table 4.4. There are no operators with dimension less or equal to one that do not break the symmetry of the system, hence the fixed point is stable. This Table can also provide information on the stability with respect to different symmetry breaking. Indeed the pair of operators $(0, 0, 0, \epsilon)$ and $(2, 0, 0, \sigma)$ of dimension $\Delta = 2/5$, as we have already seen, correspond to the operator $I = 1$ in a theory with unbroken hypercharge symmetry. This means that the fixed point becomes unstable to a local perturbation in the hypercharge channel of the form $-\vec{\mu} \cdot \vec{I}$, where $\vec{I}$ is the hypercharge operator e.g. of the impurity. After fusion, this operator will induce a perturbation $\propto \vec{\mu} \cdot \vec{\phi}_1^I$, where $\vec{\phi}_1^I$ is the $I = 1$ primary field in the hypercharge sector. It would correspond either to the particle-hole symmetry breaking channel, $(0, 0, 0, \epsilon)$, when $\vec{\mu} = (0, 0, \mu_z)$, or to the Cooper channel $(2, 0, 0, \sigma)$, when $\vec{\mu} = (\mu_x, \mu_y, 0)$. On the contrary, the behavior of the total hypercharge susceptibility is controlled by the leading irrelevant operator compatible with the symmetry properties, which is the Kac-Moody descendant $\vec{J}^I \cdot \vec{\phi}_1^I$, where $\vec{J}^I$ is the non abelian hypercharge current. The dimension of this operator being $1 + \Delta = 1 + 2/5 = 7/5$ leads to a total hypercharge susceptibility, χ^I, which behaves in temperature like

$$\chi^I \sim T^{2\Delta - 1} = T^{-1/5},$$

hence being singular. In addition there exist other instability channels. Indeed the operator $(0, 0, 2, I)$ with dimension $3/5$ represents a relevant instability towards a field which breaks the orbital symmetry, while the operator $(0, 1, 1, I)$ with the same dimension corresponds to an instability in the $\vec{S}\vec{T}$ channel.

For the unstable fixed point it is much more difficult to guess the correct fusion rules. The only hint is that it is more likely that the sector involved is the Potts sector

Table 4.3: Spectrum at the non-Fermi liquid stable fixed point for $n_0 = 3$.

Q	S	T	Z_3	$x - 3/20$	E_{NRG}
1	0	0	σ	0	0
0	1/2	1	I	1/5	0.199
0	1/2	1	ϵ	3/5	0.603
1	0	2	σ	3/5	0.599
1	1	1	σ	3/5	0.599
2	1/2	1	σ	3/5	0.603
0	1/2	2	ϵ	1	0.998
0	3/2	0	ϵ	1	0.998
1	1	2	σ	1	1.011
2	1/2	2	σ	1	0.998
2	3/2	0	σ	1	0.998
3	0	0	ϵ	1	0.998
0	1/2	3	I	6/5	1.204
0	3/2	2	I	6/5	1.204
1	0	2	Z	6/5	1.204
1	1	1	Z	6/5	1.204
2	1/2	1	Z	6/5	1.224
3	0	2	I	6/5	1.204
3	1	1	I	6/5	1.204
0	1/2	1	ϵ'	8/5	
0	1/2	3	ϵ	8/5	
0	3/2	2	ϵ	8/5	
1	1	3	σ	8/5	
2	1/2	3	σ	8/5	
2	3/2	2	σ	8/5	
3	0	2	ϵ	8/5	
3	1	1	ϵ	8/5	

Q	S	T	Z_3	$x - 3/20$
0	1/2	2	ϵ'	2
0	3/2	0	ϵ'	2
1	0	4	σ	2
3	0	0	ϵ'	2
3	1	2	ϵ	2
1	1	3	Z	11/5
2	1/2	3	Z	11/5
2	3/2	2	Z	11/5
3	1	3	I	11/5
0	1/2	3	ϵ'	13/5
0	3/2	2	ϵ'	13/5
3	0	2	ϵ'	13/5
3	1	1	ϵ'	13/5
3	1	3	ϵ	13/5
0	3/2	4	ϵ	3
2	3/2	4	σ	3
3	0	4	ϵ	3
3	1	2	ϵ'	3
0	1/2	1	W	16/5
3	1	3	ϵ'	18/5
0	3/2	4	ϵ	4
3	0	4	ϵ'	4
0	1/2	3	W	21/5
0	3/2	2	W	21/5
3	0	2	W	21/5
3	1	1	W	21/5
3	1	3	W	26/5

Table 4.4: Most relevant operators present at the non-Fermi liquid stable fixed point for $n_0 = 3$.

Q	S	T	Z_3	x
0	0	0	I	0
0	0	0	ϵ	2/5
2	0	0	σ	2/5
1	1/2	1	σ	1/2
0	0	2	I	3/5
0	1	1	I	3/5
1	1/2	2	σ	9/10
1	3/2	0	σ	9/10
0	0	2	ϵ	1
0	1	1	ϵ	1
0	1	2	I	1
2	0	0	Z	1
2	0	2	σ	1
2	1	1	σ	1
1	1/2	1	Z	11/10
3	1/2	1	I	11/10
0	0	0	ϵ'	7/5
0	1	2	ϵ	7/5
2	1	2	σ	7/5

due to the non-Fermi liquid character of the fixed point. The surprise is that the fusion with any of the primary fields of the Potts sector does not describe the UFP. The puzzle has to be solved considering that the primary operators of the Potts model are a subset of the primary fields of the $\mathcal{M}(6,5)$ minimal model. It has been demonstrated that in order to obtain all the possible boundary condition for the three-state Potts model it is necessary to consider the fusion also with those fields that are present in the $\mathcal{M}(6,5)$ Kac table but are not included in the Potts theory[56, 73, 74].

On inspection of the (few) possible cases we found that the UFP is described by the fusion of the spectrum of the Kondo fixed point with the operator $1/8$ of the Potts sector. The spectrum predicted by CFT is presented in Table 4.5 together with the NRG energies for the lowest states. This time the accuracy is lower mainly due to the difficulty in arriving close enough to the fixed to get its very spectrum. Nevertheless the degeneracies of the states are well reproduced, supporting the identification of the UFP. The operator content of the fixed point is obtained by double fusion with operator $1/8$. As for the stable non-Fermi liquid fixed point the most relevant operators are reported in Table 4.6. The presence of the operator $(0,0,0,Z)$ correctly implies the instability of the fixed point, being relevant and allowed by the symmetry of the problem. This is the operator that drives the system away from the unstable fixed point either to the Kondo screened fixed point or to the non-Fermi liquid stable one.

It is also interesting to notice the presence of the operator $(2,0,0,I)$ with dimension $1/3$ that breaks the $U(1)_{charge}$ symmetry and indicates a superconducting instability of the fixed point. The other relevant operators $(0,0,2,\sigma)$ and $(0,1,1,\sigma)$ have dimension $2/3$ and correspond to instabilities in particle-hole channels.

The ground state degeneracy of the various fixed points can be calculated from the knowledge of the fusion processes that connect the fixed points as shown in Section 2.2.3.

The outcome is that at the Kondo fixed point $g_K = 1$ as expected for a perfectly screened impurity. In the non-Fermi liquid stable phase

$$g_{SNFL} = \sqrt{\frac{\sqrt{5}+1}{\sqrt{5}-1}} \simeq 1.618 \tag{4.24}$$

The fact that g_{SNFL} is larger than g_K indicates that the non-Fermi liquid phase is less stable than the Fermi liquid (either Kondo or unscreened) phase and this is indeed compatible with the instability of the former to particle-hole symmetry breaking.

Table 4.5: Spectrum at the unstable non-Fermi liquid fixed point for $n_0 = 3$.

Q	S	T	Z_3	$x - 5/24$	E_{NRG}
1	0	0	1/8	0	0
0	1/2	1	1/40	1/6	0.162
1	0	2	1/40	1/2	0.488
1	1	1	1/40	1/2	0.489
2	1/2	1	1/40	1/2	0.491
0	1/2	1	21/40	2/3	0.675
0	1/2	2	1/8	2/3	0.643
0	3/2	0	1/8	2/3	0.644
3	0	0	1/8	2/3	0.648
1	0	2	21/40	1	0.991
1	1	1	21/40	1	0.992
1	1	2	1/8	1	1.012
2	1/2	1	21/40	1	1.011
2	1/2	2	1/8	1	0.999
2	3/2	0	1/8	1	1.000
0	1/2	3	1/40	7/6	
0	3/2	2	1/40	7/6	
3	0	2	1/40	7/6	
3	1	1	1/40	7/6	
1	0	0	13/8	3/2	
1	1	3	1/40	3/2	
2	1/2	3	1/40	3/2	
2	3/2	2	1/40	3/2	

Q	S	T	Z_3	$x - 5/24$
0	1/2	3	21/40	5/3
0	3/2	2	21/40	5/3
3	0	2	21/40	5/3
3	1	1	21/40	5/3
3	1	2	1/8	5/3
1	0	4	1/8	2
1	1	3	21/40	2
2	1/2	3	21/40	2
2	3/2	2	21/40	2
0	1/2	2	13/8	13/6
0	3/2	0	13/8	13/6
3	0	0	13/8	13/6
3	1	3	1/40	13/6
1	1	2	13/8	5/2
2	1/2	2	13/8	5/2
2	3/2	0	13/8	5/2
0	3/2	4	1/8	8/3
3	0	4	1/8	8/3
3	1	3	21/40	8/3
2	3/2	4	1/8	3
3	1	2	13/8	19/6
1	0	4	13/8	7/2
0	3/2	4	13/8	25/6
3	0	4	13/8	25/6
2	3/2	4	13/8	9/2

Table 4.6: Most relevant operators present at the non-Fermi liquid unstable fixed point for $n_0 = 3$.

Q	S	T	Z_3	x
0	0	0	I	0
2	0	0	I	1/3
1	1/2	1	σ	1/2
0	0	0	Z	2/3
0	0	2	σ	2/3
0	1	1	σ	2/3
1	1/2	1	ϵ	5/6
0	0	2	ϵ	1
0	1	1	ϵ	1
0	1	2	I	1
2	0	0	Z	1
2	0	2	σ	1
2	1	1	σ	1
2	0	2	ϵ	4/3
2	1	1	ϵ	4/3
2	1	2	I	4/3

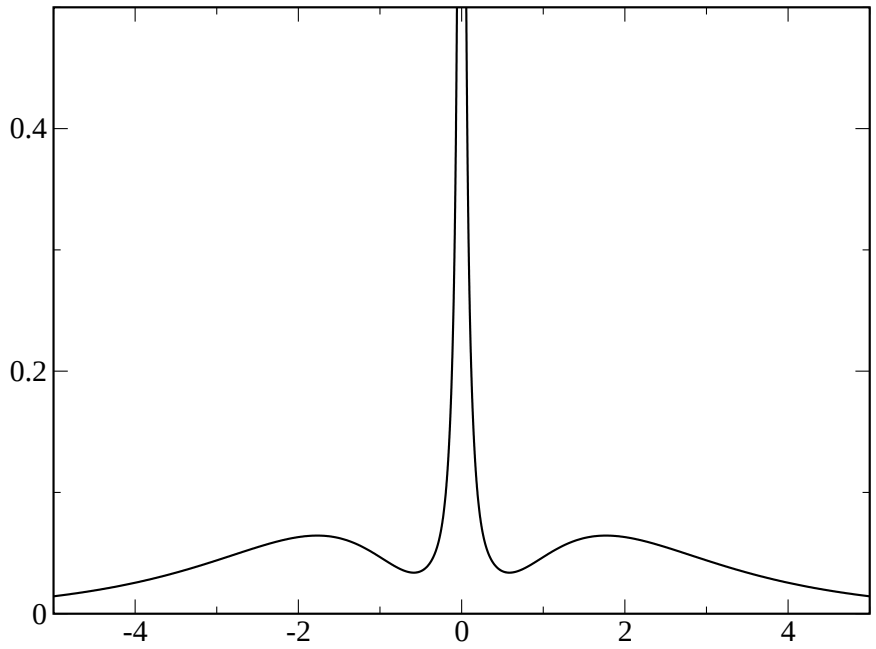

Figure 4.2: Impurity DOS in the particle-hole symmetric case $n_0 = 3$ for $J = 0$. The Kondo peak is cut off in order to make the two Hubbard bands more visible. The temperature is set by the length of the chain and is practically zero. Here $U = 2$, $\Delta_0 = U/(6\pi)$. [$\Lambda = 3$]

Eventually at the UFP we find that $g_{UNFL} = \sqrt{3}$. As expected g decreases along the renormalization group flow.

4.3.1 Impurity spectral function

From NRG we can extract the spectral function of the impurity, defined in (3.26). Arguing along the lines of Section 3.2.5, we can guess that in the Kondo screened region, where a perturbative expansion in U and J is valid, the value of the DOS at the chemical potential is fixed by the relation (3.29). On the other hand, this perturbation expansion clearly breaks down at the UFP where the value of the DOS at the chemical potential changes. We show in Fig. 4.2 the impurity spectral function on a large scale and in Fig. 4.3 the behavior in a region close to the chemical potential as obtained from NRG. The results refer to the particle-hole symmetric case across the UFP.

In the Kondo screened phase the impurity DOS has the typical behavior with two

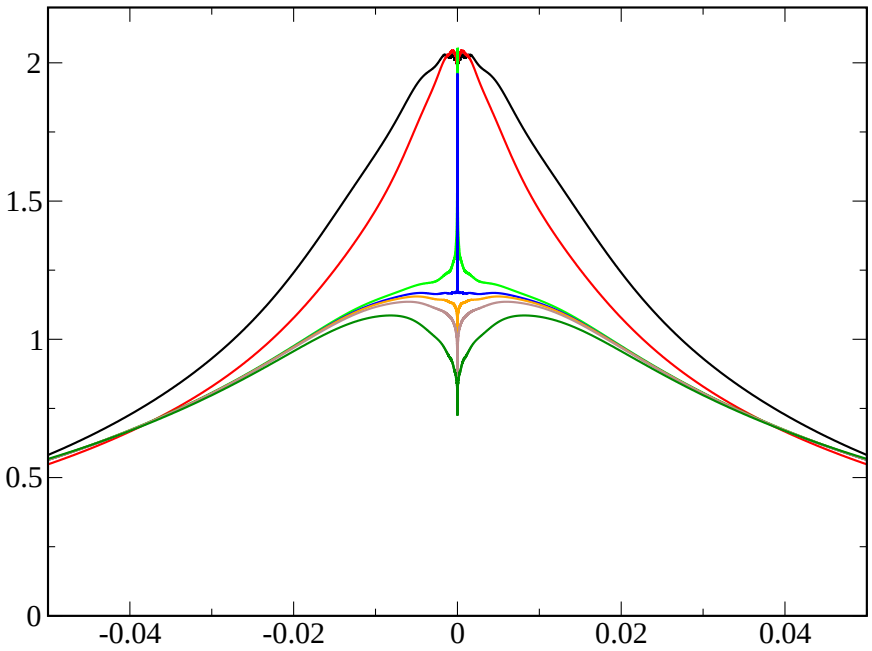

Figure 4.3: Impurity DOS close to the chemical potential in the particle-hole symmetric case $n_0 = 3$ across the UFP. From top to bottom we find the DOS's in the Kondo screened phase ($J/J^* = 0, 0.48, 0.95, 1^-$), and then in the non-Fermi liquid stable regime ($J/J^* = 1.02, 1.07, 1.31$). The other parameters are as in Fig. 4.2. In the three-orbital model, due to the high computational effort, it is more difficult to arrive close to the fixed point. Hence we don't have a precise determination of J^* and the fourth curve is indicated with the value $J/J^* = 1^-$. [$\Lambda = 3$, $U = 2$, $\Delta_0 = U/(6\pi)$, $J^* \simeq -0.042$]

peaks at energy $\pm U/2$ and the Kondo resonance at the chemical potential. As in the two-orbital model, approaching the UFP the Kondo peak becomes the superposition of a broad resonance, that remains almost constant across the UFP, and of a narrower resonance that shrinks progressively and disappears exactly at the UFP. The value of the DOS at the chemical potential in the Kondo screened phase as calculated by NRG remains constant but it is quite far from the value expected from Eq. (3.29). We postpone the discussion of this discrepancy.

As soon as the system crosses the UFP, entering the non-Fermi liquid regime, the narrow resonance becomes a narrow dip within the broad resonance. Contrary to the

two-orbital case, now the dip is not a real pseudogap and the value at the chemical potential of the DOS is finite.

At the UFP we can expect that neither the narrow resonance nor the dip are present and the DOS is given by the broad J-independent resonance.

We do not have an analytic ansatz for the spectral function of this model, but we can still compare the value of $\rho(0)$ obtained numerically by the NRG with that predicted by CFT. Using relation (3.30) we can indeed relate $\rho(0)$ to the value of the S scattering matrix at zero energy.

The discrepancy found in the NRG calculation of the DOS in the Kondo screened phase is around the 35% of the value predicted by Fermi liquid theory. This is most likely due to the very large number of states required by the calculation to give reliable results. Nevertheless we guess that this is a systematic error due to the numerical procedure and does not depend on whether the model is in the Kondo screened phase or in a non-Fermi liquid one. Hence we can consider the ratio between the values of $\rho(0)$ at the different fixed points as approximately independent on this error.

The scattering S matrix at the Kondo screened fixed point in presence of particle-hole symmetry can be calculated with the method described in Section 2.2.2 giving $S_{(1)} = -1$ and agrees with the value given by the Fermi liquid expression (3.32) with a phase shift of $\pi/2$. This in turns implies that $\rho(0)_{Kondo} = \rho_0$. If we calculate the scattering S matrix at the stable non-Fermi liquid fixed point we obtain the value

$$S_{(1)}^{SNFL} = \frac{\sqrt{5}-1}{\sqrt{5}+1} \tag{4.25}$$

that corresponds to $\rho(0)_{SNFL} = \rho_0/(1+\sqrt{5}) \sim 0.31\rho_0$. This value gives a ratio $\rho(0)_{SNFL}/\rho(0)_{Kondo}$ which is indeed compatible with the NRG result. Eventually, at the UFP, $S_{(1)}^{UNFL} = 0$, implying that $\rho(0)_{UNFL} = \rho_0/2$. Once more the ratio $\rho(0)_{UNFL}/\rho(0)_{Kondo}$ obtained numerically is in reasonable agreement.

4.3.2 Particle-hole symmetry breaking

An important issue related to the study of lattice systems through DMFT is the stability of both the non-Fermi liquid phase and the UFP to particle-hole symmetry breaking. In particular we expect from the preliminary analysis of Section 4.2 that the non-Fermi liquid phase does not survive the particle-hole symmetry breaking. At

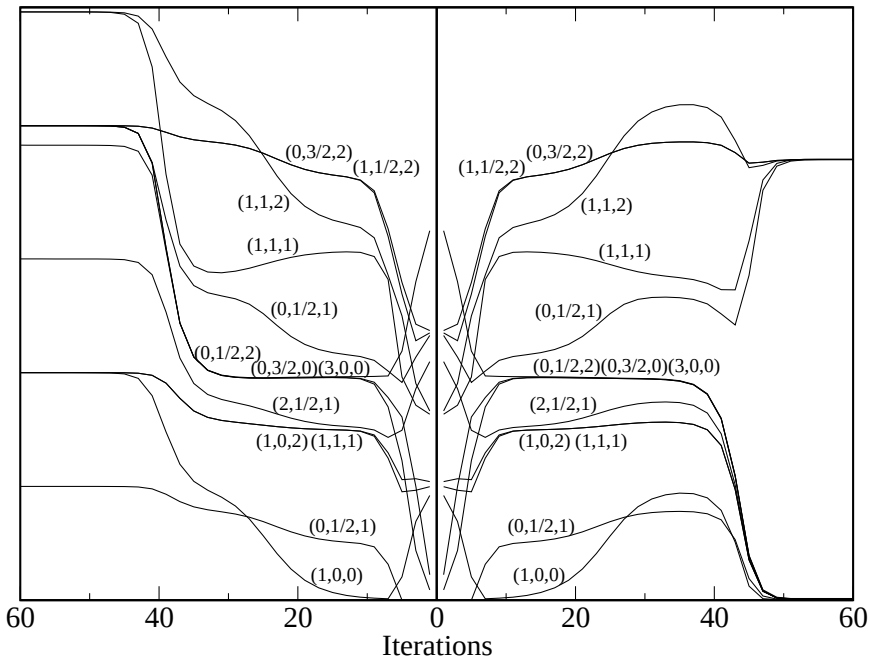

Figure 4.4: Lowest energy levels versus the chain size N (odd) for $n_0 = 2.99$. The levels are labeled by the quantum numbers (Q, S, T). The left/right panels correspond to a deviation $\delta J/J^* = \pm 3 \cdot 10^{-6}$ from the fixed point value J^*. [$\Lambda = 5$, $U = 2$, $\Delta_0 = U/(6\pi)$, $J = -0.0335918$ (left), $J = -0.0335916$ (right)]

the same time we expect that the UFP instead is not spoiled away from particle-hole symmetry.

The NRG calculations confirm this guess. In Fig. 4.4 is shown the spectrum of the system for $n_0 = 2.99$ for J close to J^*. This Figure must be compared with Fig. 4.1 which shows the particle-hole symmetric spectrum.

It is evident that the Kondo screened region is left unchanged while the non-Fermi liquid phase is completely washed out and is substituted by a Fermi liquid phase (notice the constant spacing of the lowest energy levels characteristic of a Fermi liquid spectrum).

The UFP spectrum in the first iterations of the crossover region is the same as in the particle-hole symmetric case but after a few iterations there is a change in the energy levels. This is due to the particle-hole symmetry breaking. In the first iterations the temperature is high and the symmetry breaking is not effective; as the

length of the chain increases (and the temperature decreases) the system reaches an energy scale comparable with the splitting of the levels due to the symmetry breaking and the fixed UFP spectrum is modified. Eventually the system flows to one of the stable Fermi liquid fixed points.

The UFP spectrum changes adiabatically as n_0 is varied but retains its non-Fermi liquid character. This analysis confirms the existence of a critical line of UFP's in the J-n_0 phase space that connect the UFP found at $n_0 = 3$ with the one that, as we will see in the next Section, is found for $n_0 = 2$.

The spectral function still presents the typical feature of the UFP, i.e. a jump in the value of the DOS at the chemical potential from one phase to the other.

4.3.3 Fermi liquid theory

Even if a description of the system in terms of effective Hamiltonians was not performed for the three-orbital model and we don't have access to the various Wilson ratios, nonetheless we can apply the Fermi liquid theory of Appendix A to check the validity of the approach.

The allowed configurations (T, S) for an incoming pair of electrons are three: $(0, 0)$, $(2, 0)$ and $(1, 1)$.

On the other hand, as we have already seen, the particle-hole channels are six. The $(0, 0)$-channel is the charge channel; $(0, 1)$ and $(1, 0)$ are respectively the spin and the orbital channels; $(2, 0)$ corresponds to excitations in the Hund's channel; eventually $(1, 1)$ and $(2, 1)$ mix spin and orbital.

We can define the corresponding dimensionless scattering vertices in particle-particle channels $\mathcal{A}_{(0,0)}$, $\mathcal{A}_{(2,0)}$ and $\mathcal{A}_{(1,1)}$ as in Section 3.3 and relate them to the scattering vertices in particle-hole channels. The relations between the two sets are:

$$A_{(0,0)} = \frac{5}{3}\mathcal{A}_{(2,0)} + 3\mathcal{A}_{(1,1)} + \frac{1}{3}\mathcal{A}_{(0,0)}, \tag{4.26}$$

$$A_{(0,1)} = -\frac{5}{3}\mathcal{A}_{(2,0)} + \mathcal{A}_{(1,1)} - \frac{1}{3}\mathcal{A}_{(0,0)}, \tag{4.27}$$

$$A_{(1,0)} = \frac{5}{6}\mathcal{A}_{(2,0)} - \frac{3}{2}\mathcal{A}_{(1,1)} - \frac{1}{3}\mathcal{A}_{(0,0)}, \tag{4.28}$$

$$A_{(1,1)} = -\frac{5}{6}\mathcal{A}_{(2,0)} - \frac{1}{2}\mathcal{A}_{(1,1)} + \frac{1}{3}\mathcal{A}_{(0,0)}, \tag{4.29}$$

$$A_{(2,0)} = \frac{1}{6}\mathcal{A}_{(2,0)} - \frac{3}{2}\mathcal{A}_{(1,1)} + \frac{1}{3}\mathcal{A}_{(0,0)}, \tag{4.30}$$

$$A_{(2,1)} = -\frac{1}{6}\mathcal{A}_{(2,0)} - \frac{1}{2}\mathcal{A}_{(1,1)} - \frac{1}{3}\mathcal{A}_{(0,0)}. \tag{4.31}$$

As shown in Appendix A only the Landau parameters corresponding to conserved quantities can be related to the susceptibilities of the model. The Landau parameters in non-conserved channels can only give an estimate of the corresponding susceptibility.

- When $J = 0$ the model is $SU(6)$-symmetric. Hence $\mathcal{A}_{(2,0)} = \mathcal{A}_{(1,1)} = \mathcal{A}_{(0,0)} = \mathcal{A}$. In the $s - d$ limit the model maps onto an $SU(6)$ Kondo model and the charge compressibility is negligible. This implies that $A_{(0,0)} = 5\mathcal{A} = 1$ from which we can calculate the other scattering amplitudes.

  Given the larger symmetry of the model for $J = 0$ now all the particle-hole scattering amplitudes correspond to conserved quantities and the associated Wilson ratios, defined in Eq. (3.54), can be calculated from them. In particular they have a universal value

  $$R = 6/5 \tag{4.32}$$

  in agreement with known results[58].

- In the Kondo limit for $J \gg T_K$ the impurity is frozen in a $S = 3/2$ configuration. In this regime both charge and orbital degrees of freedom are quenched, $A_{(0,0)} = A_{(1,0)} = A_{(2,0)} = 1$. This allows to extract the values for the three particle-particle scattering amplitudes:

  $$\begin{aligned} \mathcal{A}_{(2,0)} &= 1, \\ \mathcal{A}_{(1,1)} &= -1/3, \\ \mathcal{A}_{(0,0)} &= 1. \end{aligned}$$

  From this we obtain the Wilson ration in the spin channel

  $$R_{(0,1)} = 10/3 \tag{4.33}$$

  which again agrees with known results[58].

- Close to the UFP we can assume that the charge degrees of freedom are frozen below an energy scale of order U while spin and orbital one are frozen below

T_K, once again due to the lack of leading operators that generate singular behaviour at the UFP in these channels. Hence we can set $A_{(0,0)} = A_{(0,1)} = A_{(1,0)} = 1$. From this we get

$$\begin{aligned} \mathcal{A}_{(2,0)} &= 1/2, \\ \mathcal{A}_{(1,1)} &= 1/2, \\ \mathcal{A}_{(0,0)} &= -4. \end{aligned}$$

This means a dramatic enhancement of the susceptibility in the Cooper channel corresponding to the total singlet. At the same time we find $A_{(2,0)} = A_{(1,1)} = -2$ signaling a strong enhancement in the corresponding susceptibilities.

It is worth noticing that this result matches perfectly the result of the CFT analysis. Indeed in Table 4.6 the most relevant operator belongs to the total singlet particle-particle channel (with dimension $1/3$) while relevant operators in the (2,0) and (1,1) channels have a larger dimension (2/3).

4.4 Analysis of the two electrons case

As expected from our preliminary analysis, the phase diagram of the model with $n_0 = 2$ is separated into two regions characterized by different properties as in the three electron case. For J larger than a critical value $J^* < 0$ the low temperature fixed point of the model is a Kondo screened fixed point described by a Fermi liquid. For J smaller than J^* the low temperature fixed point is again a Fermi liquid but with different properties and without Kondo screening of the impurity. Once again the two phases are separated by an UFP with non-Fermi liquid properties.

The spectrum of the system obtained by NRG is shown in Fig. 4.5 for values of J close to J^* in the two phases. The left panel shows the spectrum for $J < J^*$ and the right one the spectrum for $J > J^*$. The different character of the two phases is evident.

For $J > J^*$ the spectrum is that of a chain with a $\pi/2$ phase shift and a potential scattering term. The Kondo effect takes place and the impurity is screened by the first shell of conduction electrons while the remaining conduction electrons experience a potential scattering due to the breaking of particle-hole symmetry.

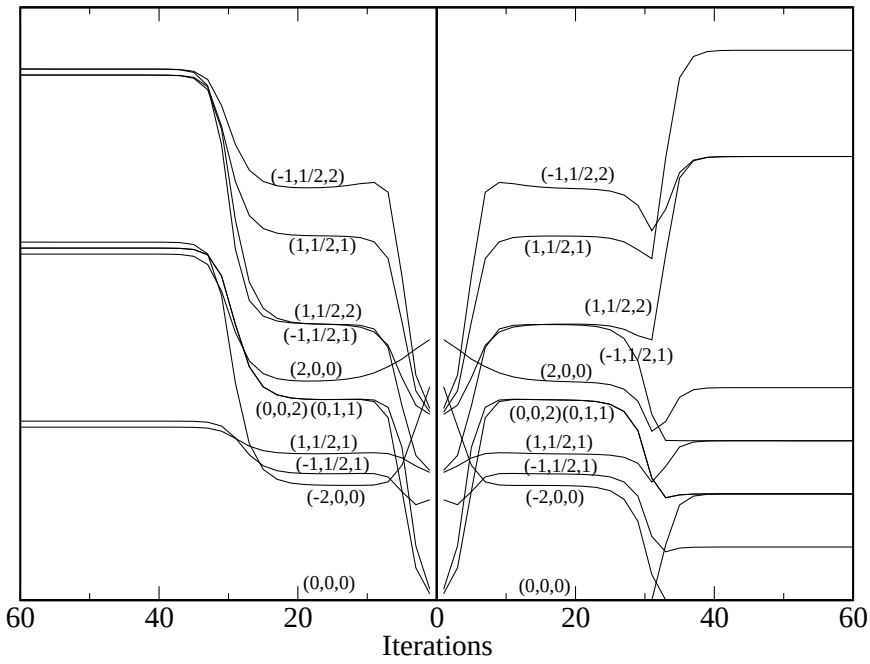

Figure 4.5: Lowest energy levels versus the chain size N (odd) for $n_0 = 2$. The levels are labeled by the quantum numbers (Q, S, T). The left/right panels correspond to a deviation $\delta J/J^* = \pm 4 \cdot 10^{-6}$ from the fixed point value J^*. [$\Lambda = 5$, $U = 2$, $\Delta_0 = U/(6\pi)$, $J = -0.0142965$ (left), $J = -0.0142964$ (right)]

For $J < J^*$ the spectrum is that of a free chain with the impurity completely decoupled from the conduction band and quenched in a total singlet configuration.

In the crossover region $J \sim J^*$ the system is initially close to an unstable fixed point with non-Fermi liquid character.

The particle-hole symmetry breaking makes the CFT description and its comparison with the numerical spectrum more involved than in the particle-hole symmetric case. In addition there is the problem that particle-hole symmetry breaking induces a splitting between charge-conjugated states and makes the comparison of the energy of these states with the numerical spectrum very difficult. The only states whose energy can be safely compared are those with $Q = 0$.

Starting from the free-fermion spectrum it is easy to find the spectrum of the fixed point corresponding to the unscreened $J < J^*$ region. Indeed in that region the phase shift is zero and the spectrum is exactly that of free fermions in presence of potential

scattering.

As we have seen in the parturbative analysis, for $J > J^*$ the system would flow to a non-Fermi liquid overscreened Kondo fixed point, but the presence of particle-hole symmetry breaking drives the flow to a conventional Fermi liquid fixed point with the first shell of conduction electrons quenched in a non degenerate configuration. The low temperature fixed point found for $J > J^*$ is hence correctly described by the spectrum of free fermions with a $\pi/2$ phase shift and a potential scattering term.

The difficult task is now to guess the correct fusion to describe the UFP. An indication comes from the fact that the UFP found for $n_0 = 3$ is stable under particle-hole symmetry breaking and that a critical line starts from that point and joins the $n_0 = 2$ UFP. Hence we can guess that, apart from the charge that will be affected when n_0 is varied, the spectrum must retain the same quantum numbers even if the energies will differ.

By inspection of the possible fusions we find that the fixed point is described by the fusion of the spectrum of the unscreened fixed point (free fermions) with operator $1/8$ of in the Potts sector. Even if it is difficult to identify the states with charge different from zero and the numerical agreement is not excellent, the fusion is the only one that reproduces correctly the succesion of states and their degeneracy. The spectrum obtained by CFT is presented in Table 4.7. It is interesting to notice that the spectrum of this UFP is the same as that of the UFP found for $n_0 = 3$ apart from the charge sector that is reshuffled. Not surprisingly also the operator content is the same of the UFP found for $n_0 = 3$ (see Table 4.6).

The spectral function, shown in Fig. 4.6, presents the already encountered jump in the value at the chemical potential in correspondence of the UFP.

4.5 Relevance of the single impurity results in connection with DMFT

The presence of symmetry breaking instabilities of the impurity model close to the UFP is relevant for lattice systems that map by DMFT onto our three-orbital model. Indeed, as we have seen in Section 3.5 for the two-orbital model, when such a lattice system is driven close to the Mott transition the corresponding impurity model is forced to enter the critical region $T_K \sim -J$. In this regime the impurity model is

Table 4.7: Spectrum at the unstable non-Fermi liquid fixed point for $n_0 = 2$.

Q	S	L	Z_3	$x - 1/8$
0	0	0	1/8	0
1	1/2	1	1/40	1/3
2	0	0	1/8	1/3
0	0	2	1/40	1/2
0	1	1	1/40	1/2
1	1/2	1	21/40	5/6
1	1/2	2	1/8	5/6
1	3/2	0	1/8	5/6
2	0	2	1/40	5/6
2	1	1	1/40	5/6
0	0	2	21/40	1
0	1	1	21/40	1
0	1	2	1/8	1
3	1/2	1	1/40	1
1	1/2	3	1/40	4/3
1	3/2	2	1/40	4/3
2	0	2	21/40	4/3
2	1	1	21/40	4/3
2	1	2	1/8	4/3
0	0	0	13/8	3/2
0	1	3	1/40	3/2
3	1/2	1	21/40	3/2
3	1/2	2	1/8	3/2
3	3/2	0	1/8	3/2

Q	S	T	Z_3	$x - 1/8$
1	1/2	3	21/40	11/6
1	3/2	2	21/40	11/6
2	0	0	13/8	11/6
2	1	3	1/40	11/6
0	0	4	1/8	2
0	1	3	21/40	2
3	1/2	3	1/40	2
3	3/2	2	1/40	2
1	1/2	2	13/8	7/3
1	3/2	0	13/8	7/3
2	0	4	1/8	7/3
2	1	3	21/40	7/3
0	1	2	13/8	5/2
3	1/2	3	21/40	5/2
3	3/2	2	21/40	5/2
1	3/2	4	1/8	17/6
2	1	2	13/8	17/6
3	1/2	2	13/8	3
3	3/2	0	13/8	3
0	0	4	13/8	7/2
3	3/2	4	1/8	7/2
2	0	4	13/8	23/6
1	3/2	4	13/8	13/3
3	3/2	4	13/8	5

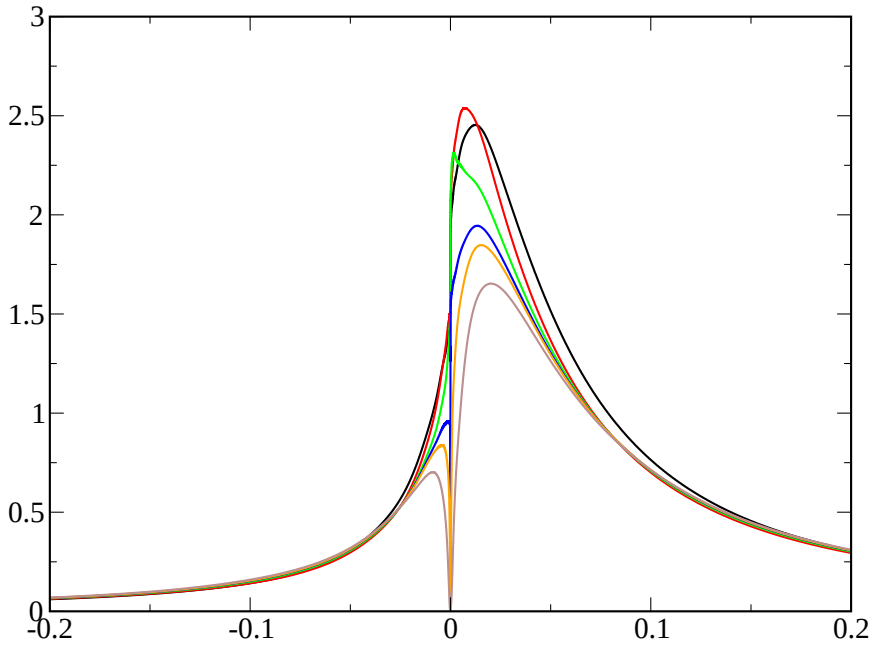

Figure 4.6: Impurity DOS close to the chemical potential for $n_0 = 2$ across the UFP. From top, the first three curves correspond to the Kondo screened phase and the last three to the unscreened one. [$\Lambda = 3$, $U = 2$, $\Delta_0 = U/(6\pi)$]

unstable in different channels and the lattice system chooses the most divergent one to develop a bulk symmetry breaking order-parameter to avoid the single impurity instability.

In the particle-hole symmetric case with three electrons on the impurity, the instabilities of the UFP are those associated to the relevant operators. From the list of operators in Table 4.6 we see that the most relevant operator, corresponding to the most divergent susceptibility close to the UFP, is $(2, 0, 0, I)$ with dimension $1/3$, i.e. the Cooper particle-particle channel. This implies that a lattice system at half filling that maps onto the three-orbital model, when driven towards the Mott transition, will develop a superconducting phase right before the transition.

Contrary to the two-orbital case, where the Cooper instability was competing with several other instabilities in different particle-hole channels, in this case the superconducting instability is the strongest. Indeed the other relevant operators $(0, 0, 2, \sigma)$ and $(0, 1, 1, \sigma)$, corresponding respectively to a Jahn-Teller and to a spin-orbit instability,

have dimension $2/3$.

The robustness of the UFP to particle-hole symmetry breaking implies that the superconducting region should extend in the phase diagram also to lattice systems away from half filling.

It is interesting to analyze also the stability of the non-Fermi liquid phase found for $J < J^*$. We have seen that this low temperature fixed point is stable only if particle-hole symmetry is preserved, disappearing from the phase diagram for $n_0 \neq 3$. This is demonstrated by the presence in Table 4.4 of the operator $(0, 0, 0, \epsilon)$ with dimension $2/5$. Nevertheless there are other symmetry breaking unstable channels at this fixed point. The most relevant is the Cooper channel and $(2, 0, 0, \sigma)$ with dimension $2/5$, and next the particle-hole channels $(0, 0, 2, I)$ and $(0, 1, 1, I)$ with dimension $3/5$. They all indicate that, were particle-hole symmetry be preserved, the fixed point would be unstable towards a perturbation in the $S = T = 0$ Copper channel and, to a lesser extent, in the particle-hole channels corresponding to a Jahn-Teller distortion and to a spin-orbit coupling.

The corresponding lattice model, once crossed the superconducting phase generated by the UFP instability, should enter a phase in which the dominant instability is towards a local particle-hole symmetry breaking. On the other hand, if the particle-hole symmetry is enforced, the lattice has still other instabilities at its disposal to avoid the non-Fermi liquid fixed point, namely the Cooper instability, the cooperative Jahn-Teller distortion or finally a spin accompanied by an orbital ordering of the bulk.

Perspectives

In this thesis we have studied the phase diagram of two Anderson impurity models which are characterized by an opposite sign of the conventional exchange splitting, namely by inverted Hund's rules. This interaction, which favors low degenerate impurity configurations, provides an alternative mechanism for freezing the impurity degrees of freedom which competes against the ordinary Kondo effect and may give rise to peculiar effects.

Indeed the impurities studied, having respectively two and three orbitals at disposal, thus representing the simplest models showing this competition, share the presence in the phase diagram of an unstable fixed point with non-Fermi liquid properties which separate the ordinary Kondo screened phase from an unscreened one where the inverted exchange splitting takes responsibility of quenching the impurity degeneracy.

The two-orbital model unstable fixed point is the analog of that found in the two-impurity Kondo model by Jones and Varma[14–16] and analyzed with conformal field theory by Affleck and Ludwig[17] and with bosonization by Sire, Varma and Krishnamurthy[45] and by Gan[46].

The three-orbital model phase diagram is even richer since, besides the already mentioned unstable fixed point, we find also a *stable* non-Fermi liquid phase when particle-hole symmetry holds. In the framework of boundary conformal field theory the various fixed points are described by a critical theory involving the two-dimensional three-state Potts model with different boundary conditions.

Beyond the interest for the impurity models per se, these results may also be of relevance for strongly correlated lattice models which are mapped by dynamical mean field theory on those Anderson impurity models.

In any strongly correlated system the competition between different energy scales, already encoded in our impurity models, is at the heart of a correct description close to a Mott transition. In the idealized picture of a Mott insulator, an integer number of

electrons is localized on each site irrespectively of the particular electronic configuration. This state would have a finite residual entropy per site, since there always exist more than a single state with that fixed number of electrons. Obviously in any realistic situation the Mott insulator will get rid of this entropy below an energy scale typically much smaller than the Mott-Hubbard gap. This scale, which we keep denoting as J, is controlled by a variety of mechanisms. For instance, in the single band Hubbard model, this mechanism is provided by the antiferromagnetic exchange, which may induce magnetic ordering of the residual spin degrees of freedom. In our multiband models it is the inverted exchange splitting which plays this role, which has the advantage of being an intra-site effect which is suitable to a DMFT analysis, unlike the inter-site antiferromagnetic exchange in the single-band Hubbard model.

When the metal is driven towards the Mott transition the coherent quasiparticle bandwidth goes to zero. Hence, before the Mott transition, it has to become of the same order as J. Translated by DMFT into the Anderson impurity language, this implies that the effective impurity model reaches a regime where the Kondo temperature is of order J. This is just the critical region around the impurity unstable fixed point, where all susceptibilities in the instability channels get hugely enhanced. This translates within DMFT into strongly enhanced local susceptibilities. We have argued that, unlike the single impurity, the lattice model may respond to this singular behavior by spontaneously generating an order parameter in any of the equivalent instability channels. Which of them is going to prevail may depend on band structure details. Therefore our conjecture is that, just before the Mott transition, a realistic model should undergo a transition from a correlated normal metal into an ordered phase which can be smoothly transformed into the zero-entropy Mott insulator. This phase should be quite anomalous in the sense that the ordering temperature should have the same order of magnitude as the energy scale below which the Mott insulator quenches its residual entropy. In our cases with inverted Hund's rules the ordered phase is likely to be superconducting. Indeed in our two-orbital model the susceptibility in the Cooper channel diverges in the same way as the susceptibilities in other particle-hole channels, mirroring a hidden symmetry of the unstable fixed point. In this case the superconducting instability of a lattice model corresponding to this impurity is expected to be favored in absence of band structure singularities or nesting. In the three-orbital model instead the superconducting susceptibility is the most diverging one close to the unstable fixed point. These speculations have indeed been

confirmed in the two-orbital model by DMFT[24] and agree with the DMFT analysis of the three-orbital model with two electrons per site[23]. On the other hand it would be extremely interesting to understand within the DMFT approach the role of the non Fermi-liquid stable phase in the three-orbital model at particle-hole symmetry.

Even though our analysis has been limited to models where the mechanism of entropy-quenching acting in the Mott insulator is on-site, thus allowing a DMFT calculation, we are tempted to believe that the outcoming scenario is more generic. In particular we think that the existence of a broad *incoherent* resonance at the chemical potential, whose typical energy scale smoothly transforms into the previously defined J-scale of the Mott insulator, on top of which there may be a narrow quasiparticle resonance or a narrow deep/pseudo-gap is a quite simple and appealing scenario for many realistic strongly correlated systems.

Appendix A

Fermi liquid theory for the Anderson model

We introduce in this appendix a Fermi liquid theory for generic multi-orbital Anderson models that will provide a useful framework to analyze NRG results and will allows us to introduce within DMFT the concept of a local Fermi liquid description in addition to the conventional one, which refers instead to low frequency and momentum scattering amplitudes. In particular this approach will prove very useful to interpret the data obtained in Section 3.2.3.

Let us consider more generally a multi-orbital Anderson impurity model. We assume that besides spin rotational symmetry also orbital degeneracy is preserved, so that the fully interacting impurity Green's functions are diagonal and independent either upon spin and orbital indices.

The variation of the electron number with orbital symmetry a and spin α associated with the presence of the impurity is given by[75]

$$\begin{aligned}\Delta n_{a\alpha} &= n_{d\,a\alpha} + \sum_{\mathbf{k}} (n_{\mathbf{k}\,a\alpha} - n^0_{\mathbf{k}\,a\alpha}) \\ &= -\frac{1}{\pi}\int_{-\infty}^{+\infty} d\epsilon\, f(\epsilon)\,\mathrm{Im}\Bigg\{ G_{a\alpha}(\epsilon+i\delta) \\ &\quad + \sum_{\mathbf{k}} \Big[\mathcal{G}_{\mathbf{k}\mathbf{k}\,a\alpha}(\epsilon+i\delta) - \mathcal{G}^{(0)}_{\mathbf{k}\mathbf{k}\,a\alpha}(\epsilon+i\delta)\Big] \Bigg\} \qquad \text{(A.1)}\end{aligned}$$

where δ is a positive infinitesimal number, $f(\epsilon)$ is the Fermi distribution function, $\mathcal{G}_{\mathbf{k}\mathbf{k}\,a\alpha}$ and $\mathcal{G}^{(0)}_{\mathbf{k}\mathbf{k}\,a\alpha}$ are respectively the interacting and non-interacting conduction elec-

tron Green's function, and $G_{a\alpha}$ is the impurity single-particle Green's function given by

$$G_{a\alpha}(\epsilon) = \left(\epsilon - \sum_{\mathbf{k}} |V_{\mathbf{k}}|^2 \mathcal{G}^{(0)}_{\mathbf{k}\mathbf{k}\,a\alpha}(\epsilon) - \Sigma_{a\alpha}(\epsilon) \right)^{-1}. \tag{A.2}$$

Plugging (A.2) in the expression (3.31) for the T-matrix, we have

$$\mathcal{G}_{\mathbf{k}\mathbf{k}\,a\alpha}(\epsilon) = \mathcal{G}^{(0)}_{\mathbf{k}\mathbf{k}\,a\alpha}(\epsilon) + \left(\mathcal{G}^{(0)}_{\mathbf{k}\mathbf{k}\,a\alpha}(\epsilon) \right)^2 |V_{\mathbf{k}}|^2 G_{a\alpha}(\epsilon) \tag{A.3}$$

and after some manipulations expression (A.1) can be also transformed into

$$\Delta n_{a\alpha} = -\frac{1}{\pi} \int_{-\infty}^{\infty} d\epsilon \, \frac{\partial f(\epsilon)}{\partial \epsilon} \, \mathrm{Im} \ln G_{a\alpha}(\epsilon + i\delta). \tag{A.4}$$

The impurity density of states is further determined through

$$\rho_{a\alpha}(\epsilon) = -\frac{1}{\pi} \mathrm{Im}\, G_{a\alpha}\left(i\omega_n \to \epsilon + i\delta\right). \tag{A.5}$$

If we introduce a source field in the Hamiltonian by

$$\delta \hat{H} = -\sum_{a\alpha} h_{a\alpha}\, n_{a\alpha},$$

where

$$n_{a\alpha} = \sum_{\mathbf{k}} c^{\dagger}_{\mathbf{k}\,a\alpha} c_{\mathbf{k}\,a\alpha} \; + \; d^{\dagger}_{a\alpha} d_{a\alpha},$$

then

$$G_{a\alpha}(i\omega_n)^{-1} \to i\omega_n + h_{a\alpha} - \Delta_{a\alpha}(i\omega_n, h_{a\alpha}) - \Sigma_{a\alpha}(i\omega_n, \{h_{b\beta}\}),$$

where

$$\Delta_{a\alpha}(i\omega_n, h_{a\alpha}) = \sum_{\mathbf{k}} |V_{\mathbf{k}}|^2 \, \frac{1}{i\omega_n - \epsilon_{\mathbf{k}} + h_{a\alpha}},$$

is the hybridization function in the presence of the source. Therefore the derivative with respect to the external field of the variation of the electron number associated with the impurity is given by

$$\begin{aligned} \left(\frac{\partial \Delta n_{a\alpha}}{\partial h_{b\beta}} \right)_{h=0} \;\; = \;\; & \int_{-\infty}^{\infty} \frac{d\epsilon}{\pi} \, \frac{\partial f(\epsilon)}{\partial \epsilon} \, \mathrm{Im} \, \Big\{ G(\epsilon + i\delta) \\ & \Big[\delta_{ab}\delta_{\alpha\beta} \left(1 - \left(\frac{\partial \Delta(z)}{\partial z} \right)_{z=\epsilon+i\delta} \right) \end{aligned}$$

$$- \left(\frac{\partial \Sigma_{a\alpha}(\epsilon + i\delta)}{\partial h_{b\beta}} \right)_{h=0} \Bigg] \Bigg\}, \tag{A.6}$$

where $\Sigma_{a\alpha}(i\omega_n)$ is the impurity self-energy and we made use of

$$\left(\frac{\partial \Delta_{a\alpha}(z, h_{a\alpha})}{\partial h_{b\beta}} \right)_{h=0} = \delta_{ab}\delta_{\alpha\beta} \frac{\partial \Delta(z)}{\partial z},$$

being $\Delta(z)$ the hybridization function in the absence of h. On the other hand

$$\begin{aligned} \left(\frac{\partial \Sigma_{a\alpha}(i\omega_n)}{\partial h_{b\beta}} \right)_{h=0} &= -\frac{1}{\beta} \sum_m \sum_{b\beta} \Gamma_{a\alpha,b\beta;b\beta,a\alpha}(i\omega_n, i\epsilon_m; i\epsilon_m, i\omega_n) \\ & \quad G(i\epsilon_m)^2 \left(1 - \frac{\partial \Delta(i\epsilon_m)}{\partial i\epsilon_m} \right), \end{aligned} \tag{A.7}$$

where we used the property that, at $h = 0$, the Green's function does not depend on a and α. The interaction vertex is the reducible one.

Let us assume that there exists a set of conserved operators

$$\begin{aligned} \mathcal{M}^{(i)} &= \sum_{\mathbf{k}} \sum_{ab\alpha\beta} c^{\dagger}_{\mathbf{k}\, a\alpha} \, (\hat{M}^{(i)})^{\alpha\beta}_{ab} \, c_{\mathbf{k}\, b\beta} \\ & \quad + \sum_{ab\alpha\beta} d^{\dagger}_{a\alpha} \, (\hat{M}^{(i)})^{\alpha\beta}_{ab} \, d_{b\beta}, \end{aligned}$$

where $\hat{M}^{(i)}$ are Hermitean matrices and the suffix i identifies the particular conserved operator. For convenience we adopt the normalization $\mathrm{Tr}\left(\hat{M}^{(i)} \cdot \hat{M}^{(i)}\right) = 1$. Then, if we add a source field

$$\delta \hat{H} = -h^{(i)} \, \mathcal{M}^{(i)},$$

we can use the basis which diagonalizes $\hat{M}^{(i)}$ and apply the above results to find the variation of $\langle \mathcal{M}^{(i)} \rangle$ associated with the presence of the impurity at first order in the applied field. Going back to the original basis, we would find the following expression of the difference $\delta\chi^{(i)}$ between the susceptibilities in the presence and absence of the impurity:

$$\begin{aligned} \delta\chi^{(i)} &= \delta \left(\frac{\partial \langle \mathcal{M}^{(i)} \rangle}{\partial h^{(i)}} \right)_{h=0} \\ &= \int_{-\infty}^{\infty} \frac{d\epsilon}{\pi} \frac{\partial f(\epsilon)}{\partial \epsilon} \, \mathrm{Im} \left\{ G(\epsilon + i\delta) \right. \end{aligned}$$

$$\left[1-\left(\frac{\partial\Delta(i\epsilon)}{\partial i\epsilon}\right)_{i\epsilon=\epsilon+i\delta}+\frac{1}{\beta}\sum_{n}\sum_{abcd}\sum_{\alpha\beta\gamma\delta}\Gamma_{b\beta,d\delta;c\gamma,a\alpha}(\epsilon+i\delta,i\epsilon_n;i\epsilon_n,\epsilon+i\delta)\right.$$
$$\left.\left(\hat{M}^{(i)}\right)_{ab}^{\alpha\beta}\left(\hat{M}^{(i)}\right)_{cd}^{\gamma\delta}G(i\epsilon_n)^2\left(1-\frac{\partial\Delta(i\epsilon_m)}{\partial i\epsilon_m}\right)\right]\Bigg\}. \tag{A.8}$$

Hereafter we drop the suffix i. One can demonstrate that the following Ward identities hold for the impurity

$$\begin{aligned}&[\Sigma(i\epsilon+i\omega)-\Sigma(i\epsilon)]\;M_{ab}^{\alpha\beta}\\&=-\frac{1}{\beta}\sum_{n}\sum_{cd;\gamma\delta}\Gamma_{a\alpha,d\delta;c\gamma,b\beta}(i\epsilon+i\omega,i\epsilon_n;i\epsilon_n+i\omega,i\epsilon)\\&\quad M_{cd}^{\gamma\delta}\,G(i\epsilon_n+i\omega)\,G(i\epsilon_n)\;[i\omega-\Delta(i\epsilon_n+i\omega)+\Delta(i\epsilon_n)]\,.\end{aligned} \tag{A.9}$$

It then follows that

$$\begin{aligned}\frac{\partial\Sigma(i\epsilon)}{\partial i\epsilon}\,M_{ab}^{\alpha\beta}&=-\frac{1}{\beta}\sum_{n}\sum_{cd}\sum_{\gamma\delta}\Gamma_{a\alpha,d\delta;c\gamma,b\beta}(i\epsilon,i\epsilon_n;i\epsilon_n,i\epsilon)\,M_{cd}^{\gamma\delta}\,G(i\epsilon_n)^2\\&\quad-\lim_{i\omega\to0}\frac{1}{\beta}\sum_{n}\sum_{cd;\gamma\delta}\Gamma_{a\alpha,d\delta;c\gamma,b\beta}(i\epsilon+i\omega,i\epsilon_n;i\epsilon_n+i\omega,i\epsilon)\\&\qquad M_{cd}^{\gamma\delta}\,G(i\epsilon_n+i\omega)\,G(i\epsilon_n)\,\frac{[-\Delta(i\epsilon_n+i\omega)+\Delta(i\epsilon_n)]}{i\omega}\\&=-\frac{1}{\beta}\sum_{n}\sum_{cd}\sum_{\gamma\delta}\Gamma_{a\alpha,d\delta;c\gamma,b\beta}(i\epsilon,i\epsilon_n;i\epsilon_n,i\epsilon)\,M_{cd}^{\gamma\delta}\,G(i\epsilon_n)^2\left(1-\frac{\partial\Delta(i\epsilon_n)}{\partial i\epsilon_n}\right)\\&\quad+\int_{-\infty}^{\infty}\frac{d\epsilon'}{2\pi}\,\frac{\partial f(\epsilon')}{\partial\epsilon'}\sum_{cd;\gamma\delta}\Gamma_{a\alpha,d\delta;c\gamma,b\beta}(i\epsilon,\epsilon'-i\delta';\epsilon'+i\delta',i\epsilon)\\&\quad\left(M^{(i)}\right)_{cd}^{\gamma\delta}\left(M^{(i)}\right)_{ba}^{\beta\alpha}\,G(\epsilon'+i\delta')\,G(\epsilon'-i\delta')\,\mathrm{Im}\,[\Delta(\epsilon'-i\delta')-\Delta(\epsilon'+i\delta')]\,.\end{aligned} \tag{A.10}$$

Let us define the quantity

$$\bar{\rho}_*=\int_{-\infty}^{\infty}\frac{d\epsilon}{\pi}\,\frac{\partial f(\epsilon)}{\partial\epsilon}\,\mathrm{Im}\left\{G(\epsilon+i\delta)\left[1-\left(\frac{\partial\Delta(i\epsilon)}{\partial i\epsilon}\right)_{i\epsilon\to\epsilon+i\delta}-\left(\frac{\partial\Sigma(i\epsilon)}{\partial i\epsilon}\right)_{i\epsilon\to\epsilon+i\delta}\right]\right\}, \tag{A.11}$$

which plays the role of the quasiparticle DOS at the chemical potential. Then, through (A.8), (A.10) and (A.11), the following equation is readily found

$$\bar{\rho}_*\;=\;\sum_{ab}\sum_{\alpha\beta}\bar{\rho}_*\left(\hat{M}^{(i)}\right)_{ba}^{\beta\alpha}\left(\hat{M}^{(i)}\right)_{ab}^{\alpha\beta}$$

$$
\begin{aligned}
&= \delta\chi^{(i)} - \frac{1}{2\pi^2}\int_{-\infty}^{\infty} d\epsilon\, d\epsilon'\, \frac{\partial f(\epsilon)}{\partial \epsilon}\, \frac{\partial f(\epsilon')}{\partial \epsilon'}\, \mathrm{Im}\left\{ G(\epsilon + i\delta)\, \Big[\right. \\
&\quad \sum_{cd;\gamma\delta} \Gamma_{a\alpha,d\delta;c\gamma,b\beta}(\epsilon + i\delta, \epsilon' - i\delta'; \epsilon' + i\delta', \epsilon + i\delta) \\
&\quad \left. \left(M^{(i)}\right)_{cd}^{\gamma\delta} \left(M^{(i)}\right)_{ba}^{\beta\alpha} G(\epsilon' + i\delta')\, G(\epsilon' - i\delta')\, \mathrm{Im}\left[\Delta(\epsilon' - i\delta') - \Delta(\epsilon' + i\delta')\right] \Big] \right\} \\
&= \delta\chi^{(i)} + \frac{1}{2\pi}\int_{-\infty}^{\infty} d\epsilon\, d\epsilon'\, \frac{\partial f(\epsilon)}{\partial \epsilon}\, \frac{\partial f(\epsilon')}{\partial \epsilon'}\, \rho(\epsilon) \\
&\quad \sum_{cd;\gamma\delta} \Gamma_{a\alpha,d\delta;c\gamma,b\beta}(\epsilon + i\delta, \epsilon' - i\delta'; \epsilon' + i\delta', \epsilon + i\delta) \\
&\quad \left(M^{(i)}\right)_{cd}^{\gamma\delta} \left(M^{(i)}\right)_{ba}^{\beta\alpha} G(\epsilon' + i\delta')\, G(\epsilon' - i\delta')\, \mathrm{Im}\left[\Delta(\epsilon' - i\delta') - \Delta(\epsilon' + i\delta')\right]
\end{aligned}
\tag{A.12}
$$

The last expression is obtained by noticing that only the imaginary part of $G(\epsilon + i\delta)$ contributes, where Im $G(\epsilon + i\delta) = -\pi\rho(\epsilon)$. Eq. (A.12) allows to express any susceptibility to fields coupled to conserved quantities. If the hybridization function is smooth at low energies, then

$$\Delta(\epsilon' - i\delta') - \Delta(\epsilon' + i\delta') \simeq 2i\Delta_0,$$

hence we can rewrite (A.12) as follows

$$
\begin{aligned}
\delta\chi^{(i)} &= \bar{\rho}_* \left[1 - \frac{\Delta_0}{\bar{\rho}_*\pi}\int_{-\infty}^{\infty} d\epsilon\, d\epsilon'\, \frac{\partial f(\epsilon)}{\partial \epsilon}\, \rho(\epsilon)\, \frac{\partial f(\epsilon')}{\partial \epsilon'} \right. \\
&\quad \sum_{cd;\gamma\delta} \Gamma_{a\alpha,d\delta;c\gamma,b\beta}(\epsilon + i\delta, \epsilon' - i\delta'; \epsilon' + i\delta', \epsilon + i\delta) \\
&\quad \left. \left(M^{(i)}\right)_{cd}^{\gamma\delta} \left(M^{(i)}\right)_{ba}^{\beta\alpha} G(\epsilon' + i\delta')\, G(\epsilon' - i\delta') \right], \\
&\equiv \bar{\rho}_* \left[1 - A_i\right],
\end{aligned}
\tag{A.13}
$$

which allows to identify local Landau A-parameters through

$$
\begin{aligned}
A_i &= \frac{\Delta_0}{\bar{\rho}_*\pi}\int_{-\infty}^{\infty} d\epsilon\, d\epsilon'\, \frac{\partial f(\epsilon)}{\partial \epsilon}\, \rho(\epsilon)\, \frac{\partial f(\epsilon')}{\partial \epsilon'} \\
&\quad \sum_{cd;\gamma\delta} \Gamma_{a\alpha,d\delta;c\gamma,b\beta}(\epsilon + i\delta, \epsilon' - i\delta'; \epsilon' + i\delta', \epsilon + i\delta) \\
&\quad \left. \left(M^{(i)}\right)_{cd}^{\gamma\delta} \left(M^{(i)}\right)_{ba}^{\beta\alpha} G(\epsilon' + i\delta')\, G(\epsilon' - i\delta') \right].
\end{aligned}
\tag{A.14}
$$

The above expression is quite general but simplifies substantially when the imaginary part of the impurity self-energy vanishes at low real frequency. In this case

$$G(i\epsilon_n \to \pm i0^+) = \frac{1}{-\epsilon_d \pm i\,\Delta_0},$$

where $\epsilon_d = \epsilon_d^{(0)} + \mathrm{Re}\Sigma(0)$ is the actual position of the d-resonance. Then, through (A.5),

$$\rho(0) = \frac{1}{\pi}\frac{\Delta_0}{\epsilon_d^2 + \Delta_0^2} = \frac{\Delta_0}{\pi} G(i0^+)G(i0^-). \tag{A.15}$$

Analogously

$$\bar{\rho}_* = \frac{\rho(0)}{Z}, \;\; \frac{1}{Z} = 1 - \left(\frac{\partial\Sigma(i\epsilon)}{\partial i\epsilon}\right)_{i\epsilon\to i0^+}$$

hence

$$A_i = \sum_{abcd}\sum_{\alpha\beta\gamma\delta}\left[Z^2\,\bar{\rho}_*\,\Gamma_{a\alpha,d\delta;c\gamma,b\beta}(0,0;0,0)\right]\,\left(\hat{M}^{(i)}\right)_{ba}^{\beta\alpha}\,\left(\hat{M}^{(i)}\right)_{cd}^{\gamma\delta}, \tag{A.16}$$

which is the more conventional expression of the Landau parameters[75].

Appendix B

Matrix elements for the three-orbital model

In this appendix we introduce the proper notation and demonstrate Eq. (4.11). The various formulas used in this Appendix can be found for instance in Ref. [76]

Let us recall the definition (4.5) of the particle-hole operators with orbital momentum l and z-component λ and with spin s and z-component σ

$$\left\{c^\dagger \otimes c\right\}_{l\lambda,s\sigma} = \sum (-1)^{k-1} C^{l\lambda}_{1j,1-k} (-1)^{\beta-1/2} C^{s\sigma}_{1/2\alpha,1/2-\beta} c^\dagger_{j\alpha} c_{k\beta} \tag{B.1}$$

where $C^{c\gamma}_{a\alpha,b\beta}$ are the Clebsh-Gordan coefficients and summation over repeated indices is implied.

The reduced matrix elements are defined through the identity

$$\langle Q;T,\tau;S,\Sigma| \left\{c^\dagger \otimes c\right\}_{l\lambda,s\sigma} |Q;T',\tau';S',\Sigma'\rangle = (-1)^{T'+S'} \left[\frac{(2T'+1)(2S'+1)}{(2T+1)(2S+1)}\right]^{1/4}$$

$$C^{T\tau}_{l\lambda T'\tau'} C^{S\Sigma}_{s\sigma S'\Sigma'} \langle Q;T,S|| \left\{c^\dagger \otimes c\right\}_{l,s} ||Q;T',S'\rangle. \tag{B.2}$$

To simplify the notation let us drop the charge index from now on and define the symbol

$$\Pi_l = \sqrt{2l+1} \tag{B.3}$$

as well as $\Pi_{l_1 \ldots l_n} = \Pi_{l_1} \ldots \Pi_{l_n}$.

The matrix element in (4.11) can then be written

$$\langle T,\tau,T'_1,T'_d;S,\Sigma,S'_1,S'_d|\hat{J}_K|T,\tau,T_1,T_d;S,\Sigma,S_1,S_d\rangle =$$

$$\sum_{\tau_1\tau_d\tau_1'\tau_d'}\sum_{\Sigma_1\Sigma_d\Sigma_1'\Sigma_d'}\sum_{l\lambda s\sigma}(1-\delta_{l0}\delta_{s0})C^{T\tau}_{T_1\tau_1T_d\tau_d}C^{S\Sigma}_{S_1\Sigma_1S_d\Sigma_d}C^{T\tau}_{T_1'\tau_1'T_d'\tau_d'}C^{S\Sigma}_{S_1'\Sigma_1'S_d'\Sigma_d'}(-1)^{-\lambda-\sigma}$$

$$\langle T_1',\tau_1';S_1',\Sigma_1'|\left\{c^\dagger\otimes c\right\}_{l\lambda,s\sigma}|T_1,\tau_1;S_1,\Sigma_1\rangle$$

$$\langle T_d',\tau_d';S_d',\Sigma_d'|\left\{d^\dagger\otimes d\right\}_{l\lambda,s\sigma}|T_d,\tau_d;S_d,\Sigma_d\rangle=$$

$$=\sum_{\tau_1\tau_d\tau_1'\tau_d'}\sum_{\Sigma_1\Sigma_d\Sigma_1'\Sigma_d'}\sum_{l\lambda s\sigma}(1-\delta_{l0}\delta_{s0})\sqrt{\frac{\Pi_{T_1T_d}}{\Pi_{T_1'T_d'}}}(-1)^{-\lambda+T_1+T_d}C^{T\tau}_{T_1\tau_1T_d\tau_d}C^{T\tau}_{T_1'\tau_1'T_d'\tau_d'}C^{T_1'\tau_1'}_{l\lambda T_1\tau_1}C^{T_d'\tau_d'}_{l-\lambda T_d\tau_d}$$

$$\sqrt{\frac{\Pi_{S_1S_d}}{\Pi_{S_1'S_d'}}}(-1)^{-\sigma+S_1+S_d}C^{S\Sigma}_{S_1\Sigma_1S_d\Sigma_d}C^{S\Sigma}_{S_1'\Sigma_1'S_d'\Sigma_d'}C^{S_1'\Sigma_1'}_{s\sigma S_1\Sigma_1}C^{S_d'\Sigma_d'}_{s-\sigma S_d\Sigma_d}$$

$$\langle T_1',S_1'||\left\{c^\dagger\otimes c\right\}_{l,s}||T_1,S_1\rangle\langle T_d',S_d'||\left\{d^\dagger\otimes d\right\}_{l,s}||T_d,S_d\rangle. \tag{B.4}$$

We now make use of a formula to sum the various Clebsh-Gordan coefficients

$$\sum_{\beta\gamma\epsilon\phi\eta}(-1)^{-\eta+e+f}C^{a\alpha}_{b\beta c\gamma}C^{a\alpha}_{e\epsilon f\phi}C^{b\beta}_{g\eta e\epsilon}C^{c\gamma}_{g-\eta f\phi}=$$

$$=\sum_\eta(-1)^{2e+2f+g-b-c}(-1)^{g-\eta}\sum_{k\kappa}\Pi_{abck}C^{k\kappa}_{g\eta g-\eta}C^{a\alpha}_{a\alpha k\kappa}\begin{Bmatrix}a&b&c\\a&e&f\\k&g&g\end{Bmatrix} \tag{B.5}$$

where the symbol in curly braces is a $9-j$ coefficient. Since

$$\sum_\eta(-1)^{g-\eta}C^{k\kappa}_{g\eta g-\eta}=\Pi_g\delta_{k0} \tag{B.6}$$

and

$$C^{a\alpha}_{a\alpha00}=1 \tag{B.7}$$

Eq. (B.5) reduces to

$$(-1)^{2e+2f+g-b-c}\Pi_{abcg}\begin{Bmatrix}a&b&c\\a&e&f\\0&g&g\end{Bmatrix}=$$

$$=(-1)^{2e+2f+g-b-c}\Pi_{abcg}\frac{(-1)^{a+c+e+g}}{\Pi_{ag}}\begin{Bmatrix}f&e&a\\b&c&g\end{Bmatrix}=$$

$$=(-1)^{-a+b+2c+3e+2f+2g}\Pi_{bc}\begin{Bmatrix}f&e&a\\b&c&g\end{Bmatrix} \tag{B.8}$$

Applying this identity to both the orbital and the spin part of Eq. (B.4) we get for the orbital

$$\sum_{\tau_1\tau_d\tau_1'\tau_d'}\sqrt{\frac{\Pi_{T_1T_d}}{\Pi_{T_1'T_d'}}}(-1)^{-\lambda+T_1+T_d}C^{T\tau}_{T_1\tau_1T_d\tau_d}C^{T\tau}_{T_1'\tau_1'T_d'\tau_d'}C^{T_1'\tau_1'}_{l\lambda T_1\tau_1}C^{T_d'\tau_d'}_{l-\lambda T_d\tau_d}=$$

$$\sqrt{\Pi_{T_1T_dT_1'T_d'}}(-1)^{-T+T_1'+2T_d'+3T_1+2T_d+2l}\begin{Bmatrix}T_d & T_1 & T\\ T_1' & T_d' & l\end{Bmatrix} \tag{B.9}$$

and for the spin

$$\sum_{\Sigma_1\Sigma_d\Sigma_1'\Sigma_d'}\sqrt{\frac{\Pi_{S_1S_d}}{\Pi_{S_1'S_d'}}}(-1)^{-\sigma+S_1+S_d}C^{S\Sigma}_{S_1\Sigma_1S_d\Sigma_d}C^{S\Sigma}_{S_1'\Sigma_1'S_d'\Sigma_d'}C^{S_1'\Sigma_1'}_{s\sigma S_1\Sigma_1}C^{S_d'\Sigma_d'}_{s-\sigma S_d\Sigma_d}=$$

$$\sqrt{\Pi_{S_1S_dS_1'S_d'}}(-1)^{-S+S_1'+2S_d'+3S_1+2S_d+2s}\begin{Bmatrix}S_d & S_1 & S\\ S_1' & S_d' & s\end{Bmatrix}. \tag{B.10}$$

Combining Eqs. (B.4), (B.9) and (B.10) we obtain as a result Eq. (4.11).

Bibliography

[1] C. M. Varma, P. B. Littlewood, S. Schmitt-Rink, E. Abrahams, and A. E. Ruckenstein. *Phys. Rev. Lett.*, **63**:1996, 1989.

[2] I. E. Perakis, C. M. Varma, and A. E. Ruckenstein. *Phys. Rev. Lett.*, **70**:3467, 1993.

[3] T. Giamarchi, C. M. Varma, A. E. Ruckenstein, and P. Nozières. *Phys. Rev. Lett.*, **70**:3967, 1993.

[4] C. Sire, C. M. Varma, A. E. Ruckenstein, and T. Giamarchi. *Phys. Rev. Lett.*, **72**:2478, 1994.

[5] G. M. Zhang and L. Yu. *Phys. Rev. Lett.*, **72**:2474, 1994.

[6] D. L. Cox and A. Zawadowski. *Adv. Phys.*, **47**:599, 1998.

[7] A. Schroeder, G. Aeppli, R. Coldea, M. Adams, O. Stockert, H. V. Loehneysen, E. Bucher, R. Ramazashvili, and P. Coleman. *Nature*, **407**:351, 2000.

[8] Q. Si, S. Rabello, K. Ingersent, and J. L. Smith. *Nature*, **413**:804, 2001.

[9] V. Barzykin and I. Affleck. *Phys. Rev. B*, **61**:6170, 2000.

[10] A. Georges, G. Kotliar, W. Krauth, and M. J. Rozenberg. *Rev. Mod. Phys.*, **68**:13, 1996.

[11] W. Metzner and D. Vollhardt. *Phys. Rev. Lett.*, **62**:324, 1989.

[12] A. Georges and G. Kotliar. *Phys. Rev. B*, **45**:6479, 1992.

[13] P. Nozières and A. Blandin. *J. Phys. (Paris)*, **41**:193–211, 1980.

[14] B. A. Jones and C. M. Varma. *Phys. Rev. Lett.*, **58**:843, 1987.

[15] B. A. Jones, C. M. Varma, and J. W. Wilkins. *Phys. Rev. Lett.*, **61**:125, 1988.

[16] B. A. Jones and C. M. Varma. *Phys. Rev. B*, **40**:324, 1989.

[17] I. Affleck and A. W. W. Ludwig. *Phys. Rev. Lett.*, **68**:1046, 1992.

[18] I. Affleck, A. W. W. Ludwig, and B. A. Jones. *Phys. Rev. B*, **52**:9528, 1995.

[19] Q. Si and G. Kotliar. *Phys. Rev. Lett.*, **70**:3143, 1993.

[20] M. Fabrizio and E. Tosatti. *Phys. Rev. B*, **55**:13465, 1997.

[21] M. Capone, M. Fabrizio, P. Giannozzi, and E. Tosatti. *Phys. Rev. B*, **62**:7619, 2000.

[22] M. Capone, M. Fabrizio, and E. Tosatti. *Phys. Rev. Lett.*, **86**:5361, 2001.

[23] M. Capone, M. Fabrizio, C. Castellani, and E. Tosatti. *Science*, **296**:2364, 2002.

[24] M. Capone, M. Fabrizio, C. Castellani, and E. Tosatti. *Phys. Rev. Lett.*, **93**:047001, 2004.

[25] P. W. Anderson. *Phys. Rev.*, **124**:41, 1961.

[26] J. R. Schrieffer and D. C. Mattis. *Phys. Rev.*, **140**:A1412, 1965.

[27] D. C. Langreth. *Phys. Rev.*, **150**:516, 1966.

[28] J. R. Schrieffer and P. A. Wolff. *Phys. Rev.*, **149**:491, 1966.

[29] J. Kondo. *Progr. Theor. Phys.*, **32**:37, 1964.

[30] P. W. Anderson. *J. Phys. C*, **3**:2436, 1970.

[31] P. W. Anderson and G. Yuval. *Phys. Rev. Lett.*, **23**:89, 1969.

[32] G. Yuval and P. W. Anderson. *Phys. Rev. B*, **1**:1522, 1970.

[33] P. W. Anderson, G. Yuval, and D. R. Hamann. *Phys. Rev. B*, **1**:4464, 1970.

[34] P. W. Anderson and G. Yuval. *J. Phys. C*, **4**:607, 1971.

[35] K. G. Wilson. *Rev. Mod. Phys.*, **47**:773, 1975.

[36] H. R. Krishnamurthy, J. W. Wilkins, and K. G. Wilson. *Phys. Rev. B*, **21**:1003, 1980.

[37] H. R. Krishnamurthy, J. W. Wilkins, and K. G. Wilson. *Phys. Rev. B*, **21**:1044, 1980.

[38] D. M. Cragg, P. Lloyd, and P. Nozières. *J. Phys. C*, **13**:803, 1980.

[39] N. Andrei and C. Destri. *Phys. Rev. Lett.*, **52**:364, 1984.

[40] A. M. Tsvelick. *J. Phys. C*, **18**:159, 1985.

[41] P. B. Wiegmann and A. M. Tsvelick. *Z. Phys. B*, **54**:201, 1985.

[42] I. Affleck and A. W. W. Ludwig. *Nucl. Phys.*, **B360**:641–696, 1991.

[43] I. Affleck and A. W. W. Ludwig. *Phys. Rev. B*, **48**:7297, 1993.

[44] I. Affleck, A. W. W. Ludwig, H.-B. Pang, and D. L. Cox. *Phys. Rev. B*, **45**:7918, 1992.

[45] C. Sire, C. M. Varma, and H. R. Krishnamurthy. *Phys. Rev. B*, **48**:13833, 1993.

[46] J. Gan. *Phys. Rev. B*, **51**:8287, 1995.

[47] A. J. Millis, B. G. Kotliar, and B. A. Jones. in *Field Theories in Condensed Matter Physics*, pages 159–166. Addison-Wesley, Redwood City, CA, 1990.

[48] D. Withoff and E. Fradkin. *Phys. Rev. Lett.*, **64**:1835, 1990.

[49] C. Gonzales-Buxton and K. Ingersent. *Phys. Rev. B*, **57**:14254, 1998.

[50] N. Andrei. *Phys. Rev. Lett.*, **45**:379, 1980.

[51] T. A. Costi, A. C. Hewson, and V. Zlatič. *J. Phys.: Condens. Matter*, **6**:2519, 1994.

[52] R. Bulla, T. A. Costi, and D. Vollhardt. *Phys. Rev. B*, **64**:045103, 2001.

[53] I. Affleck and A. W. W. Ludwig. *Nucl. Phys.*, **B352**:849–862, 1991.

[54] J. L. Cardy. *Nucl. Phys.*, **B240**:514, 1984.

[55] J. L. Cardy. *Nucl. Phys.*, **B270**:186, 1986.

[56] J. L. Cardy. *Nucl. Phys.*, **B324**:581, 1989.

[57] P. D. Francesco, P. Mathieu, and D. Sénéchal. *Conformal Field Theory*. Springer, 1996.

[58] I. Affleck. *Nucl. Phys.*, **B336**:517, 1990.

[59] I. Affleck and A. W. W. Ludwig. *Phys. Rev. Lett.*, **67**:161–164, 1991.

[60] A. W. W. Ludwig and I. Affleck. *Phys. Rev. Lett.*, **67**:3160, 1991.

[61] N. Ishibashi. *Mod. Phys. Lett.*, **A4**:251, 1989.

[62] T. Onogi and N. Ishibashi. *Nucl. Phys.*, **B318**:239, 1989.

[63] E. Verlinde. *Nucl. Phys.*, **B300**:360, 1988.

[64] M. Fabrizio, A. F. Ho, L. D. Leo, and G. E. Santoro. *Phys. Rev. Lett.*, **91**:246402, 2003.

[65] P. Nozières. *J. Low Temp. Phys.*, **17**:31–42, 1974.

[66] J. M. Maldacena and A. W. W. Ludwig. *Nucl. Phys.*, **B506**:565, 1997.

[67] G. Zaránd, L. Borda, J. von Delft, and N. Andrei. *Phys. Rev. Lett.*, **93**:107204, 2004.

[68] We are indebted with G. Zaránd for this result.

[69] J. E. Han. *cond-mat/0401104*, 2004.

[70] A. B. Zamolodchikov and V. A. Fateev. *JETP*, **62**:215, 1985.

[71] A. B. Zamolodchikov and V. A. Fateev. *JETP*, **63**:913, 1986.

[72] A. B. Zamolodchikov. *Int. J. Mod. Phys.*, **A3**:743, 1988.

[73] I. Affleck, M. Oshikawa, and H. Saleur. *J. Phys. A: Math Gen.*, **31**:5827, 1998.

[74] I. Affleck, M. Oshikawa, and H. Saleur. *J. Phys. A: Math Gen.*, **34**:1073, 2001.

[75] L. Mihály and A. Zawadowskii. *J. Phys. (France) Lett.*, **39**:L–483, 1978.

[76] D. A. Varshalovich, A. N. Moskalev, and V. K. Kheronskii. *Quantum Theory of Angular Momentum*. World Scientific, 1988.

Acknowledgments

Now that the period in Trieste is going to finish it’s time to thank and say goodbye to many friends that shared with me these years. I apologize in advance for those I will forget but, you know, physics is a memory-consuming activity.

First of all I must thank my professor Michele Fabrizio for his endless patience and support. His knowledge of physics and his skill are so great that I often realized the deep meaning of his thoughts with terrible delay. Working with him has been an exciting experience.

My gratitude goes also to all those who contributed to this work in many different ways starting from professor Giuseppe Santoro who introduced me in the world of computations. A particular thank to Davide and Ugo, whose computer skills were equal only to their patience.

My deepest thank must go to Katrin, mis chline switzer cheferli, for the beautiful time spent together, especially on our motorbike! And for joining me in the USA adventure.

A special thank to "the snow spider" Angelo. I simply cannot list all the stupid things we have done together. For sure life in Trieste is much more boring since you left.

Many greetings to the the bio-simulator gang, the “chef” Michele Cascella for making our medieval culinary knowledge wider and our bellies fatter, Alejandro with Roxana and the terrible lovely Santiago, Alessandra the crazy shopper, Pietro and Giovanna and their sabotaged refrigerator, Matteo and Lucia, Marco and Francesca, and all the others.

Thanks to Michele Cirasuolo, with whom I share the membership of the LCA group together with Silvia. Ruben and Valentina helped us in verifying that the world is really small. Roberto and Chiara, good luck in Australia! Pedro revealed us the secrets of the original paella.

Thanks to Andrea for those poor 200 km, but also for a lot of help and fun together. We still have to do a serious tour!

Thanks to Daniele, for surviving four years in the same apartment and being always there when needed.

Many thanks to my former and present office mates, Paola, Luca, Evgeny, Tanya, Claudio, Michele, Lorenzo, Laura and Manuela for making time in SISSA always a pleasure. In particular together with three of them (they know who) we are responsible for some of the worst jokes I've ever heard!

With Alessandro, Luca and Lorenzo I'm playing the longest roleplay game of my life. Hopefully we will finish before leaving Trieste.

A great thank to all the SISSA football players (really too many to be listed!) and in particular to Fabio (the Di Biagio-like penalty expert) and Cosma for sharing the organization of the weekly match. And to Giacomo and Stefano for the assistance after my last match.

And many many others: Simone and Laura, Valentina and Carlo, Adriano, Alessandro, Vittoria, Natasha, Emanuele, Francesca, Osvaldo e Claudia, Federico, Nico, Marco, Giacomo, Anna, Gorana, Gioia ...

Last, but not least, I must thank my family for the love and the support in these, sometimes hard, years.

Grazie!

L

October 29th, 2004